UNIVERSITY OF CALIFORNIA SAN DIEGO

3D Bioprinting of Ocular Stem Cells

A dissertation submitted in partial satisfaction of the
Requirements for the degree Doctor of Philosophy

in

Nanoengineering

by

Zheng Zhong

Committee in charge

Professor Shaochen Chen, Chair
Professor Liangfang Zhang, Co-Chair
Professor Nisarg J. Shah
Professor Wei Wang
Professor Binhai Zheng

2021

The Dissertation of Zheng Zhong is approved, and it is acceptable in quality and form for publication on microfilm and electronically:

University of California San Diego

2021

TABLE OF CONTENTS

LIST OF ABBREVIATIONS

DLP: digital light processing

DMD: digital micromirror device

LAP: lithium phenyl-2,4,6-trimethylbenzoylphosphinate

PDMS: polydimethylsiloxane

SLM: spatial light modulator

UV: ultraviolet

GelMA: gelatin methacryloyl

HAGM: hyaluronic acid glycidyl methacrylate

LSC: limbal stem/progenitor cells

CjSC: conjunctival stem cells

TGF-β: transforming growth factor β

BMP: bone morphogenetic proteins

ROCK: Rho-associated protein kinase

IL: interleukin

EGF: epidermal growth factor

ITS: Insulin-Transferrin-Selenium

HUVECs: human umbilical vein endothelial cells

PAX6: Paired box protein 6

KRT: cytokeratin

ABCG2: ATP-binding cassette super-family G member 2

MUC: mucin

SPDEF: SAM-pointed domain containing ETS transcription factor

RNA-seq: RNA sequencing

LIST OF FIGURES

LIST OF TABLES

ACKNOWLEDGEMENTS

I would like to sincerely thank many people, without whom this thesis would not have been possible.

First, I must thank my advisor, Dr. Shaochen Chen, who has helped me through a very difficult time and offered me a perfect research environment. Dr. Chen is a one of the most supportive mentors I have ever met. He has always shown a lot of respect on all my work and thoughts. The whole working experience here will be long memorized.

Then, I would like to thank my dissertation committee members, Dr. Liangfang Zhang, Dr. Nisarg J. Shah, Dr. Wei Wang, Dr. Binhai Zheng, for their time and comments.

I would also like to thank my lab mentor, Dr. Pengrui Wang and Dr. Claire Yu, for their guidance and advice; my teammates and co-workers, Jing Tian, Alis Balayan, Emmie Yao, Xiaoqian Deng, Xiaokang Wu, for their trust and support; and the rest of the Chen lab family, including Dr. Shangting You, Dr. Daniel Wangpraseurt, Dr. David Berry, Henry Hwang, Kathleen Miller, Jacob Schimelman, Min Tang, Wisarut Kiratitanaporn, Yi Xiang, Yazhi Sun, Leilani Kwe, Aaron Shi, Luwen Chen, Trevor Fried, for their support. It has been a lot of fun.

Last, I would like to thank all my friends and family members for the greatest love. They forgive me for spending too much time on my work and would always be there when I need them.

Chapter 2, in full, is a reprint of the manuscript in revision, Z. Zhong, A. Balayan, J. Tian, Y. Xiang, H. Hwang, X. Wu, X. Deng, J. Schimelman, Y. Sun, C. Ma, A. Santos, S. You, M. Tang, E. Yao, X. Shi, N. Steinmetz, S. Deng, S.C. Chen. “3D Bioprinting of Dual ECM Scaffolds Encapsulating Limbal Stem/Progenitor Cells in Active and Quiescent Statuses”. The dissertation author was the primary investigator and author of this paper.

Chapter 3, in full, is a reprint of the published article, "Rapid Bioprinting of Conjunctival Stem Cell Micro-constructs for Subconjunctival Ocular Injection", Z. Zhong, X. Deng, P. Wang, C. Yu, W. Kiratitanaporn, X. Wu, J. Schimelman, M. Tang, A. Balayan, E. Yao, J. Tian, L. Chen, K. Zhang, S.C. Chen, *Biomaterials*, 2020. The dissertation author was the primary investigator and author of this paper.

Chapter 4, in full, a reprint of the manuscript in preparation, "Rapid 3D Bioprinting of Multicellular Model Recapitulating Pterygium Microenvironment", Z. Zhong, J. Wang, J. Tian, X. Deng, A. Balayan, Y. Sun, J. Schimelman, E. Yao, S.C. Chen. The dissertation author was the primary investigator and author of this paper.

VITA

2015 Bachelor of Science, Sun Yat-sen University

2017 Master of Science, University of California San Diego

2021 Doctor of Philosophy, University of California San Diego

PUBLICATIONS

[1]. Chang H, Chen Z, Anil K, Chunsik L, Mingquan C, Lijuan H, Jing W, Xiangrong R, Yida J, Wei C, Bin W, Zhiqin G, **Zheng Z**, Zijing H, Fan Z, Bing H, Hao D, Rong J, Zhongshu T, Yizhi L, Yihai C, Xuri L, Xialin L. "Vasoprotective effect of PDGF-CC mediated by HMOX1 rescues retinal degeneration." *Proceedings of the National Academy of Sciences*. *111*(41) (2014), 14806-14811.

[2]. Skowronska-K D, Zhao L, Zhu J, Weinreb RN, Cao G, Luo J, Flagg K, Patel S, Wen C, Krupa M, Luo H, Ouyang H, Lin D, Wang W, Li G, Xu Y, Li O, Chung C, Yeh E, Jafari M, Ai M, **Zhong Z**, Shi W, Zheng L, Krawczyk M, Chen D, Shi C, Zin C, Zhu J, Mellon PL, Gao W, Abagyan R, Zhang L, Sun X, Zhong S, Zhuo Y, Rosenfeld MG, Liu Y, Zhang K. "P16INK4a Upregulation Mediated by SIX6 Defines Retinal Ganglion Cell Pathogenesis in Glaucoma." *Molecular Cell*. 59 (2015):931-40.

[3]. Lin H, Ouyang H, Zhu J, Huang S, Liu Z, Chen S, Cao G, Li G, Signer R, Xu Y, Chung C, Zhang Y, Lin D, Patel S, Wu F, Cai H, Hou J, Wen C, Jarafi M, Liu X, Luo L, Zhu J, Qiu A, Hou R, Chen B, Chen J, Granet D, Heichel C, Shang F, Li X, Krawczyk M, Skowronska-Krawczyk D, Wang Y, Shi W, Chen D, **Zhong Z**, Zhong S, Zhang L, Chen S, Morrison SJ, Maas RL, Zhang K*, Liu Y*. "Lens Regeneration using endogenous stem cells with gain of visual function." *Nature*. 531(2016):323-328.

[4]. Xu RH, Wei W, Krawczyk M, Wang W, Luo H, Flagg K, Yi S, Shi W, Quan Q, Li K, Zhang H, Caughey BA, Zhao Q, Hou J, Zhang R, Xu Y, Cai H, Li G, Hou R, **Zhong Z**, Lin D, Fu X, Zhu J, Duan Y, Yu M, Ying B, Zhang W, Wang J, Zhang E, Zhang C, Li O, Guo R, Carter H, Zhu JK, Hao X, Zhang K. "Circulating tumour DNA methylation markers for diagnosis and prognosis of hepatocellular carcinoma." *Nature Materials*. 16(11) (2017), 1155-1161.

[5]. P. Wang, X. Li, **Z. Zhong**, W. Wang, W. Zhu, A. Moran, K. Zhang, S. C. Chen. "3D Bioprinting of Hydrogels for Retina Cell Culturing." *Bioprinting*, Vo. 11(2018), e00029 (1-6).

[6]. M. Tang, Q. Xie, R. C. Gimple, **Z. Zhong**, T. Tam, J. Tian, R. L. Kidwell, Q. Wu, B. C. Prager, Z. Qiu, A. Yu, Z. Zhu, P. Mesci, H. Jing, J. Schimelman, P. Wang, D. Lee, M. H. Lorenzini, D. Dixit, L. Zhao, S. Bhargava, T. E. Miller, X. Wan, J. Tang, B. Sun, B. F. Cravatt, A. R. Muotri, S.C. Chen, J. N. Rich. "Three-dimensional bioprinting enables creation of tissue-informed glioblastoma microenvironments for modeling complex cellular interactions." *Cell Research*, 30(2020), 833–853.

[7]. **Z. Zhong**, X. Deng, P. Wang, C. Yu, W. Kiratitanaporn, X. Wu, M. Tang, E. Yao, J. Tian, L. Chen, K. Zhang, S.C. Chen. "Rapid Bioprinting of Conjunctival Stem Cell Micro-constructs for Subconjunctival Ocular Injection." *Biomaterials* 267 (2021): 120462.

[8]. **Z. Zhong**, A. Balayan, J. Tian, Y. Xiang, H. Hwang, X. Wu, X. Deng, J. Schimelman, Y. Sun, S. You, M. Tang, E. Yao, X. Shi, N. Steinmetz, S. Deng, S.C. Chen. "3D Bioprinting of Dual ECM Scaffolds Encapsulating Limbal Stem/Progenitor Cells in Active and Quiescent Statuses." In revision.

[9]. **Z. Zhong**, J. Wang, J. Tian, X. Deng, A. Balayan, Y. Sun, J. Schimelman, E. Yao, S.C. Chen. "Rapid 3D Bioprinting of Multicellular Model Recapitulating Pterygium Microenvironment." In preparation.

ABSTRACT OF DISSERTATION

3D Bioprinting of Ocular Stem Cells

by

Zheng Zhong

Doctor of Philosophy in Nanoengineering

University of California San Diego, 2021

Professor Shaochen Chen, Chair

Professor Liangfang Zhang, Co-Chair

Normal vision is important for many human activities, but many of ocular diseases could lead to vision impairment and affect millions of patients worldwide. In recent years, tissue engineering based on stem cells has been explored to develop novel therapeutic products and disease models for different types of ocular diseases. However, the fabrication of 3D scaffold

supporting the culture of ocular stem cells and the development of engineering approach mimicking the stem cell microenvironment remain challenging.

3D bioprinting is an emerging additive manufacturing technology for microscale biofabrication. Among different 3D bioprinting approaches, digital light processing (DLP)-based 3D bioprinting stands out with the rapid, scalable, robust fabrication with high resolution. And with the broad-range material choice and the well-defined mechanical property control, the DLP-based 3D bioprinting has been applied to fabricate hydrogel scaffold encapsulating various types of stem cells.

In this dissertation, the 3D bioprinting of two types of ocular stem cells, limbal stem cells and conjunctival stem cells, as well as the applications in stem cell therapy and ocular disease modeling were discussed. By performing the DLP-based bioprinting, we fabricated microscale hydrogel scaffolds encapsulating ocular stem cells while preserving the viability, stemness and potency. Based on this, we fabricated injectable hydrogel constructs encapsulating stem cell for minimally invasive stem cell transplantation. In addition, we bioprinted hydrogel scaffolds with heterogeneous extracellular matrix (ECM) an studied the ECM-dependent stem cell behaviors. Furthermore, with multicellular bioprinting, we developed a novel disease model recapitulating the pathological signatures displayed in patient tissues. These works have emphasized the role of 3D bioprinting in developing stem cell therapy and personalized medicine for ocular diseases.

Chapter 1 Introduction

1.1 Motivation

The eye is one of the most vital organs. Keeping a normal vision is critical for human being in conducting daily life activities while any compromises on the vision would be disastrous both physically and mentally. However, various types of severe ocular diseases and injuries caused by physical or chemical threats are jeopardizing the eye, especially the ocular surface, of millions of patients worldwide [1,2]. And in many of these cases, the vision of the patient might not be fully restored by exciting surgical interventions or therapeutic approaches [1,3]. In the last decade, as multiple sources of ocular stem cells were discovered and a variety of tissue engineering approaches using biocompatible materials have been integrated for them, regenerative medicine based on stem cells has become the potential solution for many types of ocular disorders [4–8]. Current methods for ocular stem cell transplantation largely adopt feeder layer-supported (3T3 cells, etc.) culture and natural materials-based (amniotic membrane, etc.) approaches [9–12]. The efficient in vitro expansion of stem cells, the high-throughput fabrication of cellularized constructs with precise control over the geometry and mechanical properties, as well as the maintenance of stem cell phenotypes during the fabrication remain challenging.

3D bioprinting as an emerging technology for micro- or nanoscale biomedical scaffold fabrication for tissue engineering applications, has shown tremendous potential in fabricating stem cell products [13–15]. And among different types of 3D bioprinting approaches, digital light processing (DLP)-based 3D bioprinting stands out on the high-throughput fabrication, the precise control on geometry and mechanical property of micro- or nanoscale constructs and the varsity of biocompatible material choice [16]. The unique features of this bioprinting platform have enable the fabrication of the synthetic microenvironment recapitulating not just the biochemical and

biomechanical properties of the extracellular matrix (ECM) but also the intracellular interaction by building multicellular niches [15,16]. With the DLP-based 3D bioprinting, microscale hydrogel scaffolds encapsulating primary mammalian cells, stem cells, and iPSC-derived cells have been successfully fabricated while the cell property being maintained [17–20]. The resultant cellularized constructs have also been applied for various biomedical applications, including cell transplantation and disease modeling.

This thesis aimed to develop tissue engineering approaches using DLP-based 3D bioprinting of ocular stem cells for regenerative medicine and disease modeling of ocular surface diseases. In the following chapters, we will discuss the 3D bioprinting of hydrogel scaffolds encapsulating ocular stem cells, the in vitro expansion of primary stem cells, and the fabrication of multicellular and multi-ECM in vitro bioprinted models using ocular stem cells. These studies provided engineering insights for the ocular tissue engineering and biological insights for the cell-cell, and cell-ECM interactions in the microenvironments of the ocular surface.

1.2 Tissue Engineering and Endogenous Stem Cells

Tissue engineering typically uses living cells as building blocks, assisted with the use of biomaterials, and engineering approaches to manipulate the physical properties and functions of tissues under physiological or pathological conditions [21]. Stem cells are commonly used in tissue engineering for their potency for regeneration. Endogenous stem cells are specialized unipotent or multipotent stem/progenitor cells residing in specific niches in adult tissues [22]. They largely remain quiescent and conduct self-renewal of the tissue under physiological conditions but can be activated to proliferation and differentiation for tissue repair by the stimulus from the niche, such as injury and inflammation signals [22]. Using engineered scaffolds as instructive niches, the stem

cell fate and behaviors can be guided for the application of regenerative medicine [23,24].

As the stem cell technologies developed, various types of endogenous stem cells have been studied and applied for translational research or clinical trials of novel stem cell therapy [25]. Mesenchymal stem cell (MSC) is one of the most typical multipotent stem cells [26]. They reside in different tissue niches of adult body, and can be readily isolated from bone marrow, and adipose tissues [27]. Since MSCs can be differentiated into multiple lineages, including muscle myocytes, adipocytes, osteocytes, and chondrocytes, they have been widely used for the remodeling of muscle, heart, and skeleton [28,29]. Another popular type of multipotent endogenous stem cell, hematopoietic stem cell (HSC), serves as the progenitor cell of all the differentiated blood cells from lymphoid and myeloid lineages [30]. HSCs extracted from bone marrow and peripheral blood have been extensively used for transplantation to treat blood diseases, such as leukemia, and non-blood diseases, like cerebral ischemia [31–34]. Unlike the multipotent stem cells, unipotent or bipotent stem/progenitor cells have limited potency to be differentiated into only one or two types of cells, but they are still highly valuable for the therapeutic applications of specific diseases or injuries [22,35]. For instance, limbal epithelial stem/progenitor cells (LSCs) are unipotent progenitor cells that are capable of the self-renewal and differentiation of corneal epithelium [36–38]. On the other hand, conjunctival stem cells (CjSCs) are bipotent progenitor cells on the conjunctival epithelium that give rise to both the keratinocytes and goblet cells [39,40]. Both LSCs and CjSCs have been explored as building block cells for the tissue engineering and regenerative medicine for the ocular surface reconstruction [41].

For the tissue engineering of endogenous stem cells, the efficient in vitro expansion of stem cells is the first obstacle to be overcome [42]. To eliminate or alleviate the effects of cellular senescence and the loss of stemness during the culture, a broad range of cytokines and small

molecules that activate or inhibit the signaling pathways involved in the stem cell fate decision have been tested as supplements in the stem cell culture medium [42]. Evolutionary conserved signaling pathways are often ubiquitous in various stem cell niches. They can have similar regulation effects on different cells but can also perform distinctive regulation in a tissue-specific way. For example, the inhibition of Rho/ROCK signaling, a central mechanotransduction signaling pathway, enhanced the in vitro expansion efficiency of both the mesoderm-derived HSCs and the surface ectoderm-derived epithelial stem cells [43–45]. On the other hand, Notch signaling, a highly conserved signaling pathway based on cell-cell junctions, maintains the stemness of MSCs while promotes the differentiation of LSCs [46,47]. Therefore, identifying the principle signaling pathways that control the stem cell fate decision is critical for building an efficient *in vitro* stem cell culture system.

1.3 Ocular Stem Cells and Ocular Surface Regeneration

Ocular surface is a vital component of vision as the smooth transparent surface of the cornea functions as the refractive surface of the visual system [48]. It provides the structural and immunologic protection and mainly consists of the corneal epithelium, the corneoscleral limbus, and the conjunctival epithelium, as well as some functional glands, such as the lacrimal glands and the meibomian glands [48]. In addition, ocular surface epithelia are covered by the tear film, a dynamic structure composed of the mucous proteins, aqueous and lipidic layers, for the moisturization and maintaining the hemostasis of the functional ocular surface [49].

As a major threat to the vision, ocular surface disorders are a class of disorders damaging the ocular surface, mainly the cornea and the conjunctiva. Prevalent conditions include dry eye diseases, blepharitis, allergy, meibomian gland dysfunction, while severe conditions like limbal

stem cell deficiency (LSCD), Stevens-Johnson syndrome, toxic epidermal necrolysis, recurring pterygium, as well as physical and chemical burns can cause irreversible blindness [7,50–55]. Despite of the high prevalence of the ocular surface disorders, the mechanism of pathogenesis in many cases, especially the severe forms, remained unclean and the effective approaches for evaluation, therapy, and management of these diseases are largely wanted [56]. As the most common way of treatment, administration of artificial teardrops containing steroids, antibiotics, recombinant growth factors, anti-inflammation drugs or autologous serum have been widely used in clinical practices to alleviate symptoms and attenuate signs to resist the disease progression [57–60]. In many cases, surgical interventions, such as autograft or allograft transplantation, become necessary to rebuild the structure and function of the ocular surface [61,62]. However, these approaches can hardly be radical cure and share limitation in the comprehensive restoration of the ocular surface microenvironments and the prevention of persistent inflammation.

In the past decades, as the understanding and technologies in stem cell biology and tissue engineering developed, increasing attention has been turned towards the stem cell therapy of ocular surface disorders. Among all the different cell sources, LSCs and CjSCs, as the endogenous stem cells residing on the ocular surface, have showed highly valuable application potentials for their use in regenerative medicine.

1.3.1 Limbal Stem Cells

LSCs are endogenous stem cells located in the basement membrane of the corneosceral limbus and enriched in the rete ridges of the palisades of Vogt [61,62]. LSCs are essential for the function and homeostasis of cornea and responsible for the sustain self-renewal and regeneration of the corneal epithelium [37]. When injury signals are sensed, quiescent LSCs in the basal crypts

will be activated, migrate centripetally, proliferate as transient amplifying cells (TACs), and differentiate to corneal epithelium for post-injury regeneration of corneal epithelium [63–65]. The deficiency of LSC population with congenital or acquired causes, LSCD, is a devastating ocular surface disease with high risk of visual loss [66]. As one of the most well-characterized endogenous stem cells, the cell programming, and clinical applications of LSCs have been extensively studied. The WNT protein family has been found involved in the different aspects of the LSC fate decision, as the canonical WNT pathways regulating the self-renewal and corneal epithelial differentiation while the non-canonical WNT (planar cell polarity) pathways contributed to the transition of quiescence and activation [67–69]. In addition, responded to Notch, WNT, and TGF-β signaling pathways, the transcription factor paired box 6 (PAX6) is the key regulator for LSC fate decision and the loss of PAX6 converted LSCs to epidermal lineages [37,70]. For the biomedical applications, LSCs have been integrated with various types of biomaterials, including natural and compressed collagen, gelatin, modified amniotic membranes and decellularized corneal basement membrane [64]. But more efficient approach for the fabrication of hydrogel scaffolds encapsulating LSCs is still highly desired.

1.3.2 Conjunctival Stem Cells

CjSCs are bipotent endogenous stem cells that can give rise to both conjunctival epithelial keratinocytes and conjunctival goblet cells [40]. In human conjunctiva, CjSCs localize in the epithelial basal layer and predominantly enrich in the forniceal regions [39]. As a newly defined endogenous stem cell, the physiological and pathological functions of CjSCs remained debatable. CjSCs undergo self-renewal like LSCs and react to the injury and inflammation on the conjunctival epithelium with proliferation and differentiation [41]. The stemness and differentiation of CjSCs

are manipulated by exterior niche signals like TGF-β, BMP, WNT/ β-Catenin, as a transcription factor, SPDEF, being the central regulator for goblet cell differentiation [40,71,72]. Although the application of CjSC on ocular surface regeneration has promising future, the development of CjSC-based therapeutic approaches was challenged by the lack of efficiency in the in vitro expansion and the poor understanding in CjSC engineering [9,11,41,73,74]. Existing methods often employed feeder layers to support the culture of CjSCs with issues in acquiring stem cell population with high purity [5,39,75]. A variety of engineered approaches using synthetic material membranes or hydrogel constructs have also been reported, but the maintenance of CjSC properties and the high-throughput fabrication are still challenging [6,76,77]. Therefore, new methods in the primary culture and the engineering of CjSCs are needed to better address the issue.

1.4 3D Bioprinting

As a rising technology, 3D bioprinting is a type of additive manufacturing that utilize bioinks containing biomaterials and cells to print cellular or acellular structures in a controlled manner [14,15]. Typically, 3D bioprinting techniques adopt the deposition-based method and deposit the bioinks with a nozzle in a layer-by-layer manner following designed patterns to fabricate 3D structure, such as ink-jet printing [78,79]. However, challenges remained in 1) the resolution of the fabricated features were limited by the size of nozzle or inkjet head; 2) the solidification of the bioinks in this case usually require thermal or chemical stimulus, which could compromise the biological properties of the laden cells; 3) the liquid-solid interface or meniscus will usually disrupt the surface of the printed structure [79]. In the last decade, 3D bioprinting techniques based on localized polymerization have been explored to overcome these issues and one of the most advanced way to do that is the DLP-based 3D bioprinting using

photopolymerization [16,79].

1.4.1 Photopolymerizable Biomaterials in 3D Bioprinting

A variety of biomaterials have been used in 3D bioprinting to provide biochemical and biomechanical support for the cell in tissue engineering applications. In deposition-based printing, the biomaterials for bioinks are usually thermogelling, with little chemical modification required [14]. As the DLP-based 3D bioprinting utilize photopolymerization to solidify the structure, the bioink materials need to be photocrosslinkable [16].

As one of the most widely investigated biomaterials, gelatin is a biodegradable peptide derived from collagen that is highly biocompatible and enriched with arginine-glycine-aspartic (RGD) motifs for cell adhesion [80]. By modifying gelatin with methacryloyl group, photocrosslinkable gelatin, gelatin methacrylate (GelMA) can be synthesized [81,82]. GelMA has been used for the encapsulation of various types of stem cells, as collagen being the most abundant components in many of the stem cell niche [83]. In addition to the excellent biocompatibility, GelMA has also performed to cover a board range of biomimetic stiffness in the photopolymerization-based fabrication, which is useful for recapitulating the modulus of tissues in both physiological and pathological conditions [84].

Hyaluronic acid (HA) is a type of non-sulfated glycosaminoglycan that is distributed in ECM of different tissues, such as epithelial and neural tissues [85]. Other than physical functions like hydration and lubrication, HA is also bioactive and found to regulate cellular behaviors by interacting with various surface receptor/ligand like CD44[86]. However, the printability of HA is limited by the instable mechanical property [87]. For tissue engineering applications, HA has been modified using chemicals like glycidyl methacrylate to form photopolymerizable HA glycidyl

methacrylate (HAGM) [87,88]. With the preserved biological functionality and the robust mechanical properties, HAGM has been used for the fabrication of various types of stem cell niche, including retinal progenitor cells and glioblastoma stem cells [17,89].

1.4.2 DLP-based 3D Bioprinting

The DLP-based 3D bioprinting is a light-assisted 3D additive manufacturing technology [16,90]. With photopolymerization, this method can rapidly solidify photo-polymerizable materials upon light exposure. The light source on the DLP bioprinter for inducing photopolymerization can be blue light or ultraviolet (UV) [16]. One of the most prevailing mechanism for the DLP-based 3D bioprinting is the free radical-initiating photopolymerization, as the free radicals excised by light exposure released from the photoinitiator and react with the reactive double bonds on the pre-polymer materials and trigger the chain-growth polymerization [16]. The DLP-based 3D bioprinter was equipped with a DMD chip that can convert the inputted digital designs into optical patterns that are projected on the photopolymerized pre-polymer materials to form defined objective patterns [79]. In addition, by spatiotemporally regulating the light exposure, the degree of crosslinking during the photopolymerization can be controlled and thereby the mechanical property of the bioprinted structures can be tuned [20].

In a stem cell niche, ECM provides necessary physical supports for the inhabiting cells and biological components [22]. ECM also contains bioactive molecules that interact with the receptors and ligands on the cell membrane. Because cell-ECM interactions are essential determinant of stem cell fate, biomaterials with relevant biochemical and biomechanical features as well as engineering approaches have been extensively used to build instructive microenvironments that can regulate and guide stem cells for transplantation and tissue repair [24,91]. The DLP-based

bioprinting has been reported to fabricate hydrogel scaffolds encapsulating different kinds of cells, including primary cells from human and animal sources, endogenous stem cells, iPSC-derived stem cells and cancer stem cells [15,16,18,92]. A variety of biomaterials, including gelatin, collagen, hyaluronic acid, alginate, chitosan, have been modified and used for DLP-based bioprinting, which essentially enrich available components for the ECM-recapitulating capacity of the technology [16]. Furthermore, with spatiotemporal control of light exposure enabled by the DLP-based bioprinting, hydrogel constructs with tunable mechanical property can be fabricated, which can further manipulate the phenotypes of the encapsulated cells through biomechanical interactions [13].

1.5 Research Objectives

As aforementioned, the application of ocular stem cells in developing regenerative medicine treatments for ocular diseases has a promising future, but innovative tissue engineering approaches for the ocular stem cells are wanted. At first, the lack of understanding in the stem cell biology, the efficient way of primary culture of endogenous ocular stem cells was under exploration. In addition, the complicated and diverse mechanical properties of the stem cell residing niches increased the difficulty in recapitulating the microenvironment with engineering methods. Furthermore, although some approaches for the hydrogel encapsulation of ocular stem cells have been reported, the high-throughput fabrication of the scaffolds encapsulating stem cells while preserving their biological integrity remained challenging.

The following chapters are dedicated to exploring the 3D bioprinting of ocular stem cells with the DLP-based 3D bioprinting platform by studying the stem cell biology, cell-ECM interaction and the applications in cell therapy and disease modeling.

In Chapter 2, the 3D bioprinting of dual ECM hydrogel scaffold encapsulating primary LSCs was developed, and the ECM-specific stem cell phenotypes related to the quiescence and proliferative activation were studied.

In Chapter 3, an integrative tissue engineering strategy of rabbit primary CjSCs was developed based on the DLP bioprinting, as a feeder-free in vitro expansion method for CjSCs was developed and the bioprinting of CjSC-encapsulated constructs with ECM stiffness optimized was explored, as well as a methodology of the injectable delivery of CjSCs with bioprinted hydrogel constructs was established on an ex vivo model.

In Chapter 4, the primary culture methods, and the 3D bioprinting of human primary CjSCs were studied. Upon the demonstration of 3D bioprinting of human CjSCs, a multicellular bioprinted disease model of pterygium was developed and studied on the transcriptomic level.

Reference

[1] N.N. Ashraf, M.I. Adhi, Outcome of application of amniotic membrane graft in ocular surface disorders, J. Pak. Med. Assoc. (2017).

[2] D. Meller, R.T.F. Pires, R.J.S. Mack, F. Figueiredo, A. Heiligenhaus, W.C. Park, P. Prabhasawat, T. John, S.D. McLeod, K.P. Steuhl, S.C.G. Tseng, Amniotic membrane transplantation for acute chemical or thermal burns, Ophthalmology. (2000). https://doi.org/10.1016/S0161-6420(00)00024-5.

[3] S. Barabino, M. Rolando, G. Bentivoglio, C. Mingari, S. Zanardi, R. Bellomo, G. Calabria, Role of amniotic membrane transplantation for conjunctival reconstruction in ocular-cicatricial pemphigoid, Ophthalmology. (2003). https://doi.org/10.1016/S0161-6420(02)01892-4.

[4] S.S. Mahdavi, M.J. Abdekhodaie, S. Mashayekhan, A. Baradaran-Rafii, A.R. Djalilian, Bioengineering Approaches for Corneal Regenerative Medicine, Tissue Eng. Regen. Med. 17 (2020) 567–593. https://doi.org/10.1007/s13770-020-00262-8.

[5] M. Bertolin, C. Breda, S. Ferrari, S.I. Van Acker, N. Zakaria, E. Di Iorio, A. Migliorati, D. Ponzin, B. Ferrari, Z. Lužnik, V. Barbaro, Optimized protocol for regeneration of the conjunctival epithelium using the cell suspension technique, Cornea. (2019).

https://doi.org/10.1097/ICO.0000000000001670.

[6] M. He, T. Storr-Paulsen, A.L. Wang, C.E. Ghezzi, S. Wang, M. Fullana, D. Karamichos, T.P. Utheim, R. Islam, M. Griffith, M.M. Islam, R.R. Hodges, G.E. Wnek, D.L. Kaplan, D.A. Dartt, Artificial polymeric scaffolds as extracellular matrix substitutes for autologous conjunctival goblet cell expansion, Investig. Ophthalmol. Vis. Sci. (2016). https://doi.org/10.1167/iovs.16-20081.

[7] E. Clearfield, V. Muthappan, X. Wang, I.C. Kuo, Conjunctival autograft for pterygium, Cochrane Database Syst. Rev. (2016). https://doi.org/10.1002/14651858.CD011349.pub2.

[8] M. Li, M. Zhu, Y. Yu, L. Gong, N. Zhao, M.J. Robitaille, Comparison of conjunctival autograft transplantation and amniotic membrane transplantation for pterygium: A meta-analysis, Graefe's Arch. Clin. Exp. Ophthalmol. (2012). https://doi.org/10.1007/s00417-011-1820-8.

[9] C.C. Drechsler, A. Kunze, A. Kureshi, G. Grobe, S. Reichl, G. Geerling, J.T. Daniels, S. Schrader, Development of a conjunctival tissue substitute on the basis of plastic compressed collagen, J. Tissue Eng. Regen. Med. 11 (2017) 896–904. https://doi.org/10.1002/term.1991.

[10] R. Williams, R. Lace, S. Kennedy, K. Doherty, H. Levis, Biomaterials for Regenerative Medicine Approaches for the Anterior Segment of the Eye, Adv. Healthc. Mater. 7 (2018). https://doi.org/10.1002/adhm.201701328.

[11] N. Nassiri, M. Eslani, N. Panahi, S. Mehravaran, A. Ziaei, A.R. Djalilian, Ocular graft versus host disease following allogeneic stem cell transplantation: A review of current knowledge and recommendations, J. Ophthalmic Vis. Res. (2013). https://doi.org/10.1038/s41409-018-0090-z.

[12] D. Meller, V. Dabul, S.C.G. Tseng, Expansion of conjunctival epithelial progenitor cells on amniotic membrane, Exp. Eye Res. (2002). https://doi.org/10.1006/exer.2001.1163.

[13] C. Yu, W. Zhu, B. Sun, D. Mei, M. Gou, S. Chen, Modulating physical, chemical, and biological properties in 3D printing for tissue engineering applications, Appl. Phys. Rev. 5 (2018). https://doi.org/10.1063/1.5050245.

[14] M. Askari, M. Afzali Naniz, M. Kouhi, A. Saberi, A. Zolfagharian, M. Bodaghi, Recent progress in extrusion 3D bioprinting of hydrogel biomaterials for tissue regeneration: A comprehensive review with focus on advanced fabrication techniques, Biomater. Sci. 9 (2021) 535–573. https://doi.org/10.1039/d0bm00973c.

[15] X. Ma, J. Liu, W. Zhu, M. Tang, N. Lawrence, C. Yu, M. Gou, S. Chen, 3D bioprinting of functional tissue models for personalized drug screening and in vitro disease modeling, Adv. Drug Deliv. Rev. (2018). https://doi.org/10.1016/j.addr.2018.06.011.

[16] C. Yu, J. Schimelman, P. Wang, K.L. Miller, X. Ma, S. You, J. Guan, B. Sun, W. Zhu, S.

Chen, Photopolymerizable Biomaterials and Light-Based 3D Printing Strategies for Biomedical Applications, Chem. Rev. 120 (2020) 10695–10743. https://doi.org/10.1021/acs.chemrev.9b00810.

[17] P. Wang, X. Li, W. Zhu, Z. Zhong, A. Moran, W. Wang, K. Zhang, S. Chen, 3D bioprinting of hydrogels for retina cell culturing, Bioprinting. (2018). https://doi.org/10.1016/j.bprint.2018.e00029.

[18] X. Ma, X. Qu, W. Zhu, Y.S. Li, S. Yuan, H. Zhang, J. Liu, P. Wang, C.S.E. Lai, F. Zanella, G.S. Feng, F. Sheikh, S. Chien, S. Chen, Deterministically patterned biomimetic human iPSC-derived hepatic model via rapid 3D bioprinting, Proc. Natl. Acad. Sci. U. S. A. (2016). https://doi.org/10.1073/pnas.1524510113.

[19] K.C. Hribar, D. Finlay, X. Ma, X. Qu, M.G. Ondeck, P.H. Chung, F. Zanella, A.J. Engler, F. Sheikh, K. Vuori, S.C. Chen, Nonlinear 3D projection printing of concave hydrogel microstructures for long-term multicellular spheroid and embryoid body culture, Lab Chip. (2015). https://doi.org/10.1039/c5lc00159e.

[20] X. Ma, C. Yu, P. Wang, W. Xu, X. Wan, C.S.E. Lai, J. Liu, A. Koroleva-Maharajh, S. Chen, Rapid 3D bioprinting of decellularized extracellular matrix with regionally varied mechanical properties and biomimetic microarchitecture, Biomaterials. (2018). https://doi.org/10.1016/j.biomaterials.2018.09.026.

[21] S.G. Kwon, Y.W. Kwon, T.W. Lee, G.T. Park, J.H. Kim, Recent advances in stem cell therapeutics and tissue engineering strategies, Biomater. Res. 22 (2018) 1–8. https://doi.org/10.1186/s40824-018-0148-4.

[22] H. Xia, X. Li, W. Gao, X. Fu, R.H. Fang, L. Zhang, K. Zhang, Tissue repair and regeneration with endogenous stem cells, Nat. Rev. Mater. 3 (2018) 174–193. https://doi.org/10.1038/s41578-018-0027-6.

[23] R.X. Wu, X.Y. Xu, J. Wang, X.T. He, H.H. Sun, F.M. Chen, Biomaterials for endogenous regenerative medicine: Coaxing stem cell homing and beyond, Appl. Mater. Today. 11 (2018) 144–165. https://doi.org/10.1016/j.apmt.2018.02.004.

[24] S. Pacelli, S. Basu, J. Whitlow, A. Chakravarti, F. Acosta, A. Varshney, S. Modaresi, C. Berkland, A. Paul, Strategies to develop endogenous stem cell-recruiting bioactive materials for tissue repair and regeneration, Adv. Drug Deliv. Rev. 120 (2017) 50–70. https://doi.org/10.1016/j.addr.2017.07.011.

[25] C.M. Madl, S.C. Heilshorn, H.M. Blau, Bioengineering strategies to accelerate stem cell therapeutics, Nature. 557 (2018) 335–342. https://doi.org/10.1038/s41586-018-0089-z.

[26] J. Ankrum, J.M. Karp, Mesenchymal stem cell therapy: Two steps forward, one step back, Trends Mol. Med. 16 (2010) 203–209. https://doi.org/10.1016/j.molmed.2010.02.005.

[27] D.J. Prockop, J. Youn Oh, Mesenchymal stem/stromal cells (MSCs): Role as guardians of inflammation, Mol. Ther. 20 (2012) 14–20. https://doi.org/10.1038/mt.2011.211.

[28] M.J. Dalby, A.J. García, M. Salmeron-Sanchez, Receptor control in mesenchymal stem cell engineering, Nat. Rev. Mater. 3 (2018) 1–14. https://doi.org/10.1038/natrevmats.2017.91.

[29] H.J. Anderson, J.K. Sahoo, R. V. Ulijn, M.J. Dalby, Mesenchymal stem cell fate: Applying biomaterials for control of stem cell behavior, Front. Bioeng. Biotechnol. 4 (2016) 38. https://doi.org/10.3389/fbioe.2016.00038.

[30] Q. Wei, P.S. Frenette, Niches for Hematopoietic Stem Cells and Their Progeny, Immunity. 48 (2018) 632–648. https://doi.org/10.1016/j.immuni.2018.03.024.

[31] S. Masson, Potential of Hematopoietic Stem Cell Therapy in Hepatology: A Critical Review, Stem Cells. 22 (2004) 897–907. https://doi.org/10.1634/stemcells.22-6-897.

[32] S. Schwarting, S. Litwak, W. Hao, M. Bähr, J. Weise, H. Neumann, Hematopoietic stem cells reduce postischemic inflammation and ameliorate ischemic brain injury, Stroke. 39 (2008) 2867–2875. https://doi.org/10.1161/STROKEAHA.108.513978.

[33] S.T. Gangaram-Panday, M.M. Faas, P. de Vos, Towards stem-cell therapy in the endocrine pancreas, Trends Mol. Med. 13 (2007) 164–173. https://doi.org/10.1016/j.molmed.2007.02.002.

[34] E. Gunsilius, G. Gastl, A.L. Petzer, Hematopoietic stem cells, Biomed. Pharmacother. 55 (2001) 186–194. https://doi.org/10.1016/S0753-3322(01)00051-8.

[35] F. Majo, A. Rochat, M. Nicolas, G.A. Jaoudé, Y. Barrandon, Oligopotent stem cells are distributed throughout the mammalian ocular surface, Nature. (2008). https://doi.org/10.1038/nature07406.

[36] J.H. Stern, Y. Tian, J. Funderburgh, G. Pellegrini, K. Zhang, J.L. Goldberg, R.R. Ali, M. Young, Y. Xie, S. Temple, Regenerating Eye Tissues to Preserve and Restore Vision, Cell Stem Cell. (2018). https://doi.org/10.1016/j.stem.2018.05.013.

[37] H. Ouyang, Y. Xue, Y. Lin, X. Zhang, L. Xi, S. Patel, H. Cai, J. Luo, M. Zhang, M. Zhang, Y. Yang, G. Li, H. Li, W. Jiang, E. Yeh, J. Lin, M. Pei, J. Zhu, G. Cao, L. Zhang, B. Yu, S. Chen, X.D. Fu, Y. Liu, K. Zhang, WNT7A and PAX6 define corneal epithelium homeostasis and pathogenesis, Nature. (2014). https://doi.org/10.1038/nature13465.

[38] T.T. Sun, S.C. Tseng, R.M. Lavker, Location of corneal epithelial stem cells, Nature. 463 (2010) E10–E11. https://doi.org/10.1038/nature08805.

[39] R.M.K. Stewart, C.M. Sheridan, P.S. Hiscott, G. Czanner, S.B. Kaye, Human Conjunctival Stem Cells are Predominantly Located in the Medial Canthal and Inferior Forniceal Areas, Invest. Ophthalmol. Vis. Sci. 56 (2015) 2021–2030. https://doi.org/10.1167/iovs.14-16266.

[40] I.K. Gipson, Goblet cells of the conjunctiva: A review of recent findings, Prog. Retin. Eye Res. (2016). https://doi.org/10.1016/j.preteyeres.2016.04.005.

[41] T. Ramos, D. Scott, S. Ahmad, An Update on Ocular Surface Epithelial Stem Cells: Cornea and Conjunctiva, Stem Cells Int. (2015). https://doi.org/10.1155/2015/601731.

[42] C.A. Heath, Cells for tissue engineering, Trends Biotechnol. 18 (2000) 17–19. https://doi.org/10.1016/S0167-7799(99)01396-7.

[43] C. Zhang, H.J. Lee, A. Shrivastava, R. Wang, T.J. McQuiston, S.S. Challberg, B.A. Pollok, T. Wang, Long-Term In Vitro Expansion of Epithelial Stem Cells Enabled by Pharmacological Inhibition of PAK1-ROCK-Myosin II and TGF-β Signaling, Cell Rep. 25 (2018) 598-610.e5. https://doi.org/10.1016/j.celrep.2018.09.072.

[44] R.E. Hynds, P. Bonfanti, S.M. Janes, Regenerating human epithelia with cultured stem cells: feeder cells, organoids and beyond, EMBO Mol. Med. 10 (2018) 139–150. https://doi.org/10.15252/emmm.201708213.

[45] M. Jiang, H. Chen, S. Lai, R. Wang, Y. Qiu, F. Ye, L. Fei, H. Sun, Y. Xu, X. Jiang, Z. Zhou, T. Zhang, Y. Li, J. Xie, Q. Fang, R.P. Gale, X. Han, H. Huang, G. Guo, Maintenance of human haematopoietic stem and progenitor cells in vitro using a chemical cocktail, Cell Discov. 4 (2018) 59. https://doi.org/10.1038/s41421-018-0059-5.

[46] Y. Tian, Y. Xu, T. Xue, L. Chen, B. Shi, B. Shu, C. Xie, M. Max Morandi, T. Jaeblon, J. V. Marymont, Y. Dong, Notch activation enhances mesenchymal stem cell sheet osteogenic potential by inhibition of cellular senescence, Cell Death Dis. 8 (2017) e2595–e2595. https://doi.org/10.1038/cddis.2017.2.

[47] S. González, M. Halabi, D. Ju, M. Tsai, S.X. Deng, Role of Jagged1-mediated Notch Signaling Activation in the Differentiation and Stratification of the Human Limbal Epithelium, Cells. 9 (2020) 1945. https://doi.org/10.3390/cells9091945.

[48] I.K. Gipson, The ocular surface: The challenge to enable and protect vision. The Friedenwald lecture, in: Investig. Ophthalmol. Vis. Sci., NIH Public Access, 2007: pp. 4391–4398. https://doi.org/10.1167/iovs.07-0770.

[49] S. Barabino, Y. Chen, S. Chauhan, R. Dana, Ocular surface immunity: Homeostatic mechanisms and their disruption in dry eye disease, Prog. Retin. Eye Res. (2012). https://doi.org/10.1016/j.preteyeres.2012.02.003.

[50] J. Vazirani, D. Nair, S. Shanbhag, S. Wurity, A. Ranjan, V. Sangwan, Limbal Stem Cell Deficiency—Demography and Underlying Causes, Am. J. Ophthalmol. 188 (2018) 99–103. https://doi.org/10.1016/j.ajo.2018.01.020.

[51] S. Kohanim, S. Palioura, H.N. Saeed, E.K. Akpek, G. Amescua, S. Basu, P.H. Blomquist,

C.S. Bouchard, J.K. Dart, X. Gai, J.A.P. Gomes, D.G. Gregory, G. Iyer, D.S. Jacobs, A.J. Johnson, S. Kinoshita, I.S. Mantagos, J.S. Mehta, V.L. Perez, S.C. Pflugfelder, V.S. Sangwan, K.C. Sippel, C. Sotozono, B. Srinivasan, D.T.H. Tan, R. Tandon, S.C.G. Tseng, M. Ueta, J. Chodosh, Stevens-Johnson Syndrome/Toxic Epidermal Necrolysis - A Comprehensive Review and Guide to Therapy. I. Systemic Disease, Ocul. Surf. 14 (2016) 2–19. https://doi.org/10.1016/j.jtos.2015.10.002.

[52] J. SMITH, The epidemiology of dry eye disease, Acta Ophthalmol. Scand. 85 (2007) 0–0. https://doi.org/10.1111/j.1600-0420.2007.01063_2858.x.

[53] A.R. Thode, R.A. Latkany, Current and Emerging Therapeutic Strategies for the Treatment of Meibomian Gland Dysfunction (MGD), Drugs. 75 (2015) 1177–1185. https://doi.org/10.1007/s40265-015-0432-8.

[54] T.F. Bernardes, A.A. Bonfioli, Blepharitis, Semin. Ophthalmol. 25 (2010) 79–83. https://doi.org/10.3109/08820538.2010.488562.

[55] A. Leonardi, E. Bogacka, J.L. Fauquert, M.L. Kowalski, A. Groblewska, M. Jedrzejczak-Czechowicz, S. Doan, F. Marmouz, P. Demoly, L. Delgado, Ocular allergy: Recognizing and diagnosing hypersensitivity disorders of the ocular surface, Allergy Eur. J. Allergy Clin. Immunol. 67 (2012) 1327–1337. https://doi.org/10.1111/all.12009.

[56] M.E. Stern, C.S. Schaumburg, R. Dana, M. Calonge, J.Y. Niederkorn, S.C. Pflugfelder, Autoimmunity at the ocular surface: Pathogenesis and regulation, Mucosal Immunol. 3 (2010) 425–442. https://doi.org/10.1038/mi.2010.26.

[57] A. Lambiase, L. Aloe, M. Centofanti, V. Parisi, F. Mantelli, V. Colafrancesco, G.L. Manni, M.G. Bucci, S. Bonini, R. Levi-Montalcini, Experimental and clinical evidence of neuroprotection by nerve growth factor eye drops: Implications for glaucoma, Proc. Natl. Acad. Sci. U. S. A. 106 (2009) 13469–13474. https://doi.org/10.1073/pnas.0906678106.

[58] M.J. Lavin, G.E. Rose, Use of steroid eye drops in general practice, Br. Med. J. (Clin. Res. Ed). 292 (1986) 1448–1450. https://doi.org/10.1136/bmj.292.6533.1448.

[59] D. Bremond-Gignac, F. Chiambaretta, S. Milazzo, A European perspective on topical ophthalmic antibiotics: current and evolving options., Ophthalmol. Eye Dis. 3 (2011) 29–43. https://doi.org/10.4137/OED.S4866.

[60] R.M. Shtein, J.F. Shen, A.N. Kuo, K.M. Hammersmith, J.Y. Li, M.P. Weikert, Autologous Serum-Based Eye Drops for Treatment of Ocular Surface Disease: A Report by the American Academy of Ophthalmology, in: Ophthalmology, Elsevier Inc., 2020: pp. 128–133. https://doi.org/10.1016/j.ophtha.2019.08.018.

[61] N. Koizumi, Ocular surface reconstruction, amniotic membrane, and cultivated epithelial cells from the limbus, Br. J. Ophthalmol. 87 (2003) 1437-a-1439. https://doi.org/10.1136/bjo.87.12.1437-a.

[62] Ö. Özdemir, O. Tekeli, K. Örnek, A. Arslanpençe, N.F. Yalçindağ, Limbal autograft and allograft transplantations in patients with corneal burns, Eye. 18 (2004) 241–248. https://doi.org/10.1038/sj.eye.6700640.

[63] S. Dou, Q. Wang, B. Zhang, H. Jiang, S. Chen, X. Qi, H. Duan, Y. Lu, J. Dong, Y. Cao, L. Xie, Q. Zhou, W. Shi, Molecular identity of human limbal heterogeneity involved in corneal homeostasis and privilege, Ocul. Surf. (2021). https://doi.org/10.1016/j.jtos.2021.04.010.

[64] G. Yazdanpanah, Z. Haq, K. Kang, S. Jabbehdari, M. l. Rosenblatt, A.R. Djalilian, Strategies for reconstructing the limbal stem cell niche, Ocul. Surf. 17 (2019) 230–240. https://doi.org/10.1016/j.jtos.2019.01.002.

[65] D.Q. Li, S. Kim, J.M. Li, Q. Gao, J. Choi, F. Bian, J. Hu, Y. Zhang, J. Li, R. Lu, Y. Li, S.C. Pflugfelder, H. Miao, R. Chen, Single-cell transcriptomics identifies limbal stem cell population and cell types mapping its differentiation trajectory in limbal basal epithelium of human cornea, Ocul. Surf. 20 (2021) 20–32. https://doi.org/10.1016/j.jtos.2020.12.004.

[66] Q. Le, J. Xu, S.X. Deng, The diagnosis of limbal stem cell deficiency, Ocul. Surf. 16 (2018) 58–69. https://doi.org/10.1016/j.jtos.2017.11.002.

[67] S.-Y. Chen, B.O. Han, Y.-T. Zhu, M. Mahabole, J. Huang, D.C. Beebe, S.C.G. Tseng, HC-HA/PTX3 Purified From Amniotic Membrane Promotes BMP Signaling in Limbal Niche Cells to Maintain Quiescence of Limbal Epithelial Progenitor/Stem Cells, (n.d.). https://doi.org/10.1002/stem.2091.

[68] M. Zheng, C. Tian, T. Fan, B. Xu, Fibronectin regulates the self-renewal of rabbit limbal epithelial stem cells by stimulating the Wnt11/Fzd7/ROCK non-canonical Wnt pathway, Exp. Eye Res. 185 (2019) 107681. https://doi.org/10.1016/j.exer.2019.05.021.

[69] M.N. Nakatsu, Z. Ding, M.Y. Ng, T.T. Truong, F. Yu, S.X. Deng, Wnt/β-catenin signaling regulates proliferation of human cornea epithelial stem/progenitor cells, Investig. Ophthalmol. Vis. Sci. 52 (2011) 4734–4741. https://doi.org/10.1167/iovs.10-6486.

[70] G. Li, F. Xu, J. Zhu, M. Krawczyk, Y. Zhang, J. Yuan, S. Patel, Y. Wang, Y. Lin, M. Zhang, H. Cai, D. Chen, M. Zhang, G. Cao, E. Yeh, D. Lin, Q. Su, W.W. Li, G.L. Sen, N. Afshari, S. Chen, R.L. Maas, X.D. Fu, K. Zhang, Y. Liu, H. Ouyang, Transcription factor PAX6 (paired box 6) controls limbal stem cell lineage in development and disease, J. Biol. Chem. 290 (2015) 20448–20454. https://doi.org/10.1074/jbc.M115.662940.

[71] H.A. McCauley, C.Y. Liu, A.C. Attia, K.A. Wikenheiser-Brokamp, Y. Zhang, J.A. Whitsett, G. Guasch, TGFβ signaling inhibits goblet cell differentiation via SPDEF in conjunctival epithelium, Dev. (2014). https://doi.org/10.1242/dev.117804.

[72] H.A. McCauley, G. Guasch, Three cheers for the goblet cell: Maintaining homeostasis in mucosal epithelia, Trends Mol. Med. (2015). https://doi.org/10.1016/j.molmed.2015.06.003.

[73] S. Kasbekar, S.B. Kaye, R.L. Williams, R.M.K. Stewart, S. Leow-Dyke, P. Rooney, Development of decellularized conjunctiva as a substrate for the ex vivo expansion of conjunctival epithelium, J. Tissue Eng. Regen. Med. 12 (2018) e973–e982. https://doi.org/10.1002/term.2419.

[74] S. Dehghani, M. Rasoulianboroujeni, H. Ghasemi, S.H. Keshel, Z. Nozarian, M.N. Hashemian, M. Zarei-Ghanavati, G. Latifi, R. Ghaffari, Z. Cui, H. Ye, L. Tayebi, 3D-Printed membrane as an alternative to amniotic membrane for ocular surface/conjunctival defect reconstruction: An in vitro & in vivo study, Biomaterials. (2018). https://doi.org/10.1016/j.biomaterials.2018.05.013.

[75] E. Tóth, D. Beyer, B. Zsebik, G. Vereb, L. Takács, Limbal and conjunctival epithelial cell cultivation on contact lenses - Different affixing techniques and the effect of feeder cells, Eye Contact Lens. 43 (2017) 162–167. https://doi.org/10.1097/ICL.0000000000000259.

[76] U. Agraval, P. Rundle, I.G. Rennie, S. Salvi, Fresh frozen amniotic membrane for conjunctival reconstruction after excision of neoplastic and presumed neoplastic conjunctival lesions, Eye. (2017). https://doi.org/10.1038/eye.2016.322.

[77] J.R.S. Ricardo, P.C. Cristovam, P.A.N. Filho, C.C. Farias, A.L. De Araujo, R.R. Loureiro, J.L. Covre, J.N. De Barros, T.P. Barreiro, M.S. Dos Santos, J.A.P. Gomes, Transplantation of conjunctival epithelial cells cultivated ex vivo in patients with total limbal stem cell deficiency, Cornea. (2013). https://doi.org/10.1097/ICO.0b013e31825034be.

[78] R. Raman, R. Bashir, Stereolithographic 3D bioprinting for biomedical applications, in: Essentials 3D Biofabrication Transl., Elsevier Inc., 2015: pp. 89–121. https://doi.org/10.1016/B978-0-12-800972-7.00006-2.

[79] S. You, K. Miller, S. Chen, Chapter 1. Microstereolithography, in: Royal Society of Chemistry, 2019: pp. 1–21. https://doi.org/10.1039/9781788012683-00001.

[80] S. Xiao, T. Zhao, J. Wang, C. Wang, J. Du, L. Ying, J. Lin, C. Zhang, W. Hu, L. Wang, K. Xu, Gelatin Methacrylate (GelMA)-Based Hydrogels for Cell Transplantation: an Effective Strategy for Tissue Engineering, Stem Cell Rev. Reports. 15 (2019) 664–679. https://doi.org/10.1007/s12015-019-09893-4.

[81] H. Shirahama, B.H. Lee, L.P. Tan, N.J. Cho, Precise tuning of facile one-pot gelatin methacryloyl (GelMA) synthesis, Sci. Rep. (2016). https://doi.org/10.1038/srep31036.

[82] B.H. Lee, N. Lum, L.Y. Seow, P.Q. Lim, L.P. Tan, Synthesis and characterization of types A and B gelatin methacryloyl for bioink applications, Materials (Basel). (2016). https://doi.org/10.3390/ma9100797.

[83] A.B. Bello, D. Kim, D. Kim, H. Park, S.H. Lee, Engineering and functionalization of gelatin biomaterials: From cell culture to medical applications, Tissue Eng. - Part B Rev. 26 (2020)

164–180. https://doi.org/10.1089/ten.teb.2019.0256.

[84] C. Kim, J.L. Young, A.W. Holle, K. Jeong, L.G. Major, J.H. Jeong, Z.M. Aman, D.W. Han, Y. Hwang, J.P. Spatz, Y.S. Choi, Stem Cell Mechanosensation on Gelatin Methacryloyl (GelMA) Stiffness Gradient Hydrogels, Ann. Biomed. Eng. 48 (2020) 893–902. https://doi.org/10.1007/s10439-019-02428-5.

[85] M.N. Collins, C. Birkinshaw, Hyaluronic acid based scaffolds for tissue engineering - A review, Carbohydr. Polym. 92 (2013) 1262–1279. https://doi.org/10.1016/j.carbpol.2012.10.028.

[86] K. Fuchs, A. Hippe, A. Schmaus, B. Homey, J.P. Sleeman, V. Orian-Rousseau, Opposing effects of high-and low-molecular weight hyaluronan on CXCL12-induced CXCR4 signaling depend on CD44, Cell Death Dis. 4 (2013) 819. https://doi.org/10.1038/cddis.2013.364.

[87] J.B. Leach, K.A. Bivens, C.W. Patrick, C.E. Schmidt, Photocrosslinked hyaluronic acid hydrogels: Natural, biodegradable tissue engineering scaffolds, Biotechnol. Bioeng. 82 (2003) 578–589. https://doi.org/10.1002/bit.10605.

[88] B.S. Spearman, N.K. Agrawal, A. Rubiano, C.S. Simmons, S. Mobini, C.E. Schmidt, Tunable methacrylated hyaluronic acid-based hydrogels as scaffolds for soft tissue engineering applications, J. Biomed. Mater. Res. - Part A. 108 (2020) 279–291. https://doi.org/10.1002/jbm.a.36814.

[89] M. Tang, Q. Xie, R.C. Gimple, Z. Zhong, T. Tam, J. Tian, R.L. Kidwell, Q. Wu, B.C. Prager, Z. Qiu, A. Yu, Z. Zhu, P. Mesci, H. Jing, J. Schimelman, P. Wang, D. Lee, M.H. Lorenzini, D. Dixit, L. Zhao, S. Bhargava, T.E. Miller, X. Wan, J. Tang, B. Sun, B.F. Cravatt, A.R. Muotri, S. Chen, J.N. Rich, Three-dimensional bioprinted glioblastoma microenvironments model cellular dependencies and immune interactions, Cell Res. (2020). https://doi.org/10.1038/s41422-020-0338-1.

[90] J. Zhang, Q. Hu, S. Wang, J. Tao, M. Gou, Digital light processing based three-dimensional printing for medical applications, Int. J. Bioprinting. 6 (2020) 12–27. https://doi.org/10.18063/ijb.v6i1.242.

[91] M.P. Lutolf, H.M. Blau, Artificial stem cell niches, Adv. Mater. 21 (2009) 3255–3268. https://doi.org/10.1002/adma.200802582.

[92] C. Yu, X. Ma, W. Zhu, P. Wang, K.L. Miller, J. Stupin, A. Koroleva-Maharajh, A. Hairabedian, S. Chen, Scanningless and continuous 3D bioprinting of human tissues with decellularized extracellular matrix, Biomaterials. 194 (2019) 1–13. https://doi.org/10.1016/j.biomaterials.2018.12.009.

Chapter 2 3D Bioprinting of Dual ECM Scaffolds Encapsulating Limbal Stem/Progenitor Cells in Active and Quiescent Statuses

Abstract

Limbal stem cell deficiency (LSCD) and corneal disorders are among the top global threats for human vision. Emerging therapies that integrate stem cell transplantation with engineered hydrogel scaffolds for biological and mechanical support are becoming a rising trend in the field. However, methods for high-throughput fabrication of hydrogel scaffolds, as well as knowledge of the interaction between limbal stem/progenitor cells (LSCs) and the surrounding extracellular matrix (ECM) are still much needed. Here, we employed digital light processing (DLP)-based 3D bioprinting to fabricate hydrogel scaffolds encapsulating primary LSCs and studied the ECM-dependent LSC phenotypes. The DLP-based 3D bioprinting with gelatin methacrylate (GelMA) or hyaluronic acid glycidyl methacrylate (HAGM) generated microscale hydrogel scaffolds that could support the viability of the encapsulated primary rabbit LSCs (rbLSCs) in culture. Immunocytochemistry and transcriptional analysis showed that the encapsulated rbLSCs remained active in GelMA-based scaffolds while exhibited quiescence in the HAGM-based scaffolds. The primary human LSCs (hLSCs) encapsulated within bioprinted scaffolds showed consistent ECM-dependent active/quiescent statuses. Based on these results, we have developed a novel 3D bioprinted dual ECM 'Yin-Yang' model encapsulating LSCs to support both active and quiescent statues. Our findings provide valuable insights towards stem cell therapies and regenerative medicine for corneal reconstruction.

2.1 Introduction

Corneal epithelium is a transparent nonkeratinized epithelium that contributes to the refractive power of eye and serves as the first protective barrier against the outside world [1,2]. Limbal stem/progenitor cells (LSCs) are endogenous stem cells that reside at the limbus, the periphery of the cornea [3]. LSCs are responsible for the homeostasis of corneal epithelium, thus, facilitating optical clarity and light transmission [2,3]. Worldwide, there are over 5 million individuals affected by corneal blindness and limbal stem cell deficiency (LSCD) being a common etiology [4–6]. Conventional LSCD treatments employ surgical repair interventions using such sources as amniotic membrane (AM) as substrate or scaffold combined with keratolimbal autografts, or allografts [7]. These treatment approaches are limited by the lack of standardized preparation of AM, risk of developing iatrogenic LSCD and immunologic rejection [8–10].

Recent advances in regenerative medicine and tissue engineering have facilitated the development of novel transplantation approaches using advanced biomaterials for the treatment of LSCD [11]. Hydrogel scaffolds based on collagen, gelatin, hyaluronic acid (HA), and synthetic polymers have been investigated as LSC carriers for transplantation [12–15]. Among the various approaches of hydrogel scaffold fabrication, digital light processing (DLP)-based 3D bioprinting stands out as a high-throughput platform allowing rapid fabrication of hydrogel scaffolds that support the encapsulation of numerous types of stem cells including retinal progenitor cells, conjunctival stem cells, mesenchymal stem cells, neural progenitor cells and cancer stem cells [16–21]. The spatiotemporal control of light exposure afforded by DLP-based 3D bioprinting also enables the stiffness tunability within desired regions of the fabricated hydrogel scaffolds, thus also allowing manipulate the phenotypes of the encapsulated cells [19,22–25]. Moreover, DLP-based 3D bioprinting enables the use of multiple extracellular matrix (ECM) components and

multiple cell types during hydrogel fabrication to better recapitulate the complex native microenvironment of stem cells [16,17,26].

Biological and biomechanical interactions between stem cells and their ECM have been shown to manipulate cell fate and phenotype [27–29]. Biomechanical factors such as substrate stiffness have been shown to regulate the activities of LSCs and the corneal regeneration under physiological and pathological conditions [30]. Stem cells can also interact with the scaffolds in a composition-dependent way as various types of cell surface receptors responding to the ECM by triggering downstream intracellular signaling pathways that dynamically and comprehensively manipulate cell programming [12,31–35]. The delicate balance between activation and quiescence of endogenous stem cells, including LSCs, is critical for the system homeostasis under varying healthy, aging, and diseased circumstances [36–38]. Recent studies have showed that engineered scaffolds are able to tune the transition of activation/quiescence in LSCs [33,39]. Therefore, understanding how the different ECM compositions regulate LSCs in a 3D microenvironment is important for developing novel transplantable LSC scaffolds.

In this study, we present a 3D bioprinting approach in generating primary LSC-encapsulated microscale hydrogel scaffolds to study the ECM-dependent LSC activities. With the customized DLP-based 3D bioprinting system, we fabricated microscale hydrogel scaffolds with gelatin methacrylate (GelMA) and hyaluronic acid glycidyl methacrylate (HAGM) that supported the encapsulation and cell viability of primary rabbit LSCs (rbLSCs). Next, we analyzed the different phenotypes of encapsulated rbLSCs at mRNA and protein levels. In addition, we extended the study on primary human LSCs (hLSCs) from different individuals with 3D bioprinting. Furthermore, we performed multi-material 3D bioprinting and fabricated a dual ECM 'Yin-Yang' model encapsulating primary rbLSCs in active/quiescent status. Overall, we developed

an innovative DLP-based 3D bioprinting approach for LSC engineering while broadening the understanding of ECM-dependent LSCs phenotypes, which is a meaningful step towards the development of regenerative medicine for LSCD and other severe ocular surface diseases.

2.2 Materials and Methods

Primary rabbit, human LSCs isolation and culture

The rabbit tissues from 10-12 weeks old New Zealand White rabbit eyes (Oryctolagus Cuniculus) were acquired from Sierra for Medical Science, Inc. (Whittier, CA). The human corneoscleral rims were acquired from One Legacy or Saving Sight eye banks. Consent was obtained by the eye banks for the tissues to be used for research. Experimentation on human tissue adhered to the tenets of the Declaration of Helsinki. The protocol for human corneal tissue collection and dissection was evaluated and exempted by the University of California, Los Angeles (UCLA) Institutional Review Boards (IRB#12-000363). The overall procedure was approved by University of California San Diego Institutional Biosafety Committee.

For rabbit LSCs (rbLSCs), rabbit eyeballs were washed in Dulbecco's phosphate-buffered saline (DPBS) and Dulbecco's Modified Eagle Medium (DMEM, ThermoFisher Scientific) with penicillin-streptomycin, respectively, and the corneoscleral rims were isolated for further dissection. Human LSCs (hLSCs) were harvested from donor corneoscleral rims stored in Optisol-GS. Corneoscleral rims from three different donors with no significant history of corneal diseases were used in this study. The isolation of both rbLSCs and hLSCs was performed as previously described [40]. Briefly, limbal epithelium with underlying stroma was excised circumferentially and minced using Vannas scissors. Type IV collagenase (0.2%, Sigma Aldrich) was used for digestion at 37℃ with constant shaking at 120 rpm for 1-1.5 hr. Following the incubation, cells

were pelleted and washed with PBS. Following a 10 min digestion with 0.25% Trypsin-EDTA (Sigma Aldrich) digestion, the cells were filtered through a 70 μm cell strainer (Corning) to obtain single cells. The cells were seeded onto Collagen I coated plates (ThermoFisher Scientific). The culture medium used was composed of DMEM /F-12 (3:1, ThermoFisher Scientific) with 10% Fetal Bovine Serum (ThermoFisher Scientific), penicillin-streptomycin (ThermoFisher Scientific), 400 ng/ml hydrocortisone (Sigma Aldrich), 1x insulin-transferrin-selenium (Corning), 2 nM reverse T3 (Sigma Aldrich), and 0.1 nM cholera toxin (Sigma Aldrich), 10 ng/ml epidermal growth factor (EGF, R&D System), and 10 μM Y27632 (Tocris Bioscience).

Material synthesis and photocrosslinkable bioink preparation

The synthesis of GelMA and HAGM was performed following previously established protocols [16,17,19,26,41]. Briefly, for GelMA, a 10% (w/v) gelatin solution was prepared by dissolving porcine skin gelatin type A (Sigma Aldrich) in a 0.25 M carbonate-bicarbonate (3:7) buffer at pH 9 while stirring at 50℃. Methacrylic anhydride (Sigma Aldrich) was then mixed in a dropwise fashion to the gelatin solution to reach 100 μl methacrylic anhydride per gram of gelatin. Then, following 1 hour of continuous stirring at 50℃, the product was subjected to overnight fluid dynamic dialysis using 13.5 kDa dialysis tubes (Repligen). Lyophilization for three days was then used to produce GelMA powder which was then stored at -80℃. The degree of methacrylation of the resultant GelMA is approximately 95% [17].

For the synthesis of HAGM, 1.0 g of Sodium Hyaluronate (Lifecore Biomedical) was dissolved in 100 mL water: acetone solution (1:1 ratio) and stirred at room temperature overnight

to prepare a 1% (w/v) HA solution. The flask was subjected to vacuum for 3 sec or until the solution boils then flooded with Argon. This step was repeated two more times and the solution was stirred overnight protected from light. On the next day, 7.2 ml triethylamine (Sigma Aldrich) 20-fold in excess was slowly added to the reaction flask until thoroughly mixed. The reaction was then flooded with argon gas, then immediately sealed, and mixed for 30 min. Using a syringe, 7.2 mL of glycidyl methacrylate (GM, Sigma Aldrich) in 20-fold excess was added dropwise to the reaction. Afterwards, the reaction was flooded with Argon, sealed, and stirred overnight at room temperature. The resulting material was precipitated using acetone and vacuum filtration was used to collect the precipitate which was dissolved in DI water. The dissolved material was then dialyzed, lyophilized, and stored at -80℃ until further use. The degree of methacrylation of the resultant HAGM is approximately 35% [17].

For photopolymerization, lithium phenyl-2,4,6-trimethylbenzoylphosphinate (LAP) was used as photoinitiator and synthesized per previously published protocols [16,19]. Briefly, dimethyl phenylphosphonite (18 mmol, Sigma Aldrich) was added dropwise to an equimolar 2,4,6-trimethylbenzoyl chloride (Acros Organics). The reaction was constantly stirred for 18 hours at room temperature. A solution of lithium bromide (6.1g, Sigma Aldrich) in 100 ml of 2-butanone (Sigma Aldrich) was then mixed into the reaction. Following a 10-minute stirring at 50℃, the mixture was incubated overnight at room temperature. Filter-washing with 2-butanone for three times was used to get rid of unreacted lithium bromide. The LAP solids that resulted from the reaction were crushed into powder and stored under argon in the dark at 4 ℃.

8% (w/v) GelMA with 0.25% (w/v) LAP and 4% (w/v) HAGM with 0.25% (w/v) LAP were dissolved in warm DPBS, filtered using 0.22 μm syringe and used as prepolymer solutions

for DLP-based 3D bioprinting with or without LSCs. The cells were detached from the culture plates with 0.25% trypsin-EDTA, and then neutralized with a pre-made culture medium. The cell solution was then filtered with a 70 μm cell strainer and the cell concentration was measured with a hemocytometer. The bioink containing 1-2×107 cells/mL LSCs and GelMA/HAGM prepolymer solution was prepared right before printing.

3D bioprinting of GelMA and HAGM hydrogel scaffolds

Our in-house DLP-based 3D bioprinting system was used for the rapid biofabrication of hydrogel scaffolds. The system is composed of a 365 nm light source (Hamamatsu), a projection optics assembly, a motion-controlled stage (Newport) and a digital micromirror device (DMD, Texas Instruments.) used for patterning the light. We generated digital patterns using Adobe photoshop which were imported into the custom operation software that controls the DMD chip to modulate the projection of light depending on the imported pattern. For the bioprinting setup, two polydimethylsiloxane (PDMS) spacers with thickness of 250 μm were set between a PDMS base that is attached to a glass slide and a methacrylated coverslip. This creates a gap of desired thickness where the prepolymer bioink was loaded. Then, photopolymerization was performed with the DLP bioprinter and the printed constructs were immediately moved to a 24-well plate and washed in pre-warmed DPBS to remove the excess bioink materials. The DPBS was then substituted with warmed culture medium and the bioprinted constructs were incubated in 5% CO2 at 37℃.

Immunofluorescence staining

Primary LSCs cultured on Millicell EZ slides (Millipore Sigma) were washed twice with

DPBS to prepare for 2D cell staining. The cells were fixed at room temperature for 20 min with 4% (w/v) paraformaldehyde (FUJIFILM Wako), followed by three washes with DPBS, each for 10 min. Then, the samples underwent blocking and permeabilization for 1 hour using 5% bovine serum albumin (Sigma Aldrich) and 0.3% triton X-100 (Sigma Aldrich) in DPBS at room temperature. Primary antibody incubation was done at 4℃ overnight followed by three DPBS washes for 10 min each. Afterwards, the cells were incubated with secondary antibodies (Alexa Fluor-conjugated, Invitrogen) for 1 hour at room temperature. The samples were further washed with DPBS, and nuclear staining was done with 1:500 DAPI (4',6-Diamidino-2-Phenylindole; ThermoFisher Scientific) in DPBS for 10 min. After a final DPBS wash, the samples were left to air-dry for 30 sec and mounted with Fluoromount-G™ Mounting Medium (ThermoFisher Scientific). Hydrogel cells staining was performed with the exact same procedure, except without mounting, where the samples were left in DPBS to be imaged. The samples were all imaged within 48 hours of the staining to preserve clarity. Further information on details of antibodies and dilution rates are mentioned in Supplementary Table 2.1.

Mechanical properties characterization

A micromechanical testing machine (Microsquisher, CellScale) was used to determine Young's modulus of the bioprinted scaffolds based on GelMA and HAGM. Cylinders test specimens (500 μm diameter, 500 μm height) printed with 8% GelMA or 4% HAGM were fabricated and incubated at 37℃ for overnight. The measurement of the compressive modulus followed the manufacturer's instructions. The sample's hysteresis was removed using two cycles of predetermined compression. During the mechanical testing, the samples were compressed at a

10% strain with strain rate of 2 μm/s. After the force and displacement data was collected from the Microsquisher, they were processed via a custom MATLAB script to calculate the compressive Young's modulus.

Viability evaluation

The viability of the LSCs encapsulated in the hydrogels were studied with the Viability/Cytotoxicity kit (Thermo Fisher), also known as Live/Dead™ staining. They were incubated with 2 μM calcein acetoxymethyl ester, along with 4 μM ethidium homodimer in DPBS, for 30 min at 37℃. Fluorescent imaging was done with a Leica microscope (DMI 6000-B). The viability test was carried out in triplicates.

RNA isolation, reverse transcription, and real time quantitative PCR

For RNA extraction, a TRIzol® reagent (Ambion Thermo Fisher) was continuously pipetted into the pelleted 2D-cultured cells. For the encapsulated LSCs in GelMA- and HAGM-based bioprinted hydrogel scaffolds, the constructs were stripped off their coverslips using a scalpel and subjected to enzymatic digestion with 0.2% Type IV collagenase (Sigma Aldrich) and 1kU/ml hyaluronidase (STEMCELL Technologies), respectively, at 37℃ for 15 min. The resulting cell solution was pelleted with centrifugation immediately followed by addition of TRIzol® reagent to the pellet. The lysate was then used directly or stored in -80℃. Direct-zol™ RNA Purification kit (Zymo Research) was used for the extraction of RNA following the manufacturer's protocol. NanoDropTM 2000 (Thermo Fisher Scientific) was used to quantify the purified RNA. The RNA was then used for cDNA synthesis and reverse transcription using the iScript™ cDNA Synthesis Kit (Bio-Rad) with thermal cycler StepOneTM Real-Time PCR System (Thermo Fisher

Scientific). Luna® Universal qPCR Master Mix was used for Real-Time quantitative polymerase chain reaction (qPCR). The primer details used in the qPCR can be found in Supplementary Table 2.2.

Flow cytometry

For flow cytometry, GelMA- and HAGM-based bioprinted scaffolds were enzymatically digested to isolate the encapsulated LSCs. Following the enzymatic digestion, the cells extracted from the scaffolds and 2D-cultured cells were digested with 0.25% trypsin-EDTA and filtered with a 70 µm cell strainer. After centrifugation, cell pellets were resuspended and fixed with Cytofix™ Fixation Buffer (BD) for 20 min followed by three 5-minute wash with Cell Staining Buffer (Biolegend) supplemented with 0.2% triton X-100. Primary antibodies were diluted with Cell Staining Buffer and applied for 20 min. Following a wash, secondary antibodies were diluted with Cell Staining Buffer and applied for 20 min. All the antibody incubations were performed at room temperature. Cell solutions were then kept on ice in the dark until use. The propidium iodide (Biolegend) viability staining was performed following the manufacturer's procedures. Briefly, 10 µl per million cells of the propidium iodide solution was added in the cell suspension. The solution was then incubated for 15 minutes at 4 °C avoiding light before analysis. Flow cytometry was performed using BD Accuri™ C6 flow cytometer following the instructions of the manufacturer. The data was collected from at least 100,000 events for each group and processed using FlowJo.

Imaging and processing

Confocal and brightfield/regular fluorescence imaging of the samples were taken using SP8 Confocal and DMI 6000-B Leica microscopes, respectively. ImageJ and LAS X were used to

further process the images.

Statistical analysis

Data obtained from the experiments were processed with Microsoft Excel and presented in a way of mean ± standard deviations Student's t-test (two tailed) or one-way ANOVA were applied to determine statistical significance which was denoted on the figures with an asterisk where appropriate (*: $P < 0.05$; **: $P < 0.01$; ***: $P < 0.001$.).

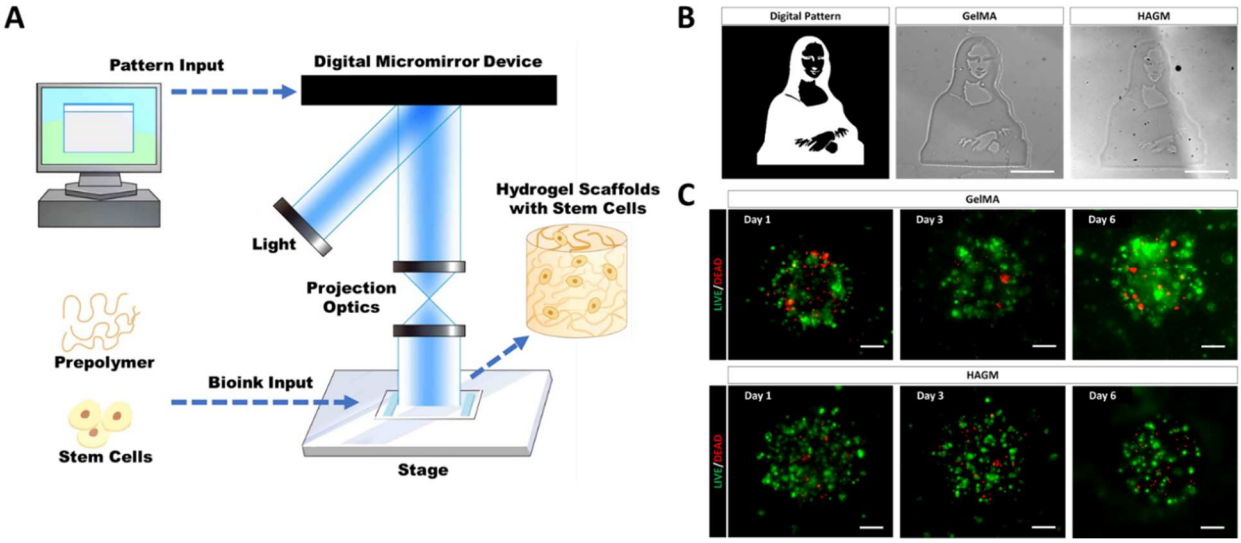

Figure 2.1. Bioprinting of GelMA- or HAGM-based bioprinted scaffolds encapsulating primary rbLSCs. (A) Schematic of DLP-based 3D bioprinting workflow; (B) representative bright field images of bioprinted Mona Lisa with acellular GelMA or HAGM; (C) representative images of Live/DeadTM staining of rbLSCs encapsulated with GelMA- or HAGM-based bioprinted scaffolds at Day 1, Day 3 and Day 6 of culture (scale bars: 100 μm).

2.3 Results

2.3.1 3D bioprinted GelMA and HAGM hydrogel scaffolds supported the viability of encapsulated primary rbLSCs

Our customized DLP-based 3D bioprinting system can spatially manipulate light based on

user-defined input designs, allowing for precise photopolymerization-based patterning of cellularized hydrogel constructs containing different material compositions (Figure 2.1A) [18,19,24]. GelMA is a photocrosslinkable gelatin that has been extensively studied as bioink for 3D bioprinting of stem cells including conjunctival stem cells and mesenchymal stem cells [19,42]. HAGM as another photocrosslinkable bioink, was found to support the encapsulation of retinal progenitor cells and cancer stem cells [16,17]. Using DLP-based 3D bioprinting techniques, we were able to fabricate GelMA- or HAGM-based hydrogel scaffolds with a complex pattern and microscale resolution within a matter of seconds (Figure 2.1B). For the encapsulation of LSCs in 3D scaffolds, primary rbLSCs were isolated and expanded from fresh rabbit limbal tissues and characterized with immunofluorescence staining of various LSC markers (Supplementary Figure S2.1A). To test biocompatibility, we fabricated GelMA- or HAGM-based bioprinted scaffolds encapsulating primary rbLSCs. Long-term culture confirmed that both types of bioprinted scaffolds were able to support the viability of the encapsulated rbLSCs as shown by the Live/DeadTM staining (Figure 2.1C). We have also quantified the viability of the encapsulated rbLSC in both types of bioprinted scaffolds by flow cytometry with propidium iodide staining (Supplementary Figure S1B). Based on the results, the live cell ratios were 86.7±1.65% in GelMA scaffolds and 92.1±0.8 % in HAGM scaffolds after 7 days of culture. In brief, we were able to fabricate both GelMA- and HAGM-based scaffolds encapsulating viable primary rbLSCs using our DLP-based 3D bioprinting system.

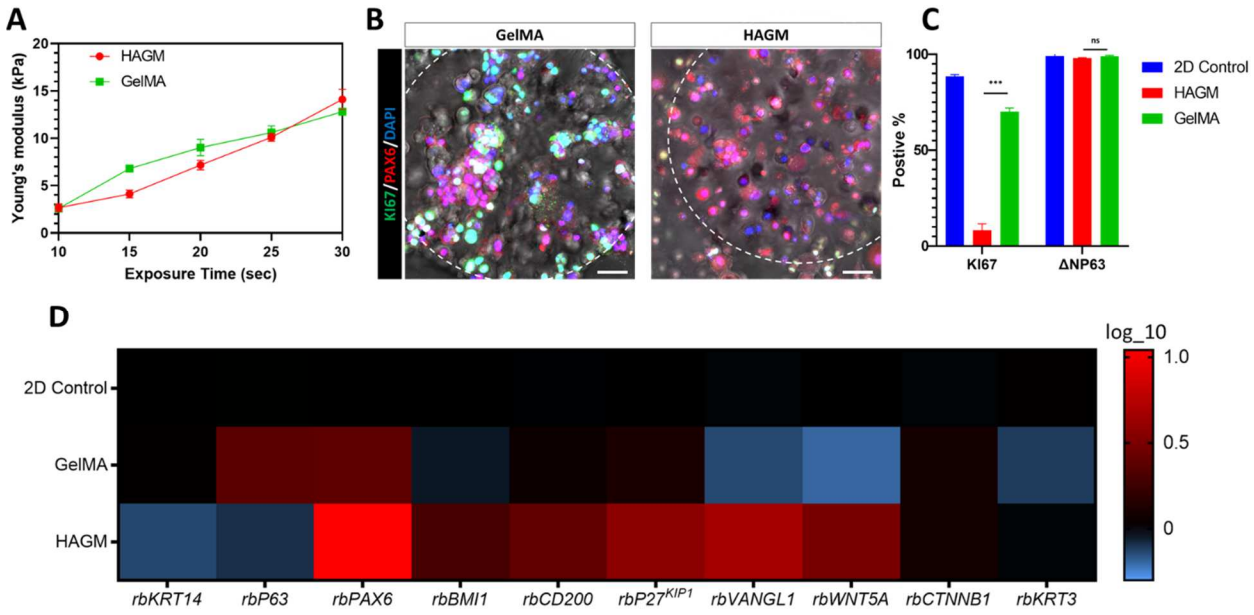

Figure 2.1. Encapsulated primary rbLSCs displayed different status in GelMA- or HAGM-based bioprinted scaffolds. (A) Linear plot of compressive modulus of the GelMA- or HAGM-based bioprinted scaffolds versus light exposure time (mean ± SD, n ≥ 3); (B) representative images of immunofluorescence staining of proliferation marker KI67 and LSC lineage marker PAX6 on rbLSCs encapsulated in GelMA- or HAGM-based bioprinted scaffolds after 2 days of culture (scale bars: 50 μm); (C) KI67-positive and ΔNP63-positve populations of the primary rbLSCs cultured in 2D and encapsulated in GelMA- or HAGM-based bioprinted scaffolds after 2 days of culture as determined by flow cytometry (mean ± SD, n = 3); (D) heatmap of real-time qPCR data showing relative mRNA expression of LSC markers (KRT14, P63, PAX6, BMI1), LSC quiescent markers (CD200, $P27^{KIP1}$), corneal epithelium differentiation marker (KRT3), canonical WNT signaling pathway marker (CTNNB1) and non-canonical WNT signaling pathway markers (WNT5A, VANGL1) on rbLSCs on 2D surface or encapsulated in GelMA- or HAGM-based bioprinted scaffolds after 2 days of culture.

2.3.2 Encapsulated primary rbLSCs displayed active status in GelMA-based bioprinted scaffolds while exhibiting quiescence in HAGM-based bioprinted scaffolds

While both GelMA- and HAGM-based bioprinted scaffolds maintained viable encapsulated primary rbLSCs, the cells displayed different behaviors depending on which scaffold they were cultured in. More cell aggregates or colonies were observed in GelMA-based bioprinted scaffolds, while rbLSCs encapsulated with HAGM-based scaffolds largely remained as single-

cells after 6 days of culture (Supplementary Figure S2.1C). These results suggest that the interaction between rbLSCs and surrounding ECM in the different bioprinted scaffolds influenced the stem cell status following the encapsulation. To further explore the effect of the scaffold matrix material on LSC-ECM interaction, we first needed to control the stiffness. Our DLP-based 3D bioprinting system enables us to control mechanical properties of the fabricated hydrogel scaffolds via spatiotemporal regulation of light exposure [23,24]. Mechanical testing of GelMA- and HAGM-based bioprinted scaffolds indicated positive linear correlation between Young's modulus and light exposure time in our printing system (Figure 2.2A, Supplementary Figure S2.1D). Based on the results, GelMA and HAGM scaffolds had a similar Young's modulus with light exposure time set to 25 seconds which was adopted as the primary bioprinting parameters for subsequent experiments.

To investigate the behavior of LSCs in the different scaffolds, we examined the expression of various LSC markers. Immunofluorescence staining showed the expression of PAX6, an ocular lineage marker, in both GelMA- and HAGM-encapsulated rbLSCs while the expression of proliferation marker, KI67, was present only in the GelMA-based scaffolds (Figure 2.2B). Consistently, flow cytometry identified significantly smaller percentage of KI67 positive rbLSCs encapsulated in HAGM-based bioprinted scaffolds compared to the population encapsulated in GelMA, while the positive ratio of stemness marker, ΔNP63, remained identical in both scaffolds (Figure 2.2C, Supplementary Figure S2.2A). The decreased KI67 positive population of rbLSCs encapsulated in HAGM-based bioprinted scaffolds can be reversed by releasing the cells from scaffolds (Supplementary Figure S2.2B). We have also performed transcriptional analysis with real-time qPCR to compare rbLSCs in 2D culture or encapsulation with GelMA- or HAGM-based bioprinted scaffolds (Figure 2.2D). We found up-regulated mRNA expression of PAX6 and BMI1

in the HAGM group compared to the 2D control, while P63 was up-regulated in the GelMA group. In addition, the expression of two previously reported LSC quiescence markers, CD200 and P27KIP1, were up-regulated in the HAGM group [43–45]. The expression of corneal epithelium differentiation marker, KRT3, was downregulated in the GelMA group and showed no significant change in the HAGM group in compare with the 2D control. Furthermore, mRNA expression of markers of non-canonical WNT pathway, VANGL1 and WNT5A, were up-regulated in the HAGM group but down-regulated in the GelMA group. Meanwhile, the expression of marker of canonical WNT pathway, CTNNB1, remained unchanged among the three groups. These results indicated the potential participation of non-canonical WNT pathway in the LSCs-ECM interactions [46–49].

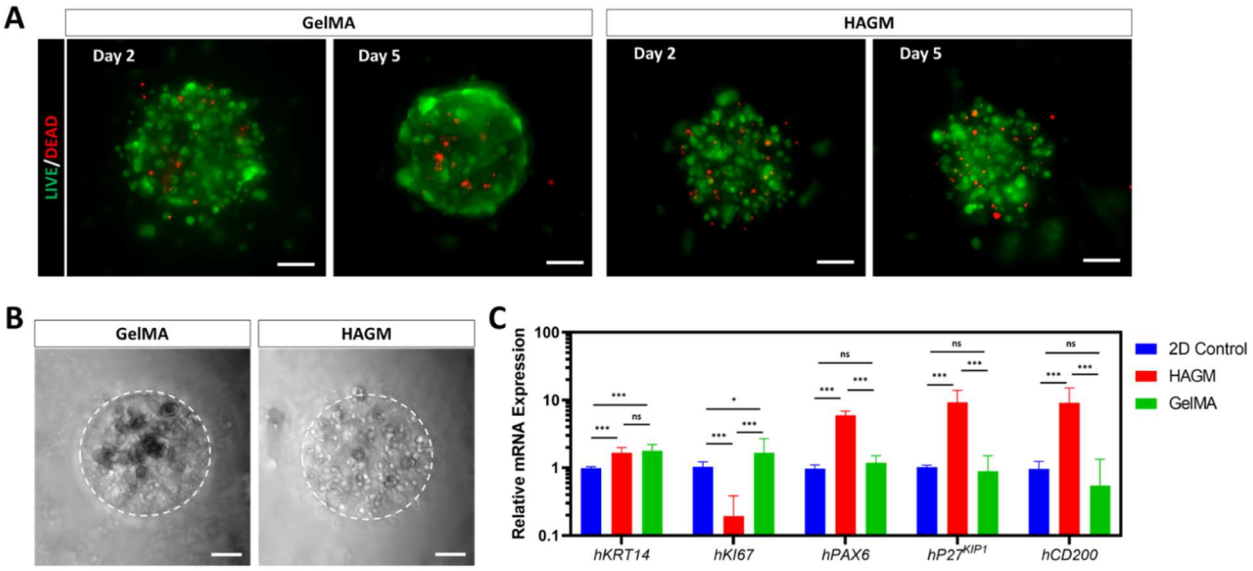

Figure 2.2. Encapsulated primary hLSCs remained viable and displayed different status in GelMA- or HAGM-based bioprinted scaffolds. (A) Representative images of Live/Dead™ staining of hLSCs encapsulated with GelMA- or HAGM-based bioprinted scaffolds at Day 2 and Day 5 of culture (scale bars: 100 μm); (B) representative bright field images of bioprinted scaffolds with GelMA/HAGM encapsulating primary hLSCs after 5 days of culture (scale bars: 100 μm); (C) real-time qPCR data showing relative mRNA expression of proliferation marker (KI67), LSC markers (KRT14, PAX6), LSC quiescent markers (CD200, $P27^{KIP1}$) of the primary hLSCs on 2D surface or encapsulated in GelMA- or HAGM-based bioprinted scaffolds after 2 days of culture (mean ± SD, n = 3).

2.3.3 Encapsulated primary hLSCs were viable but displayed different status in GelMA- or HAGM-based bioprinted scaffolds

Based on the ECM-dependent response of rbLSCs in the GelMA- or HAGM-based bioprinted scaffolds, we further explored the LSC-ECM interaction in human LSCs. Primary hLSCs were isolated and expanded from human corneoscleral rims of three different donors and subjected to 3D bioprinting with GelMA and HAGM. Similar to the rbLSCs, Live/DeadTM staining showed that most of the encapsulated hLSCs remained viable in both types of bioprinted scaffolds during culture (Figure 2.3A). Consistent with rbLSCs, aggregated colonies of hLSCs were largely found in the GelMA-based bioprinted scaffolds but rarely observed in the HAGM-based bioprinted scaffolds (Figure 2.3B). Real-time qPCR showed that the hLSCs encapsulated in HAGM-based bioprinted scaffolds had significantly higher expression of PAX6, CD200 and P27KIP1, while the expression of KI67 was significantly down-regulated compared to the 2D control and the GelMA group (Figure 2.3C). In addition, KRT14 expression was significantly up-regulated in both bioprinted groups comparing with the 2D control. These results reinforce the observation that LSCs respond differently (e.g., exhibiting active proliferation or quiescence) to the surrounding ECM composition, and appears to be consistent whether the LSCs are isolated from rabbits or humans, suggesting that this may be highly valuable for future clinical studies.

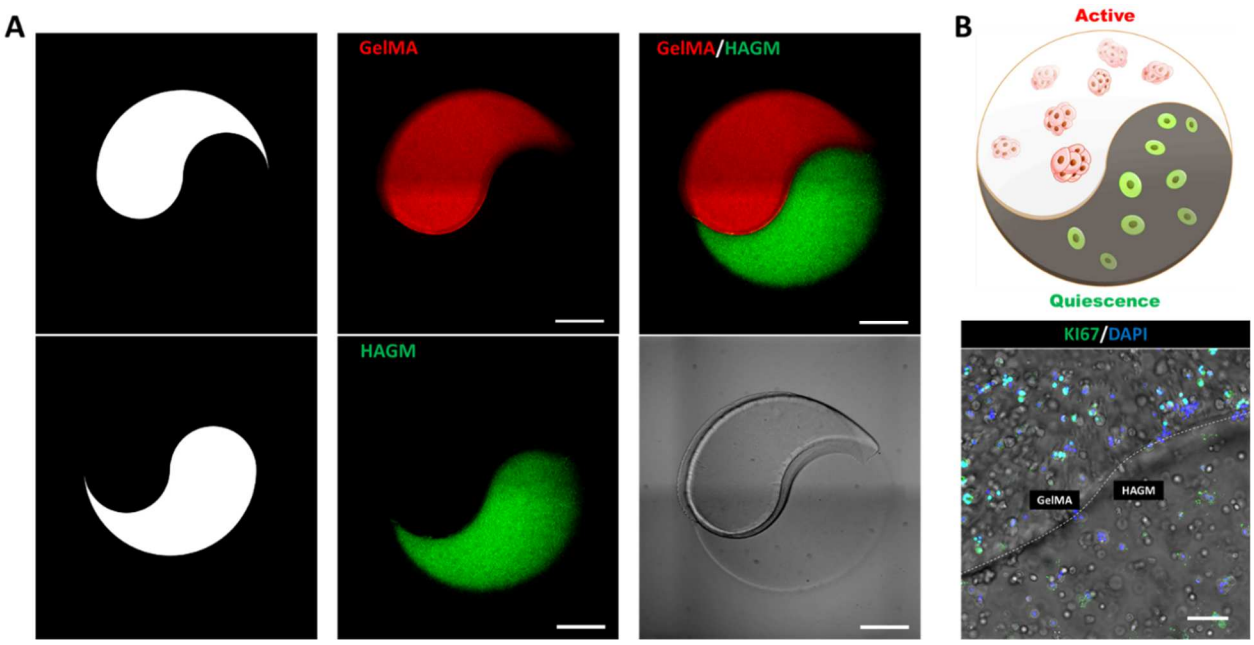

Figure 2.3. 3D bioprinting of a dual ECM 'Yin-Yang' model encapsulating rbLSCs. (A) Illustration of the design patterns and bright field images of the acellular dual ECM 'Yin-Yang' models encapsulating fluorescent microspheres (scale bars: 500 μm); (B) illustration and a representative image of immunofluorescence staining of KI67 on dual ECM 'Yin-Yang' models encapsulating primary rbLSCs after 2 days of culture (scale bars: 100 μm).

2.3.4 DLP-based 3D bioprinting of dual ECM 'Yin-Yang' LSC model

After ascertaining the ECM-dependent active/quiescent status of encapsulated LSCs in GelMA- and HAGM-based bioprinted scaffolds, we aimed to build a dual in vitro ECM model that could facilitate these differential statuses of cells within the same hydrogel, thus coming closer to recapitulating native LSC niches where cells in both activated/quiescent states coexist [3]. For this, we chose to utilize a 'Yin-Yang' pattern that allows for the placement of GelMA and HAGM distinctly separate yet spatially close regions. To demonstrate the feasibility of our design, we first printed the 'Yin-Yang' pattern in microscale with GelMA and HAGM mixed with fluorescence microspheres (Figure 2.4A). Fluorescent microscopic imaging showed the precise patterning of the acellular hydrogel materials matching our design specification. In follow-up prints, we replaced fluorescent microspheres with primary rbLSCs and verified the status of the encapsulated

rbLSCs in different parts of the dual ECM model (Figure 2.4B). Immunofluorescence staining showed the positive expression of KI67 in the GelMA-based region while few KI67 positive cells were found in the HAGM-based region (Figure 2.4B). Therefore, with our bioprinting system, we were able to fabricate the dual ECM 'Yin-Yang' model whose separate ECM-portions induced active/quiescent statuses for the LSC.

2.4 Discussion

With the recent technological advances in tissue engineering and regenerative medicine, stem cell therapies based on hydrogel scaffolds have become popular for the treatment of LSCD [12]. However, cost effective approaches for the high-throughput fabrication of hydrogel scaffolds encapsulating primary LSCs remains an active area of research. Furthermore, behavior that LSCs exhibit in response to different 3D matrices presents an attractive challenge in formulating scaffolds that can effectively recapitulate the native microenvironment of the LSC niche. Our study presents a novel engineering approach applying DLP-based 3D bioprinting for the fabrication of hydrogel scaffolds encapsulating both rabbit and human primary LSCs. We successfully printed GelMA- and HAGM-based microscale hydrogel scaffolds that maintained the viability of the encapsulated primary rbLSCs. The cells exhibited ECM-dependent phenotypes with an active status in GelMA- and quiescent status in HAGM-based scaffolds. We repeated the bioprinting experiments with hLSCs and confirmed the consistency of the ECM-dependent phenotype in primary human cells. Moreover, we applied DLP-based 3D bioprinting to build a dual ECM 'Yin-Yang' model encapsulating LSCs in active/quiescent status.

Tissue regeneration using endogenous stem cell is a promising solution for many medical conditions [2,28,50,51]. As the essential endogenous epithelial stem cell contributing to corneal

regeneration, LSCs have been explored in various approaches in combination with hydrogel scaffolds for corneal epithelium reconstruction [52,53]. DLP-based 3D bioprinting has been instrumental in tissue engineering as it facilitated the fabrication of high-throughput hydrogel scaffolds encapsulating various types of stem cells [18]. We used DLP-based 3D bioprinting to produce GelMA- or HAGM-based hydrogel scaffolds encapsulating of primary rbLSCs and hLSCs. DLP-based 3D bioprinting maintained the viability and stemness of the encapsulated LSCs in both materials. With flexible and precise control over morphological structures, the microscale hydrogel scaffolds encapsulating LSCs can be optimized by our bioprinting system to serve various therapeutic purposes including minimally invasive injectable stem cell transplantation [54]. Furthermore, the translucent nature of the GelMA and HAGM scaffolds not only enabled facile monitoring of cell morphology and behaviors, but also makes ideal candidates for corneal tissue-on-a-chip in vitro disease modeling.

The ECM-dependent regulation and reprogramming of epithelial stem cell fate have been indicated as prevalent mechanisms in different tissues including epidermis, lung, intestine, colon and cornea [30,55–58]. By controlling the matrix stiffness with our bioprinting system, we were able to compare the influence of ECM component on the encapsulated LSCs. As a result, we found that primary rbLSCs and hLSCs actively proliferated and formed aggregated colonies in the GelMA-based scaffolds while showed inhibited proliferation and aggregation in the HAGM-based scaffolds. Further analysis showed the active/quiescent status of encapsulated LSCs by comparing proliferation and stemness markers. The quiescence of LSCs in HAGM-based scaffolds can potentially be mediated by the HA-specific cell adhesion excluding integrins [59–61]. We also found the HAGM-encapsulated rbLSCs presented proliferative status after being released from scaffolds and cultured for a week, indicating that the HAGM-encapsulated rbLSCs were reversibly

quiescent [62]. Non-canonical WNT signaling pathways (planar cell polarity) have been reported to modify the activation/quiescence in multiple endogenous stem cells [48,49,63]. Notably, we found upregulated mRNA expression of markers related to non-canonical WNT signaling pathways in primary LSCs encapsulated in HAGM-based scaffolds, which is consistent with the previously reported ECM-response of primary LSCs cultured on engineered HA scaffolds [39,64]. As a proof-of-concept, we further combined these findings with multi-material bioprinting to fabricate a dual ECM 'Yin-Yang' model simultaneously encapsulating primary LSCs in active/quiescent status. The dual ECM model can be an attractive platform for drug screening since it reproduced stem cell quiescence that was correlated to drug-resistance and recapitulated the stem cells in heterogeneous status that could react to drugs differently [65–67].

2.5 Conclusions

We applied DLP-based 3D bioprinting to fabricate engineered microscale hydrogel scaffolds based on GelMA and HAGM. These scaffolds supported not only the viability of encapsulated primary rbLSCs and hLSCs, but also exhibited differential regulation. LSCs were found to display an ECM-dependent active/quiescent status as they actively proliferated in the GelMA-based scaffolds and took on quiescent characteristics in the HAGM-based scaffolds. A bioprinted dual-ECM 'Yin-Yang' model encapsulating both active and quiescent LSCs were fabricated based on these findings. Together, these results illustrated an innovative engineering approach for disease modeling, drug screening and the development of an LSC-based regenerative therapy for the treatment of LSCD and related ocular diseases. Future studies exploring other types of biomaterials or integrating different cell types would be valuable to investigate.

Acknowledgements

Chapter 2, in full, is a reprint of the unpublished manuscript in review, “3D Bioprinting of Dual ECM Scaffolds Encapsulating Limbal Stem/Progenitor Cells in Active and Quiescent Statuses”, Z. Zhong, A. Balayan, J. Tian, Y. Xiang, H. H. Hwang, X. Wu, X. Deng, J. Schimelman, Y. Sun, S. You, M. Tang, E. Yao, X. Shi, N. F. Steinmetz, S. X. Deng, S.C. Chen. *Biofabrication*, 2021. The dissertation author was the primary investigator and author of this paper. This work was supported in part by grants from the NIH to S.C. (R21EY031122, R01EB02185) and S.D. (R01EY021797), National Science Foundation (NSF) to S.C. (1937653), and California Institute for Regenerative Medicine to S.D. (CLIN1-08686 and CLIN2-11650).

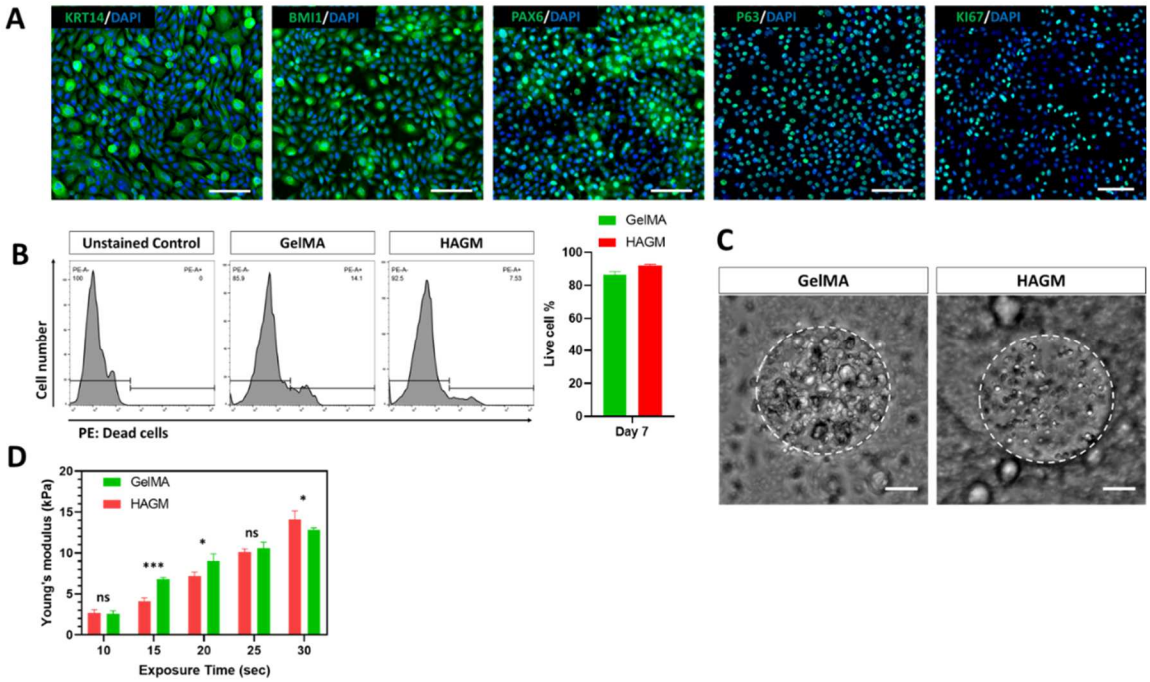

Supplementary Figure S2.1. LSC Characterization. (A) Immunofluorescence staining of LSC lineage markers (BMI1 and PAX6) stemness markers (KRT14, ΔNP63), and proliferation marker (KI67) on primary rbLSCs expanded in 2D condition (scale bars: 100 μm); (B) representative gating and statics of the flow cytometry analysis with propidium iodide staining on the different groups of primary rbLSCs after 7 days of culture. The PE positive cell populations represent the dead cells (mean ± SD, n ≥ 3); (C) representative bright field images of bioprinted microscale cylinders with GelMA/HAGM encapsulating primary rbLSCs after 6 days of culture (scale bars: 100 μm); (D) column plot of compressive modulus of the GelMA- or HAGM-based bioprinted scaffolds versus light exposure time (mean ± SD, n ≥ 3).

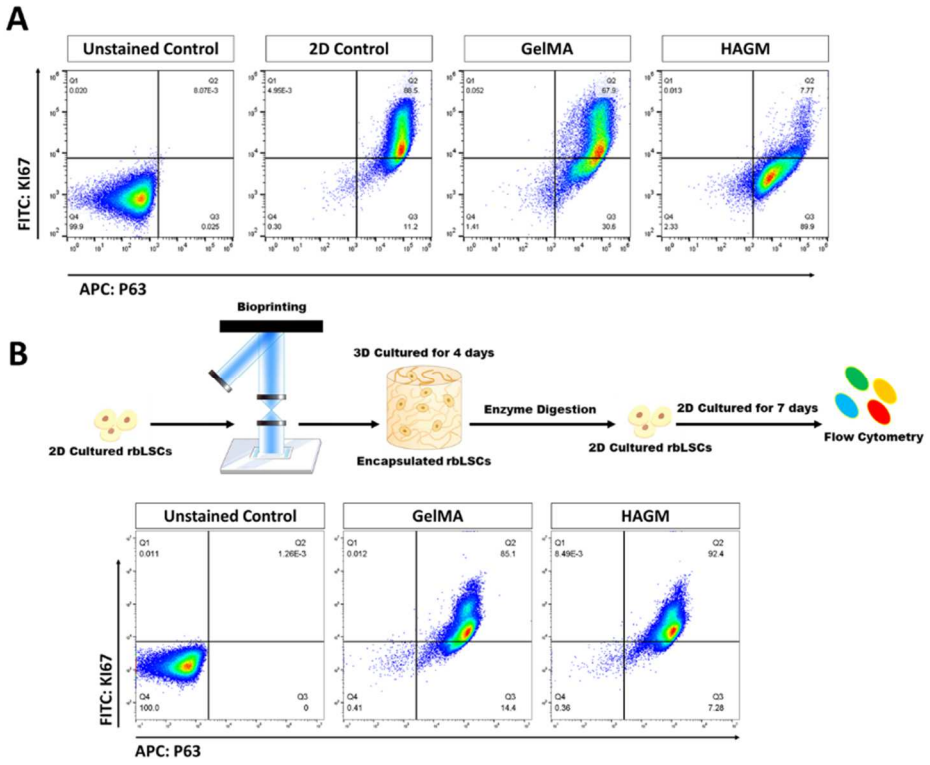

Supplementary Figure S2.2. Flow cytometry of LSCs. (A) The representative gating on the different groups of primary rbLSCs after flow cytometry analysis of KI67 and ΔNP63 positive cell populations; (B) the schematic showing the ECM-dependent phenotype reversal test and the representative flow cytometry gating on the different groups of primary rbLSCs released from GelMA- or HAGM-based scaffolds.

Supplementary Table 2.1. Antibody List

Antibody	Catalog	Vendor	Dilution	Application
Anti-mouse IgG (H+L), F(ab')2 Fragment (Alexa Fluor® 488 Conjugate) #4408	4408S	Cell Signaling Technologies	1:500	IF staining; Flow cytometry
Anti-rabbit IgG (H+L), F(ab')2 Fragment (Alexa Fluor® 555 Conjugate) #4413	4413S	Cell Signaling Technologies	1:500	IF staining
Anti-rat IgG (H+L), (Alexa Fluor® 647 Conjugate) #4418	4418S	Cell Signaling Technologies	1:500	IF staining; Flow cytometry
Keratin 14 Polyclonal Antibody, Purified	905301	BioLegend	1:100	IF staining
Purified anti-Pax-6 Antibody	901301	BioLegend	1:200	IF staining
Purified anti-p63 (ΔN) Antibody	699501	BioLegend	1:250	IF staining; Flow cytometry
Purified Mouse Anti-Ki-67	550609	BD Pharmagin	1:100	IF staining; Flow cytometry
Anti-Bmi1 antibody	ab85688	Abcam	1:500	IF staining
DAPI (4',6-Diamidino-2-Phenylindole, Dihydrochloride)	D1306	ThermoFisher Scientific	1:500	IF staining

Supplementary Table 2.2. Primers for Real Time qPCR

Rabbit Gene		5' → 3'
rbCTNNB1	Forward	CGGAGCCTGCCATCTGTGCT
	Reverse	GATGGCGGGTGCAGGAGCTT
rbWNT5A	Forward	CGCGCGCATCCTCATGAACC
	Reverse	CGGCCGCGCTGTCGTATTTC
rbBMI1	Forward	ACGATGCCCAGCAGCAATGA
	Reverse	TGCTGGGCTGTTGGCCTTGT
rbCD200	Forward	ATGGAGAGGCTGGTGTTCGG
	Reverse	CACCACCACCCCATGGTTCT
rbP27^{KIP1}	Forward	CCTGCCACAGACGATTCTTCC
	Reverse	GTTCGGGGAACCGTCGGAAC
rbVANGL1	Forward	ACGGCCATCACAGGCACCTC
	Reverse	AGGCGATGGGCGTGAGGAAC
rbPAX6	Forward	GTATTCTTGCTTCAGGTAGAT
	Reverse	GAGGCTCAAATGCGACTTCAGCT
rbKRT14	Forward	CCCAGTTCTCCTCGGGCTCT
	Reverse	GTGGGAGGACACCACCTTGC
rbP63	Forward	GAACGGCTCCTCGTCCACCA
	Reverse	GACGGCGAGAGGGCATCGAA
rbGADPH	Forward	TGGTGAAGGTCGGAGTGAAC
	Reverse	ATGTAGTGGAGGTCAATGAATGG
rbKRT3	Forward	CGGAGCTGTCCCAGATGCAG
	Reverse	CACCTCGGCGATGATGCTGT

Human Gene		5' → 3'
hKI67	Forward	CTTTGGGTGCGACTTGACG
	Reverse	GTCGACCCCGCTCCTTTT
hP27^{KIP1}	Forward	GACCTGCAACCGACGATTC
	Reverse	GTCCATTCCATGAAGTCAGCG
hPAX6	Forward	GTATTCTTGCTTCAGGTAGAT
	Reverse	GAGGCTCAAATGCGACTTCAGCT
hKRT14	Forward	GACCATTGAGGACCTGAGGA
	Reverse	ATTGATGTCGGCTTCCACAC
hCD200	Forward	ATGGAGAGGCTGACTCTGACCA
	Reverse	GGGCATTTTGCAGAGAGCATT
hGADPH	Forward	CGACCACTTTGTCAAGCTCA
	Reverse	AGGGGTCTACATGGCAACTG

Reference

[1] D. Dhouailly, D.J. Pearton, F. Michon, The vertebrate corneal epithelium: From early specification to constant renewal, Dev. Dyn. 243 (2014) 1226–1241. https://doi.org/10.1002/dvdy.24179.

[2] H. Ouyang, Y. Xue, Y. Lin, X. Zhang, L. Xi, S. Patel, H. Cai, J. Luo, M. Zhang, M. Zhang, Y. Yang, G. Li, H. Li, W. Jiang, E. Yeh, J. Lin, M. Pei, J. Zhu, G. Cao, L. Zhang, B. Yu, S. Chen, X.D. Fu, Y. Liu, K. Zhang, WNT7A and PAX6 define corneal epithelium homeostasis and pathogenesis, Nature. 511 (2014) 358–361. https://doi.org/10.1038/nature13465.

[3] M.A. Dziasko, J.T. Daniels, Anatomical Features and Cell-Cell Interactions in the Human Limbal Epithelial Stem Cell Niche, Ocul. Surf. 14 (2016) 322–330. https://doi.org/10.1016/j.jtos.2016.04.002.

[4] R.R.A. Bourne, S.R. Flaxman, T. Braithwaite, M. V. Cicinelli, A. Das, J.B. Jonas, J. Keeffe, J. Kempen, J. Leasher, H. Limburg, K. Naidoo, K. Pesudovs, S. Resnikoff, A. Silvester, G.A. Stevens, N. Tahhan, T. Wong, H.R. Taylor, P. Ackland, A. Arditi, Y. Barkana, B. Bozkurt, R. Wormald, A. Bron, D. Budenz, F. Cai, R. Casson, U. Chakravarthy, N. Congdon, T. Peto, J. Choi, R. Dana, M. Palaiou, R. Dandona, L. Dandona, T. Shen, I. Dekaris, M. Del Monte, J. Deva, L. Dreer, M. Frazier, L. Ellwein, J. Hejtmancik, K. Frick, D. Friedman, J. Javitt, B.

Munoz, H. Quigley, P. Ramulu, A. Robin, J. Tielsch, S. West, J. Furtado, H. Gao, G. Gazzard, R. George, S. Gichuhi, V. Gonzalez, B. Hammond, M.E. Hartnett, M. He, F. Hirai, J. Huang, A. Ingram, C. Joslin, R. Khanna, D. Stambolian, M. Khairallah, J. Kim, G. Lambrou, V.C. Lansingh, P. Lanzetta, J. Lim, K. Mansouri, A. Mathew, A. Morse, D. Musch, V. Nangia, M. Battaglia, F. Yaacov, M. Raju, L. Rossetti, J. Saaddine, M. Sandar, J. Serle, R. Shetty, P. Sieving, J.C. Silva, R.S. Sitorus, J. Tejedor, M. Tsilimbaris, J. van Meurs, R. Varma, G. Virgili, J. Volmink, Y. Xing, N.L. Wang, P. Wiedemann, Y. Zheng, Magnitude, temporal trends, and projections of the global prevalence of blindness and distance and near vision impairment: a systematic review and meta-analysis, Lancet Glob. Heal. (2017). https://doi.org/10.1016/S2214-109X(17)30293-0.

[5] S.X. Deng, V. Borderie, C.C. Chan, R. Dana, F.C. Figueiredo, J.A.P. Gomes, G. Pellegrini, S. Shimmura, F.E. Kruse, Global consensus on definition, classification, diagnosis, and staging of limbal stem cell deficiency, Cornea. 38 (2019) 364–375. https://doi.org/10.1097/ICO.0000000000001820.

[6] Q. Le, J. Xu, S.X. Deng, The diagnosis of limbal stem cell deficiency, Ocul. Surf. 16 (2018) 58–69. https://doi.org/10.1016/j.jtos.2017.11.002.

[7] D. Meller, R.T.F. Pires, R.J.S. Mack, F. Figueiredo, A. Heiligenhaus, W.C. Park, P. Prabhasawat, T. John, S.D. McLeod, K.P. Steuhl, S.C.G. Tseng, Amniotic membrane transplantation for acute chemical or thermal burns, Ophthalmology. (2000). https://doi.org/10.1016/S0161-6420(00)00024-5.

[8] A. Hopkinson, R.S. McIntosh, P.J. Tighe, D.K. James, H.S. Dua, Amniotic membrane for ocular surface reconstruction: Donor variations and the effect of handling on TGF-β content, Investig. Ophthalmol. Vis. Sci. 47 (2006) 4316–4322. https://doi.org/10.1167/iovs.05-1415.

[9] T.Ž. Ramuta, M. Starčič Erjavec, M.E. Kreft, Amniotic Membrane Preparation Crucially Affects Its Broad-Spectrum Activity Against Uropathogenic Bacteria, Front. Microbiol. 11 (2020) 469. https://doi.org/10.3389/fmicb.2020.00469.

[10] S.X. Deng, F. Kruse, J.A.P. Gomes, C.C. Chan, S. Daya, R. Dana, F.C. Figueiredo, S. Kinoshita, P. Rama, V. Sangwan, A.R. Slomovic, D. Tan, Global Consensus on the Management of Limbal Stem Cell Deficiency, Cornea. 39 (2020) 1291–1302. https://doi.org/10.1097/ICO.0000000000002358.

[11] S.S. Mahdavi, M.J. Abdekhodaie, S. Mashayekhan, A. Baradaran-Rafii, A.R. Djalilian, Bioengineering Approaches for Corneal Regenerative Medicine, Tissue Eng. Regen. Med. 17 (2020) 567–593. https://doi.org/10.1007/s13770-020-00262-8.

[12] K.N. Nguyen, S. Bobba, A. Richardson, M. Park, S.L. Watson, D. Wakefield, N. Di Girolamo, Native and synthetic scaffolds for limbal epithelial stem cell transplantation, Acta Biomater. 65 (2018) 21–35. https://doi.org/10.1016/j.actbio.2017.10.037.

[13] D. Chen, Y. Qu, X. Hua, L. Zhang, Z. Liu, S.C. Pflugfelder, D.Q. Li, A hyaluronan hydrogel

scaffold-based xeno-free culture system for ex vivo expansion of human corneal epithelial stem cells, Eye. 31 (2017) 962–971. https://doi.org/10.1038/eye.2017.8.

[14] F. Sanie-Jahromi, M. Eghtedari, E. Mirzaei, M.H. Jalalpour, Z. Asvar, M. Nejabat, F. Javidi-Azad, Propagation of limbal stem cells on polycaprolactone and polycaprolactone/gelatin fibrous scaffolds and transplantation in animal model, BioImpacts. 10 (2020) 44–54. https://doi.org/10.15171/bi.2020.06.

[15] P. Soman, J.W. Lee, A. Phadke, S. Varghese, S. Chen, Spatial tuning of negative and positive Poisson's ratio in a multi-layer scaffold, Acta Biomater. (2012). https://doi.org/10.1016/j.actbio.2012.03.035.

[16] P. Wang, X. Li, W. Zhu, Z. Zhong, A. Moran, W. Wang, K. Zhang, S. Chen, 3D bioprinting of hydrogels for retina cell culturing, Bioprinting. (2018). https://doi.org/10.1016/j.bprint.2018.e00029.

[17] M. Tang, Q. Xie, R.C. Gimple, Z. Zhong, T. Tam, J. Tian, R.L. Kidwell, Q. Wu, B.C. Prager, Z. Qiu, A. Yu, Z. Zhu, P. Mesci, H. Jing, J. Schimelman, P. Wang, D. Lee, M.H. Lorenzini, D. Dixit, L. Zhao, S. Bhargava, T.E. Miller, X. Wan, J. Tang, B. Sun, B.F. Cravatt, A.R. Muotri, S. Chen, J.N. Rich, Three-dimensional bioprinted glioblastoma microenvironments model cellular dependencies and immune interactions, Cell Res. (2020). https://doi.org/10.1038/s41422-020-0338-1.

[18] C. Yu, J. Schimelman, P. Wang, K.L. Miller, X. Ma, S. You, J. Guan, B. Sun, W. Zhu, S. Chen, Photopolymerizable Biomaterials and Light-Based 3D Printing Strategies for Biomedical Applications, Chem. Rev. 120 (2020) 10695–10743. https://doi.org/10.1021/acs.chemrev.9b00810.

[19] Z. Zhong, X. Deng, P. Wang, C. Yu, W. Kiratitanaporn, X. Wu, J. Schimelman, M. Tang, A. Balayan, E. Yao, J. Tian, L. Chen, K. Zhang, S. Chen, Rapid bioprinting of conjunctival stem cell micro-constructs for subconjunctival ocular injection, Biomaterials. (2021). https://doi.org/10.1016/j.biomaterials.2020.120462.

[20] X. Qu, W. Zhu, S. Huang, Y.S. Li, S. Chien, K. Zhang, S. Chen, Relative impact of uniaxial alignment vs. form-induced stress on differentiation of human adipose derived stem cells, Biomaterials. (2013). https://doi.org/10.1016/j.biomaterials.2013.09.009.

[21] P. Soman, B.T.D. Tobe, J.W. Lee, A.M. Winquist, I. Singec, K.S. Vecchio, E.Y. Snyder, S. Chen, Three-dimensional scaffolding to investigate neuronal derivatives of human embryonic stem cells, Biomed. Microdevices. (2012). https://doi.org/10.1007/s10544-012-9662-7.

[22] J.H. Wen, L.G. Vincent, A. Fuhrmann, Y.S. Choi, K.C. Hribar, H. Taylor-Weiner, S. Chen, A.J. Engler, Interplay of matrix stiffness and protein tethering in stem cell differentiation, Nat. Mater. (2014). https://doi.org/10.1038/nmat4051.

[23] C. Yu, X. Ma, W. Zhu, P. Wang, K.L. Miller, J. Stupin, A. Koroleva-Maharajh, A. Hairabedian, S. Chen, Scanningless and continuous 3D bioprinting of human tissues with decellularized extracellular matrix, Biomaterials. 194 (2019) 1–13. https://doi.org/10.1016/j.biomaterials.2018.12.009.

[24] X. Ma, C. Yu, P. Wang, W. Xu, X. Wan, C.S.E. Lai, J. Liu, A. Koroleva-Maharajh, S. Chen, Rapid 3D bioprinting of decellularized extracellular matrix with regionally varied mechanical properties and biomimetic microarchitecture, Biomaterials. (2018). https://doi.org/10.1016/j.biomaterials.2018.09.026.

[25] K.C. Hribar, Y.S. Choi, M. Ondeck, A.J. Engler, S. Chen, Digital plasmonic patterning for localized tuning of hydrogel stiffness, Adv. Funct. Mater. (2014). https://doi.org/10.1002/adfm.201400274.

[26] X. Ma, X. Qu, W. Zhu, Y.S. Li, S. Yuan, H. Zhang, J. Liu, P. Wang, C.S.E. Lai, F. Zanella, G.S. Feng, F. Sheikh, S. Chien, S. Chen, Deterministically patterned biomimetic human iPSC-derived hepatic model via rapid 3D bioprinting, Proc. Natl. Acad. Sci. U. S. A. (2016). https://doi.org/10.1073/pnas.1524510113.

[27] R.M. Gouveia, C.J. Connon, Biomechanical modulation therapy—a stem cell therapy without stem cells for the treatment of severe ocular burns, Transl. Vis. Sci. Technol. 9 (2020) 1–11. https://doi.org/10.1167/tvst.9.12.5.

[28] H. Xia, X. Li, W. Gao, X. Fu, R.H. Fang, L. Zhang, K. Zhang, Tissue repair and regeneration with endogenous stem cells, Nat. Rev. Mater. 3 (2018) 174–193. https://doi.org/10.1038/s41578-018-0027-6.

[29] T. Ramos, D. Scott, S. Ahmad, An Update on Ocular Surface Epithelial Stem Cells: Cornea and Conjunctiva, Stem Cells Int. (2015). https://doi.org/10.1155/2015/601731.

[30] R.M. Gouveia, G. Lepert, S. Gupta, R.R. Mohan, C. Paterson, C.J. Connon, Assessment of corneal substrate biomechanics and its effect on epithelial stem cell maintenance and differentiation, Nat. Commun. (2019). https://doi.org/10.1038/s41467-019-09331-6.

[31] A. Chakraborty, J. Dutta, S. Das, H. Datta, Comparison of ex vivo cultivated human limbal epithelial stem cell viability and proliferation on different substrates, Int. Ophthalmol. 33 (2013) 665–670. https://doi.org/10.1007/s10792-013-9765-z.

[32] C. Bonnans, J. Chou, Z. Werb, Remodelling the extracellular matrix in development and disease, Nat. Rev. Mol. Cell Biol. 15 (2014) 786–801. https://doi.org/10.1038/nrm3904.

[33] T.F. Gesteira, M. Sun, Y.M. Coulson-Thomas, Y. Yamaguchi, L.K. Yeh, V. Hascall, V.J. Coulson-Thomas, Hyaluronan rich microenvironment in the limbal stem cell niche regulates limbal stem cell differentiation, Investig. Ophthalmol. Vis. Sci. 58 (2017) 4407–4421. https://doi.org/10.1167/iovs.17-22326.

[34] I.J. Cho, P.P.W. Lui, J. Obajdin, F. Riccio, W. Stroukov, T.L. Willis, F. Spagnoli, F.M. Watt, Mechanisms, Hallmarks, and Implications of Stem Cell Quiescence, Stem Cell Reports. 12 (2019) 1190–1200. https://doi.org/10.1016/j.stemcr.2019.05.012.

[35] J. Cooper, F.G. Giancotti, Integrin Signaling in Cancer: Mechanotransduction, Stemness, Epithelial Plasticity, and Therapeutic Resistance, Cancer Cell. 35 (2019) 347–367. https://doi.org/10.1016/j.ccell.2019.01.007.

[36] I.J. Cho, P.P.W. Lui, J. Obajdin, F. Riccio, W. Stroukov, T.L. Willis, F. Spagnoli, F.M. Watt, Mechanisms, Hallmarks, and Implications of Stem Cell Quiescence, Stem Cell Reports. 12 (2019) 1190–1200. https://doi.org/10.1016/j.stemcr.2019.05.012.

[37] Y.A.Z. Wang, J.M. Plane, P. Jiang, C.J. Zhou, W. Deng, Concise review: Quiescent and active states of endogenous adult neural stem cells: Identification and characterization, Stem Cells. 29 (2011) 907–912. https://doi.org/10.1002/stem.644.

[38] N. Sagga, L. Kuffová, N. Vargesson, L. Erskine, J.M. Collinson, Limbal epithelial stem cell activity and corneal epithelial cell cycle parameters in adult and aging mice, Stem Cell Res. 33 (2018) 185–198. https://doi.org/10.1016/j.scr.2018.11.001.

[39] S.-Y. Chen, B. Han, Y.-T. Zhu, M. Mahabole, J. Huang, D.C. Beebe, S.C.G. Tseng, HC-HA/PTX3 Purified From Amniotic Membrane Promotes BMP Signaling in Limbal Niche Cells to Maintain Quiescence of Limbal Epithelial Progenitor/Stem Cells, Stem Cells. 33 (2015) 3341–3355. https://doi.org/10.1002/stem.2091.

[40] H. Ouyang, Y. Xue, Y. Lin, X. Zhang, L. Xi, S. Patel, H. Cai, J. Luo, M. Zhang, M. Zhang, Y. Yang, G. Li, H. Li, W. Jiang, E. Yeh, J. Lin, M. Pei, J. Zhu, G. Cao, L. Zhang, B. Yu, S. Chen, X.D. Fu, Y. Liu, K. Zhang, WNT7A and PAX6 define corneal epithelium homeostasis and pathogenesis, Nature. (2014). https://doi.org/10.1038/nature13465.

[41] H. Shirahama, B.H. Lee, L.P. Tan, N.J. Cho, Precise tuning of facile one-pot gelatin methacryloyl (GelMA) synthesis, Sci. Rep. (2016). https://doi.org/10.1038/srep31036.

[42] W. Zhu, H. Cui, B. Boualam, F. Masood, E. Flynn, R.D. Rao, Z.Y. Zhang, L.G. Zhang, 3D bioprinting mesenchymal stem cell-laden construct with core-shell nanospheres for cartilage tissue engineering, Nanotechnology. 29 (2018). https://doi.org/10.1088/1361-6528/aaafa1.

[43] M. Vattulainen, T. Ilmarinen, L. Koivusalo, K. Viiri, H. Hongisto, H. Skottman, Modulation of Wnt/BMP pathways during corneal differentiation of hPSC maintains ABCG2-positive LSC population that demonstrates increased regenerative potential, Stem Cell Res. Ther. 10 (2019) 236. https://doi.org/10.1186/s13287-019-1354-2.

[44] S. Bojic, D. Hallam, N. Alcada, A. Ghareeb, R. Queen, S. Pervinder, H. Buck, A. Amitai Lange, G. Figueiredo, P. Rooney, M. Stojkovic, A. Shortt, F.C. Figueiredo, M. Lako, CD200 Expression Marks a Population of Quiescent Limbal Epithelial Stem Cells with Holoclone

Forming Ability, Stem Cells. 36 (2018) 1723–1735. https://doi.org/10.1002/stem.2903.

[45] V. Barbaro, A. Testa, E. Di Iorio, F. Mavilio, G. Pellegrini, M. De Luca, C/EBPδ regulates cell cycle and self-renewal of human limbal stem cells, J. Cell Biol. (2007). https://doi.org/10.1083/jcb.200703003.

[46] R.A. Mentink, L. Rella, T.W. Radaszkiewicz, T. Gybel, M.C. Betist, V. Bryja, H.C. Korswagen, The planar cell polarity protein VANG-1/Vangl negatively regulates Wnt/β-catenin signaling through a Dvl dependent mechanism, PLoS Genet. 14 (2018). https://doi.org/10.1371/journal.pgen.1007840.

[47] M. Katoh, Canonical and non-canonical WNT signaling in cancer stem cells and their niches: Cellular heterogeneity, omics reprogramming, targeted therapy and tumor plasticity (Review), Int. J. Oncol. 51 (2017) 1357–1369. https://doi.org/10.3892/ijo.2017.4129.

[48] M. Chavali, M. Klingener, A.G. Kokkosis, Y. Garkun, S. Felong, A. Maffei, A. Aguirre, Non-canonical Wnt signaling regulates neural stem cell quiescence during homeostasis and after demyelination, Nat. Commun. 9 (2018) 1–17. https://doi.org/10.1038/s41467-017-02440-0.

[49] R. Sugimura, X.C. He, A. Venkatraman, F. Arai, A. Box, C. Semerad, J.S. Haug, L. Peng, X.B. Zhong, T. Suda, L. Li, Noncanonical Wnt signaling maintains hematopoietic stem cells in the niche, Cell. 150 (2012) 351–365. https://doi.org/10.1016/j.cell.2012.05.041.

[50] L. He, N.B. Nguyen, R. Ardehali, B. Zhou, Heart regeneration by endogenous stem cells and cardiomyocyte proliferation: Controversy, fallacy, and progress, Circulation. 142 (2020) 275–291. https://doi.org/10.1161/CIRCULATIONAHA.119.045566.

[51] H. Lin, H. Ouyang, J. Zhu, S. Huang, Z. Liu, S. Chen, G. Cao, G. Li, R.A.J. Signer, Y. Xu, C. Chung, Y. Zhang, D. Lin, S. Patel, F. Wu, H. Cai, J. Hou, C. Wen, M. Jafari, X. Liu, L. Luo, J. Zhu, A. Qiu, R. Hou, B. Chen, J. Chen, D. Granet, C. Heichel, F. Shang, X. Li, M. Krawczyk, D. Skowronska-Krawczyk, Y. Wang, W. Shi, D. Chen, Z. Zhong, S. Zhong, L. Zhang, S. Chen, S.J. Morrison, R.L. Maas, K. Zhang, Y. Liu, Lens regeneration using endogenous stem cells with gain of visual function, Nature. (2016). https://doi.org/10.1038/nature17181.

[52] M. Mobaraki, R. Abbasi, S.O. Vandchali, M. Ghaffari, F. Moztarzadeh, M. Mozafari, Corneal repair and regeneration: Current concepts and future directions, Front. Bioeng. Biotechnol. 7 (2019) 135. https://doi.org/10.3389/fbioe.2019.00135.

[53] B. Wright, S. Mi, C.J. Connon, Towards the use of hydrogels in the treatment of limbal stem cell deficiency, Drug Discov. Today. 18 (2013) 79–86. https://doi.org/10.1016/j.drudis.2012.07.012.

[54] Ö.B. Selver, A. Yağcı, S. Eğrilmez, M. Gürdal, M. Palamar, T. Çavuşoğlu, U. Ateş, A. Veral, Ç. Güven, J.M. Wolosin, Limbal stem cell deficiency and treatment with stem cell

transplantation, Turkish J. Ophthalmol. (2017). https://doi.org/10.4274/tjo.72593.

[55] W.P. Daley, S.B. Peters, M. Larsen, Extracellular matrix dynamics in development and regenerative medicine, J. Cell Sci. 121 (2008) 255–264. https://doi.org/10.1242/jcs.006064.

[56] S. Yui, L. Azzolin, M. Maimets, M.T. Pedersen, R.P. Fordham, S.L. Hansen, H.L. Larsen, J. Guiu, M.R.P. Alves, C.F. Rundsten, J. V. Johansen, Y. Li, C.D. Madsen, T. Nakamura, M. Watanabe, O.H. Nielsen, P.J. Schweiger, S. Piccolo, K.B. Jensen, YAP/TAZ-Dependent Reprogramming of Colonic Epithelium Links ECM Remodeling to Tissue Regeneration, Cell Stem Cell. 22 (2018) 35-49.e7. https://doi.org/10.1016/j.stem.2017.11.001.

[57] E. Chermnykh, E. Kalabusheva, E. Vorotelyak, Extracellular matrix as a regulator of epidermal stem cell fate, Int. J. Mol. Sci. 19 (2018). https://doi.org/10.3390/ijms19041003.

[58] L. Meran, A. Baulies, V.S.W. Li, Intestinal Stem Cell Niche: The Extracellular Matrix and Cellular Components, Stem Cells Int. 2017 (2017). https://doi.org/10.1155/2017/7970385.

[59] Y. Kim, S. Kumar, CD44-mediated adhesion to hyaluronic acid contributes to mechanosensing and invasive motility, Mol. Cancer Res. 12 (2014) 1416–1429. https://doi.org/10.1158/1541-7786.MCR-13-0629.

[60] J. Lam, N.F. Truong, T. Segura, Design of cell-matrix interactions in hyaluronic acid hydrogel scaffolds, Acta Biomater. 10 (2014) 1571–1580. https://doi.org/10.1016/j.actbio.2013.07.025.

[61] J.E. Frith, R.J. Mills, J.J. Cooper-White, Lateral spacing of adhesion peptides influences human mesenchymal stem cell behaviour, J. Cell Sci. 125 (2012) 317–327. https://doi.org/10.1242/jcs.087916.

[62] V. Barbaro, A. Testa, E. Di Iorio, F. Mavilio, G. Pellegrini, M. De Luca, C/EBPδ regulates cell cycle and self-renewal of human limbal stem cells, J. Cell Biol. 177 (2007) 1037–1049. https://doi.org/10.1083/jcb.200703003.

[63] M. Zheng, C. Tian, T. Fan, B. Xu, Fibronectin regulates the self-renewal of rabbit limbal epithelial stem cells by stimulating the Wnt11/Fzd7/ROCK non-canonical Wnt pathway, Exp. Eye Res. 185 (2019) 107681. https://doi.org/10.1016/j.exer.2019.05.021.

[64] S.C.G. Tseng, S.Y. Chen, O.G. Mead, S. Tighe, Niche regulation of limbal epithelial stem cells: HC-HA/PTX3 as surrogate matrix niche, Exp. Eye Res. 199 (2020) 108181. https://doi.org/10.1016/j.exer.2020.108181.

[65] W. Chen, J. Dong, J. Haiech, M.C. Kilhoffer, M. Zeniou, Cancer stem cell quiescence and plasticity as major challenges in cancer therapy, Stem Cells Int. 2016 (2016). https://doi.org/10.1155/2016/1740936.

[66] M.L. De Angelis, F. Francescangeli, F. La Torre, A. Zeuner, Stem cell plasticity and

dormancy in the development of cancer therapy resistance, Front. Oncol. 9 (2019) 626. https://doi.org/10.3389/fonc.2019.00626.

[67] S.K. Rehman, J. Haynes, E. Collignon, K.R. Brown, Y. Wang, A.M.L. Nixon, J.P. Bruce, J.A. Wintersinger, A. Singh Mer, E.B.L. Lo, C. Leung, E. Lima-Fernandes, N.M. Pedley, F. Soares, S. McGibbon, H.H. He, A. Pollet, T.J. Pugh, B. Haibe-Kains, Q. Morris, M. Ramalho-Santos, S. Goyal, J. Moffat, C.A. O'Brien, Colorectal Cancer Cells Enter a Diapause-like DTP State to Survive Chemotherapy, Cell. 184 (2021) 226-242.e21. https://doi.org/10.1016/j.cell.2020.11.018.

Chapter 3 Rapid Bioprinting of Conjunctival Stem Cell Micro-constructs for Subconjunctival Ocular Injection

Abstract

Ocular surface diseases including conjunctival disorders are multifactorial progressive conditions that can severely affect vision and quality of life. In recent years, stem cell therapies based on conjunctival stem cells (CjSCs) have become a potential solution for treating ocular surface diseases. However, neither an efficient culture of CjSCs nor the development of a minimally invasive ocular surface CjSC transplantation therapy has been reported. Here, we developed a robust *in vitro* expansion method for primary rabbit-derived CjSCs and applied digital light processing (DLP)-based bioprinting to produce CjSC-loaded hydrogel micro-constructs for injectable delivery. Expansion medium containing small molecule cocktail generated fast dividing and highly homogenous CjSCs for more than 10 passages in feeder-free culture. Bioprinted hydrogel micro-constructs with tunable mechanical properties enabled the 3D culture of CjSCs while supporting viability, stem cell phenotype, and differentiation potential into conjunctival goblet cells. These hydrogel micro-constructs were well-suited for scalable dynamic suspension culture of CjSCs and were successfully delivered to the bulbar conjunctival epithelium via minimally invasive subconjunctival injection. This work integrates novel cell culture strategies with bioprinting to develop a clinically relevant injectable-delivery approach for CjSCs towards the stem cell therapies for the treatment of ocular surface diseases.

3.1 Introduction

The conjunctiva is a nonkeratinized stratified epithelium that comprises the ocular surface

along with the cornea [1]. It is a transparent mucous membrane that contains mucin-producing goblet cells, which are important for tear film stability [2]. Disorders of the conjunctiva include ocular cicatricial pemphigoid, Stevens-Johnson syndrome, toxic epidermal necrolysis, pterygium, and chemical or physical damages, which can lead to further complications such as dysfunctional tear syndrome, keratinization, symblepharon formation, and increased risk of infection [1,3–6]. With more than ten million new diagnoses worldwide each year, patients suffering from these severe forms of ocular diseases will often need surgical intervention to regenerate the ocular surface, especially the conjunctiva, to restore vision [7–11]. As the damage to the ocular surface is one of the major causes of visual impairment, preserving the integrity of the conjunctiva is critical [12]. Traditional therapeutics for treating severe ocular surface diseases include an autograft of conjunctiva or nasal mucosa, an allograft of amniotic membrane (AM), and conservative medications with eye drops [13–17]. However, these approaches have limitations in complete regeneration and the sourcing of autogenic or allogenic tissue is scarce. A critical factor in their lack of effectiveness is due to persistent inflammation which can drain the endogenous stem cell reservoir and hamper the regenerative capacity of the conjunctiva [18][19]. With the development of advanced regenerative medicine and stem cell technologies, growing attention over the past decade has turned towards the utilization of stem cell therapy for ocular surface diseases [20,21].

In parallel to the identification of corneal stem cells originating from the limbus as a promising source to support stem cell therapy for corneal diseases, there is currently a large interest in exploring the use of conjunctival stem cells (CjSCs) and their clinical applications for ocular surface diseases [22–25]. CjSCs are bipotent progenitor cells of conjunctival keratinocytes and conjunctival goblet cells [24,26]. Although several studies have located and identified CjSCs populations within the conjunctival epithelium, their efficient in vitro expansion and subsequent

transplantation to the ocular surface remains a challenge [22,27]. Recent studies on epithelial stem cells have highlighted the effectiveness of small molecule based dual SMAD signaling inhibition (dSMADi) and ROCK signaling inhibition (ROCKi) for the extensive expansion of epithelial stem cells derived from the airway, esophagus, intestine, skin, mammary, epididymis, and prostate glands [28,29]. Dual SMAD signaling, encompassing the TGFβ and BMP signaling pathways, influences the epithelial basal stem cell fate by controlling their differentiation, dedifferentiation, self-renewal, and quiescence [30–33]. ROCK signaling pathways play critical roles in the regulation of the cytoskeleton, microtubule dynamics, cell membrane transportation, and polarity [34]. Therefore, integration of dSMADi with ROCKi can potentially be used towards the development of feeder-free cell culture systems for CjSCs.

As the cell-niche interactions significantly affect stem cell survival and behavior, an instructive niche is critically important for successful stem cell transplantation [19,35,36]. Present studies on conjunctival reconstruction have mostly focused on allogeneic sheet transplantation using primary conjunctival epithelium grown on AM or other substitutes [27,37–39]. However, very few studies have addressed the use of substrates supporting the transplantation of CjSCs, which is mainly due to the poor understanding of their native niche. Meanwhile, the existing methodologies largely employ surgical grafting that often involve high postoperative risks including scar formation and symblepharon, as well as elongate recovery times. Therefore, minimally invasive cell transplantation strategies have become a safe and effective alternative [40–44]. Nevertheless, the delivery of CjSCs to the conjunctiva is limited by challenges regarding poor immobilization of cells to the target site which can lead to compromised viability and rapid diffusion of the transplanted cells [45]. In recent years, encouraging progress has been made in integrating hydrogel scaffolds for therapeutic delivery of stem cells to the ocular surface [46,47].

Digital light processing (DLP)-based rapid bioprinting enables a robust platform for high throughput fabrication of cell-loaded hydrogel constructs while providing well-defined user control over key factors including cell placement, biomechanical properties, and microarchitecture to better recapitulate the native niche [48–53]. Moreover, bioprinting offers superior microscale geometric control as well as the scalable and rapid production of cellularized constructs [54,55]. Given the elastic nature of the conjunctival epithelium, subconjunctival delivery of injectable bioprinted cell-loaded hydrogel constructs could be used as a minimally invasive remedy for ocular surface regeneration [56].

In this study, we presented a DLP-based rapid bioprinting approach to fabricate microscale CjSC-loaded hydrogel constructs for subconjunctival injectable delivery. We first expanded rabbit-derived CjSCs using a feeder-free culture system containing a small molecule cocktail that performed dSMADi and ROCKi. Then, we applied our DLP-based bioprinting system to fabricate hydrogel micro-constructs with tunable mechanical properties to encapsulate CjSCs while ensuring their viability and preserving stem cell behavior. Dynamic suspension culture of the hydrogel micro-constructs was also performed to demonstrate the scalability of the process. Furthermore, we validated the injectability and post-injection viability of CjSC-loaded hydrogel micro-constructs by performing ex vivo delivery into the subconjunctival region of rabbit eyes using a 30-gauge syringe. This is the first report on the development of bioprinted injectable CjSC-loaded hydrogel micro-constructs and the establishment of protocols for robust in vitro expansion of CjSCs. Overall, this work serves as an important framework for understanding the conjunctival stem cell population, conjunctival epithelial biology, as well as the application of CjSCs as a clinically translatable strategy for minimally invasive treatments of severe ocular surface diseases.

3.2 Materials and Methods

Primary CjSCs isolation, culture, and differentiation

Fresh eyes harvested from 10-12 weeks old New Zealand White rabbits (Oryctolagus Cuniculus) were acquired from Sierra for Medical Science, Inc. (Whittier, CA) and used for conjunctival cell isolation. Rabbit conjunctival epithelium was collected from palpebral conjunctiva and bulbar conjunctiva that was 3-5 mm away from the limbus. PBS was subconjunctivally injected into the palpebral and bulbar area with a flat pinhead for the blunt dissection of conjunctival epithelium from the stroma. The dissected conjunctival epithelium was minced with a surgical blade and incubated with 0.5% type IV collagenase (Sigma Aldrich) solution at 37℃ under agitation at 150 rpm for 1 hour. After the incubation, cell pellets were collected and washed with PBS, followed by a 10-minute digestion with 0.25% trypsin-EDTA (Sigma Aldrich). The cells were filtered using a 75 μm cell strainer before seeding onto collagen I (ThermoFisher Scientific) coated 6-well plates. The epithelial basal medium was prepared as previously reported by combining DMEM/F-12 (3:1) with 10% (v/v) fetal bovine serum (FBS) (DF12) supplemented with 1% (v/v) penicillin–streptomycin (P-S, ThermoFisher Scientific), 1x insulin-transferrin-selenium (ITS, ThermoFisher Scientific), 10 ng/ml epidermal growth factor (EGF, R&D System), 400 ng/ml hydrocortisone (Sigma Aldrich), 0.1 nM cholera toxin (Sigma Aldrich), and 2 nM 3,39,5-triiodo-L-thyronine (Sigma Aldrich)[25,57]. In the medium component formulation studies, 0.1 μM, 1 μM, or 10 μM A83-01 (STEMCELL Technologies), SB431542 (Tocris Bioscience), DMH1 (STEMCELL Technologies), Dorsomorphin (STEMCELL Technologies), LDN193189 (Tocris Bioscience), or 10 μM SB505142 (Tocris Bioscience), 1 μM LY294002 (Tocris Bioscience), 10 μM Y27632 (Tocris Bioscience), 100 ng/ml bone morphogenetic protein 4 (BMP4) (Biolegend), 100 ng/ml transforming growth factor beta (TGFβ;

Biolegend) were added into the basal medium. Basal medium without these aforementioned additive components was used as the control in the primary culture study. The procedure was approved by University of California San Diego Institutional Biosafety Committee.

For the expansion of CjSCs, cells were seeded on collagen I (ThermoFisher Scientific) coated 6-well plates with the seeding density of 200,000 cells per well and cultured in conjunctival stem cell expansion medium (CjSCM) composed of epithelial basal medium supplemented with 10 μM Y27632, 1 μM A83-01, and 1 μM DMH1. Medium changes were performed every other day and cells were passaged at 80-90% confluence. For differentiation into conjunctival goblet cells, expanded CjSCs over passage 2 (P2) were seeded and cultured the same as mentioned above. The differentiation was initiated when the cells reached 90% confluence, in differentiation medium composed of Keratinocyte SFM (serum-free medium) (ThermoFisher Scientific) supplemented with 50 μg/ml bovine pituitary extract (BPE), 5 ng/ml recombinant epidermal growth factor (EGF) (ThermoFisher Scientific), 1% (v/v) P-S, 100 ng/ml BMP4, 10 ng/ml fibroblast growth factor 10 (FGF10), 100 ng/ml interleukin 13 (IL-13) and 1 μM A83-01[2,58–60]. The cells were cultured with the goblet cell differentiation medium for 7 days with the medium changed every other day. For CjSCs 3D static culture, the bioprinted hydrogel micro-constructs were cultured in a 24-well plate with CjSCM immediately after bioprinting to induce goblet cell differentiation as described above. For dynamic suspension culture, the hydrogel micro-constructs were cultured in 12-well plates and constantly agitated at a rate of 95 rpm. The cell culture was performed at 37℃ with 5% CO_2.

Material synthesis and photocrosslinkable bioink preparation

Gelatin methacryloyl (GelMA) was synthesized according to previously established

protocols [61,62]. Briefly, porcine skin gelatin type A (Sigma Aldrich) was dissolved into a 0.25 M carbonate-bicarbonate (3:7) buffer solution at pH 9 with stirring at 50℃ to prepare a 10% (w/v) solution. Once the gelatin was completely dissolved, methacrylic anhydride (MA; Sigma Aldrich) was added dropwise into the gelatin solution to a concentration of 100μl per gram of gelatin and reacted for 1 hour under continuous stirring at 50℃. The product underwent dynamic dialysis overnight using 13.5 kDa dialysis tubes (Repligen). The GelMA solution was then lyophilized for three days and stored at -80℃ for later use. Lithium phenyl-2,4,6-trimethylbenzoylphosphinate (LAP) was used as a photoinitiator and synthesized as previously described [63]. In brief, under constant stirring at room temperature, 18 mmol of dimethyl phenylphosphonite (Sigma Aldrich) was mixed equimolarly with 2,4,6-trimethylbenzoyl chloride (Acros Organics) by dropwise addition and left to react for 18 hours. Next, 6.1 g of lithium bromide (Sigma Aldrich) dissolved in 100 ml of 2-butanone (Sigma Aldrich) was added in the reaction mixture, and the reaction was continued at 50℃ for 10 minutes with stirring. The mixture was then left to incubate overnight at room temperature and the unreacted lithium bromide was removed by filter-washing with 2-butanone for a total of 3 times. The resultant LAP solids were ground into powder and stored in the dark under argon at 4℃.

To prepare the prepolymer bioinks, GelMA powders and LAP powders were dissolved with warmed DPBS to form a stock solution of 10% (w/v) GelMA and 0.5% (w/v) LAP, followed by filtering with 0.22 μm syringe filters. The cells were trypsinized with 0.25% trypsin-EDTA and neutralized with culture medium. The resultant cell solution was filtered with a 75 μm cell strainer to attain a single cell suspension. The cell suspension was then counted with a hemocytometer and

adjusted to desired concentrations. Immediately prior to bioprinting, the GelMA-LAP prepolymer solution was mixed 1:1 with single cell suspension to form a final bioink formulation composed of 5% (w/v) GelMA, 0.25% (w/v) LAP, and 107 cells/mL CjSCs. For the acellular bioprinted hydrogel micro-constructs, the prepolymer solution was mixed 1:1 with DPBS to make the bioink.

Rapid bioprinting of hydrogel micro-constructs

Rapid bioprinting of acellular or cellularized hydrogel micro-constructs was performed with our custom-built digital light projection (DLP)-based bioprinting system [51,52,64]. This DLP-based bioprinter consists of a 365 nm light source (Hamamatsu) with aligning projection optics, a digital micromirror device (DMD) chip (Texas Instruments) for optical patterning, and a stage controlled by a motion controller (Newport). User-defined patterns were fed into the computer. Using custom operation software, the DMD chip could be controlled to modulate the light projection based on the assigned patterns. All the digital patterns used for bioprinting were generated with Adobe Photoshop. For the bioprinting setup, two identical polydimethylsiloxane (PDMS) spacers with the thicknesses of 500 μm or 125 μm were placed between a methacrylated coverslip and the PDMS base attached to a glass slide. The prepolymer bioink was loaded into the gap between the coverslip and the base followed by photopolymerization. The polymerized constructs were immediately transferred to a 24-well plate containing pre-warmed DPBS and excess prepolymer was washed by gentle pipetting. The DPBS was then replaced by the culture medium which was then changed after the first 24 hours. For dynamic suspension culture, the hydrogel constructs were rinsed with DPBS and then carefully detached from the coverslips using surgical blades and placed into 12-well plates (36 constructs per well). The hydrogel constructs were resuspended with warm CjSCM and subjected to 95 rpm rotation.

Immunofluorescence staining

For 2D cell staining, CjSCs were grown on collagen-coated Millicell EZ slides (Millipore Sigma). Samples were washed twice with sterile DPBS and fixed with 4% (w/v) paraformaldehyde (FUJIFILM Wako) for 20 minutes at room temperature, followed by three 10 minutes DPBS washes. For the co-staining of ABCG2/KRT14, P63/E-Cad, and KI67/PAX6 the fixed samples were blocked with 5% (w/v) bovine serum albumin (BSA; Sigma Aldrich) containing 0.3% triton X-100 (Sigma Aldrich) for 1 hour at room temperature. For the staining of Muc5AC and MUC16, the fixed samples were permeabilized with DPBS containing 0.2% triton X-100 for 10 min, followed by blocking for 1 hour with 5% (w/v) BSA. Afterwards, samples were incubated with primary antibodies at 4 ℃ overnight. Following primary antibody incubation, cultures were washed three times for 10 minutes each in DPBS and incubated with Alexa Fluor-conjugated secondary antibodies (Invitrogen) for 1 hour at room temperature. The samples were then washed with DPBS three times before staining with DAPI (4',6-Diamidino-2-Phenylindole; ThermoFisher Scientific) diluted in DPBS (1:500) for 10 minutes. After removing the DAPI solution and a final DPBS wash, the solution was aspirated and the samples were air-dried for 30 seconds, followed by mounting with Fluoromount-G™ Mounting Medium (ThermoFisher Scientific). The immunofluorescence staining on hydrogel micro-constructs followed the same protocols with the mounting step omitted. For the staining on cryosectioned samples, the optimal cutting temperature (O.C.T.) compound was washed off with three 10 minutes DPBS washes followed by brief air drying. Then, hydrophobic circles were drawn around the sections with a PAP pen (Sigma Aldrich). The permeabilization and blocking were performed with 5% (w/v) BSA and 0.3% (v/v) triton X-100 at room temperature for 1 hour. The sequential steps are the same as described above. After

staining, samples were imaged within 48 hours. The antibody information and their dilution rates are available in the Supplementary Table 3.1.

Mechanical properties characterization

The compressive modulus (Young's modulus) of the bioprinted hydrogel micro-constructs encapsulated with CjSCs was measured using a MicroSquisher (CellScale) apparatus following the manufacturer's instructions. The 5% GelMA cylinders (250 μm in diameter; 250 μm in height) printed for the test were incubated at 37℃ before use. Prior to measurement, the hysteresis of the samples was removed with two rounds of preconditioned compression. Then, the samples were compressed at 10% strain with a 2 μm/s strain rate to record the data. The Young's modulus of measured samples was calculated using a custom MATLAB algorithm with the force and displacement data.

Rheometry was used to determine if the hydrogels are shear thinning. We adapted an established testing protocol [65] and conducted the measurements on a parallel plate rheometer (AR-G2 Rheometer, TA Instruments). The tests were conducted at 25℃ and a gap height of 1000 μm. The tests were conducted at room temperature to mimic the ambient temperature for injection. A 5% GelMA, 0.25% LAP solution in DPBS was warmed to 37℃ and 310 μl of solution was injected between the plates. The top plate was lowered to 900 μm and lifted back to 1000 μm to ensure even the spreading of solution between the plates. To form the hydrogel between the parallel plates, the solution was exposed for 5 minutes to UV light from a 395nm UV LED flashlight

(TaoTronics, Model: TT-FL001). Before each test, a 2-minute time sweep was performed at 0.2% strain and 10 Hz to recondition the hydrogel to reset its mechanical history. A frequency sweep was done from 0.01 to 100 Hz at 0.2% strain with 10 points per decade. A strain sweep was done from 0.01% to 500% strain at 10 Hz with 10 points per decade. The viscosity was measured by a continuous flow ramp from shear rates 0 to 50 s-1 in 2.5 minutes with 20 points per decade. The reported data represents 3 independent hydrogel runs.

For the characterization of equilibrium swelling ratio, acellular hydrogel micro-constructs were fabricated as described above. The hydrogel micro-constructs were dehydrated with overnight incubation at 37℃, followed by imaging and rehydration via DPBS immersion. The hydrated hydrogel micro-constructs were then imaged every 24 hours for 6 days with a Leica DMI 6000-B microscope. The cross-sectional area of the dry and wet hydrogel micro-constructs were measured using ImageJ and recorded as A_{Dry} and A_{Wet}, respectively. The equilibrium swelling ratio at each time point was calculated by A_{Wet}/A_{Dry}. All measurements were performed in triplicates.

Viability evaluation

To evaluate the viability of encapsulated CjSCs in the bioprinted hydrogel micro-constructs, samples were stained with Live/DeadTM Viability/Cytotoxicity kit (Thermo Fisher Scientific) and the metabolic activity was measured with CellTiter-Glo® 3D cell viability assay (Promega). For the Live/Dead staining, the hydrogel micro-constructs were incubated with DPBS with 2 μM calcein acetoxymethyl ester and 4 μM ethidium homodimer for 30 minutes at 37℃, followed by fluorescent imaging with Leica DMI 6000-B microscope. The Live/DeadTM staining was performed in duplicates. For the CellTiter-Glo® 3D cell viability assay, the hydrogel micro-

constructs were transferred to a 24-well plate filled with 200 µl culture medium and 200 µl CellTiter-Glo® 3D reagent (400 µl solution per well). The samples were then incubated at room temperature under constant agitation for 1 hour. After incubation, 50 µl of the lysate was transferred to a white opaque-walled 96-well plate and diluted with 150 µl of UltraPure™ water (Thermo Fisher Scientific). The adenosine triphosphate (ATP) standard curve was created with gradient dilution of ATP disodium salt (Promega) and loaded in the same 96-well plate. Each test was performed with 6 replicates. The data collection was carried out by plate-reading with the Tecan Infinite M200 PRO microplate reader.

RNA isolation, reverse transcription, and real time quantitative PCR

To extract the RNA from the 2D cultured cells, chilled TRIzol® reagent (Ambion Thermo Fisher) was added to the pelleted cells followed by repeated pipetting. To extract the RNA from encapsulated cells in hydrogel micro-constructs, the samples were physically broken down with clean pipette tips and immediately immersed into chilled TRIzol® reagent and repeatedly pipetted. The lysate was either used for extraction or immediately stored in the -80℃ freezer. RNA samples were extracted with the Direct-zolTM RNA Purification kit (Zymo Research) following the manufacturer's instructions. The products were quantified using a NanoDropTM 2000 (Thermo Fisher Scientific) instrument. The RNA samples were either used immediately for cDNA synthesis or stored at -80℃. The cDNA reverse transcription synthesis was carried out with PhotoScript® first strand cDNA synthesis kit (New England BioLabs) following the manufacturer's protocols using the thermal cycler of the StepOneTM Real-Time PCR System (Thermo Fisher Scientific). The resultant cDNAs were further diluted 10-fold with UltraPureTM water (Thermo Fisher

Scientific). Real time quantitative PCR (qPCR) was performed in triplicates using the Luna® Universal qPCR Master Mix (New England BioLabs) according to the manufacturer's instructions. The qPCR primers used are listed in Supplementary Table 3.2. For relative quantification, glyceraldehyde 3-phosphate dehydrogenase (GAPDH) was used as an internal control.

Flow cytometry

For flow cytometry, cultured cells were digested with 0.25% trypsin-EDTA, filtered with a 75 μm cell strainer, and pelleted by centrifugation. Following the manufacturer's instructions, the pellets were resuspended with a Cell Staining Buffer (Biolegend) and TruStain FcX™ (Biolegend) was used for blocking. To quantify the KRT14 positive population, anti-Keratin 14 rabbit polyclonal antibody (905304, Biolegend) and anti-rabbit IgG (H+L), F(ab')2 Fragment (Cell Signaling Tech) were applied subsequentially following the manufacturer's instructions. Flow cytometry was performed using FACSAria™ Fusion sorter (BD Biosciences) and the data was analyzed using FlowJo.

Cell doubling quantification

For the cell doubling comparison, freshly isolated, viable conjunctival epithelial cells were seeded on a collagen I coated 12-well plate with a density of 20,000 cells per well. The cells were serially expanded in CjSCM or control medium. Subculture was performed with 0.25% trypsin-EDTA every 3-4 days depending on the confluence. The number of cells were measured with hemocytometer (Fisher Scientific) and re-seeded on a collagen I coated 12-well plate with a density of 20,000 cells per well. The test was performed in triplicates and the cell doubling time (DT) was calculated with the following formula: $DT = \Delta T \cdot ln\ 2\ /ln\ (Q2/Q1)$. ΔT represents the incubation

time. *Q1* and *Q2* represents the number of cells at the beginning and at the end, respectively.

Periodic acid–Schiff (PAS) staining

PAS staining on differentiated conjunctival goblet cells was performed by Periodic Acid Schiff (PAS) Stain Kit (Abcam) following the manufacturer's instructions. Imaging was performed using the Keyence BZ-9000 microscope with a multicolor CCD camera.

Biodegradibility test

To evaluate the biodegradibility of the hydrogel materials, we synthesized fluorescein (FAM) conjugated GelMA using FAM NHS ester, 6-isomer (Lumiprobe, CAT# 55120) with guidance from the manufacturer's protocol. Briefly, lyophilized GelMA and FAM NHS ester were first homogeneously dissolved separately in 0.1M sodium bicarbonate buffer solution (pH 8.3) then combined into a 50-ml conical to make a 2% (w/v) GelMA solution with 4x molar excess of FAM NHS ester. The reaction was allowed to proceed overnight at 4℃ in the dark. The solution was filtered via ZebaTM 7K MWCO spin desalting columns (ThermoFisher, CAT# 89894) to remove excess FAM NHS ester, subsequently frozen at -20℃, and lyophilized for three days. Lyophilized FAM-GelMA was stored at -80℃ until further use.

The FAM-GelMA pre-polymer solution was prepared and used for bioprinting as described in Section 2.2. For the biodegradibility test, FAM-GelMA-based microscale cylinders (2 mm in diameter; 500 μm in height) were printed. The hydrogel constructs were then subjected to 100 rpm rotating incubation at 37℃ with 10 μg/ml collagenase Type IV (Sigma Aldrich). The supernatant

was collected every 10 minutes until the complete degradation of hydrogel constructs. The FAM concentrations in the supernatant were measured by fluorescence plate-reading with the Tecan Infinite M200 PRO microplate reader. The degree of degradation was calculated by normalizing the signal from each group to the signal from the complete degradation group (80 minutes group).

Injectability test

To evaluate the injectability of the hydrogel micro-constructs, 80 samples were suspended in 200 μl of DPBS in a microcentrifuge tube and aspirated with a 30-gauge syringe needle, followed by repeated injection and aspiration for a total of 3 times. Afterwards, the treated hydrogel micro-constructs and the non-treated controls were subjected to dynamic suspension culture. Live/DeadTM staining was performed to evaluate the influence of injection on the encapsulated cells.

Subconjunctival delivery and cryosection

Subconjunctival injection into rabbit eyes was performed using a 30-gauge syringe needle. For a single injection, 36 hydrogel micro-constructs encapsulated with GFP-labeled CjSCs were suspended in 100 μl of DPBS supplemented with 1% (v/v) P-S in a microcentrifuge tube, loaded into the syringe, and injected into the subconjunctival regions of the bulbar conjunctiva. Four injection sites in between the muscles and connective tissues were chosen to mimic the actual injection protocol. Moreover, 100 μl of single cell suspension (106 cells/ml) in DPBS with 1% (v/v) P-S was injected in the same manner to serve as the control. After injection, the rabbit eyes were incubated in DF12 supplemented with 10 ng/ml EGF and 1% (v/v) P-S, for 24 hours under constant agitation at 95 rpm.

To prepare the rabbit eyeballs for cryosectioning, dissection was performed with the anterior part (sclera ring with conjunctiva and cornea) kept intact and the excised tissue was fixed in 4% (w/v) PFA for 3 hours, followed by dehydration with 30% (w/v) sucrose (Sigma Aldrich) in 0.1 M DPBS at 4 °C overnight. The tissues were then embedded in Tissue Tek® O.C.T. Compound (Fisher Scientific) and frozen at -80℃. Serial transverse sections of 6 μm thick each were cut using a CM1900 cryostat (Leica) and stored at −80 °C until stained.

Imaging and processing

The brightfield and regular fluorescence images of the cells and hydrogel micro-constructs were captured using a Leica DMI 6000-B microscope. Confocal imaging was performed using a Leica SP8 Confocal with lighting deconvolution. All images were processed using LAS X software and ImageJ.

Statistical analysis

All the statistics in this work were processed with Microsoft Excel and GraphPad Prism (V6) and presented by mean ± standard deviation. The statistical significance was evaluated with Student's t-test (two tailed) or one-way ANOVA. Statistics with P-value < 0.05 were considered as significant and labeled with asterisks (*: $P < 0.05$; **: $P < 0.01$; ***: $P < 0.001$.).

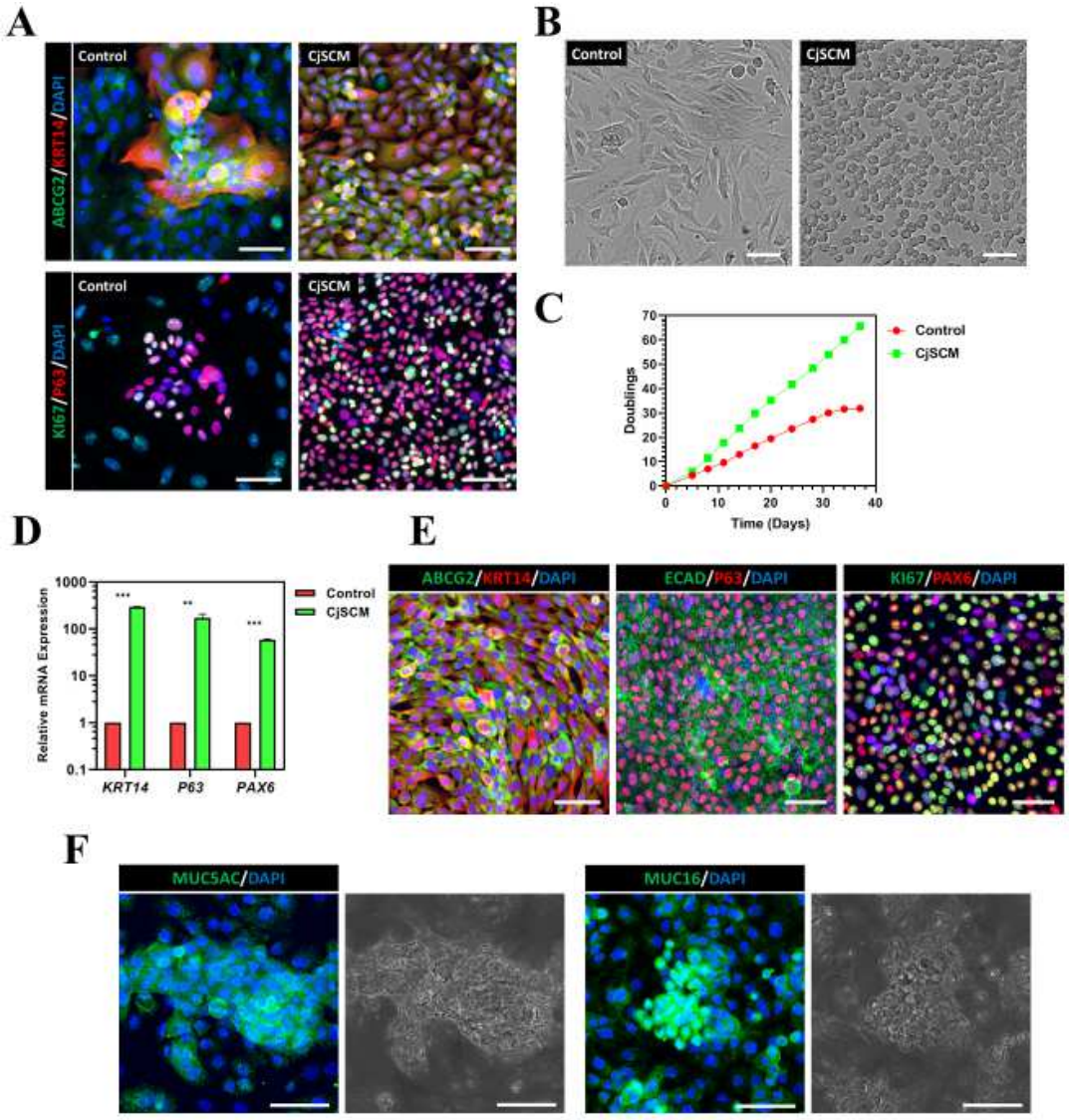

Figure 3.1. Conjunctival Stem Cell Expansion Medium (CjSCM) with Small Molecule Cocktail Facilitates *In vitro* Expansion of CjSCs. (A) Immunofluorescence staining of ABCG2/ KRT14 and KI67/P63 on primary conjunctival epithelial cells that were cultured in CjSCM or control medium for 4 days. Scale bars: 50 μm. (B) Cell morphologies of nonconfluent primary conjunctival epithelial cells cultured with CjSCM or control medium at P3. Scale bars: 50 μm. (C) Cumulative cell doubling plot showing the doublings versus the culture time of primary conjunctival epithelial cells in culture with CjSCM or control medium. (D) Real time qPCR showing the relative mRNA expression of stem cell markers (i.e., KRT14, P63) and lineage marker (i.e., PAX6) in P10 cells expanded in CjSCM or control medium (mean ± SD, n=3, **: $P < 0.01$.). (E) Immunofluorescence staining of ABCG2/ KRT14, ECAD/ P63 and KI67/PAX6 on CjSCs at P10. Scale bars: 50 μm. (F) Immunofluorescence staining of MUC5AC and MUC16 and the corresponding bright field images on the differentiated CjSCs. Scale bars: 50 μm.

3.3 Results

3.3.1 *In vitro* expansion of CjSCs with small molecule cocktail

To expand the CjSCs *in vitro*, different small molecules related to dSMADi or ROCKi at different concentrations (i.e., 0.1 μM, 1 μM, 10 μM) in the basal medium were tested. The mitotically active undifferentiated epithelial cell population represented by cytokeratin 14 (KRT14) positive cells were evaluated by flow cytometry (Supplementary S3.1A, B)[66,67]. Groups treated with A83-01 (TGFβ inhibitor) and DMH1 (BMP inhibitor) showed the most KRT14 positive population expansion among their analogues. Given the promise of the addition of A83-01 and DMH1, we further tested them along with Y27632 (ROCK inhibitor) and the related activator proteins (TGFβ, BMP4) to evaluate their efficacy in stem cell expansion. After 4 days of primary culture, more small-sized and tightly packed cells were found in the inhibitors (i.e., A83-01, DMH1, Y27632)-treated groups (Supplementary S3.1C). Real time qPCR showed up-regulated mRNA expression of stem cell markers (KRT14, P63) and ocular lineage marker (PAX6) in the inhibitors-treated groups while down-regulated expression was found in the activators (i.e. TGFβ, BMP4)-treated groups (Supplementary S3.1D)[24,68]. The three inhibitors combined group exhibited the highest expression up-regulation on all three markers, which indicated the three components synergistically stimulated stem cell expansion in primary conjunctival epithelial cell culture. Consistently, immunofluorescence staining of stem cell markers (ABCG2, KRT14, P63) and the proliferation marker (KI67) identified homogenous positive populations in the three inhibitors combined group while only small colonies of positive populations were found in the control (Fig. 3.1A)[24]. Based on these results, we combined 10 μM Y27632, 1 μM A83-01, and 1 μM DMH1 to form the small molecule cocktail for the conjunctival stem cell expansion medium (CjSCM). The cells cultured with CjSCM were homogenous in size and rounded shape whereas the control

cells showed heterogenous size and flattened, elongated morphologies (Fig. 3.1B). Furthermore, long-term culture demonstrated that cells expanded with CjSCM proliferated significantly faster than the control cells and can be expanded stably for more than 60 doublings without losing replicative potential (Fig. 3.1C, Supplementary S3.1E). Real time qPCR showed an up-regulation in expression of *KRT14*, *P63* and *PAX6*, in the expanded CjSCs in comparison to the control (Fig. 3.1D). The stem cell identity and proliferative potential of the CjSCs cultured with CjSCM were confirmed by the positive expression of the stem cell markers (i.e., ABCG2, KRT14, P63), lineage markers (i.e., E-Cadherin (ECAD), PAX6) and proliferation marker (i.e., KI67) (Fig. 3.1E). We next tested whether the expanded CjSCs are functional by differentiating them into conjunctival goblet cells. Immunofluorescence staining showed the positive expression of the characteristic mucous protein markers for mucin 5AC (MUC5AC) and mucin 16 (MUC16) in the CjSCs expanded with CjSCM after 7 days of goblet cell differentiation (Fig. 3.1F)[2,69]. This was further confirmed by positive Periodic acid-Schiff (PAS) staining for mucin expression in the cells post differentiation (Supplementary S3.1F). Together, we showed successful *in vitro* expansion of functional CjSCs while preserving differentiation potential into conjunctival goblet cells using our developed CjSCM.

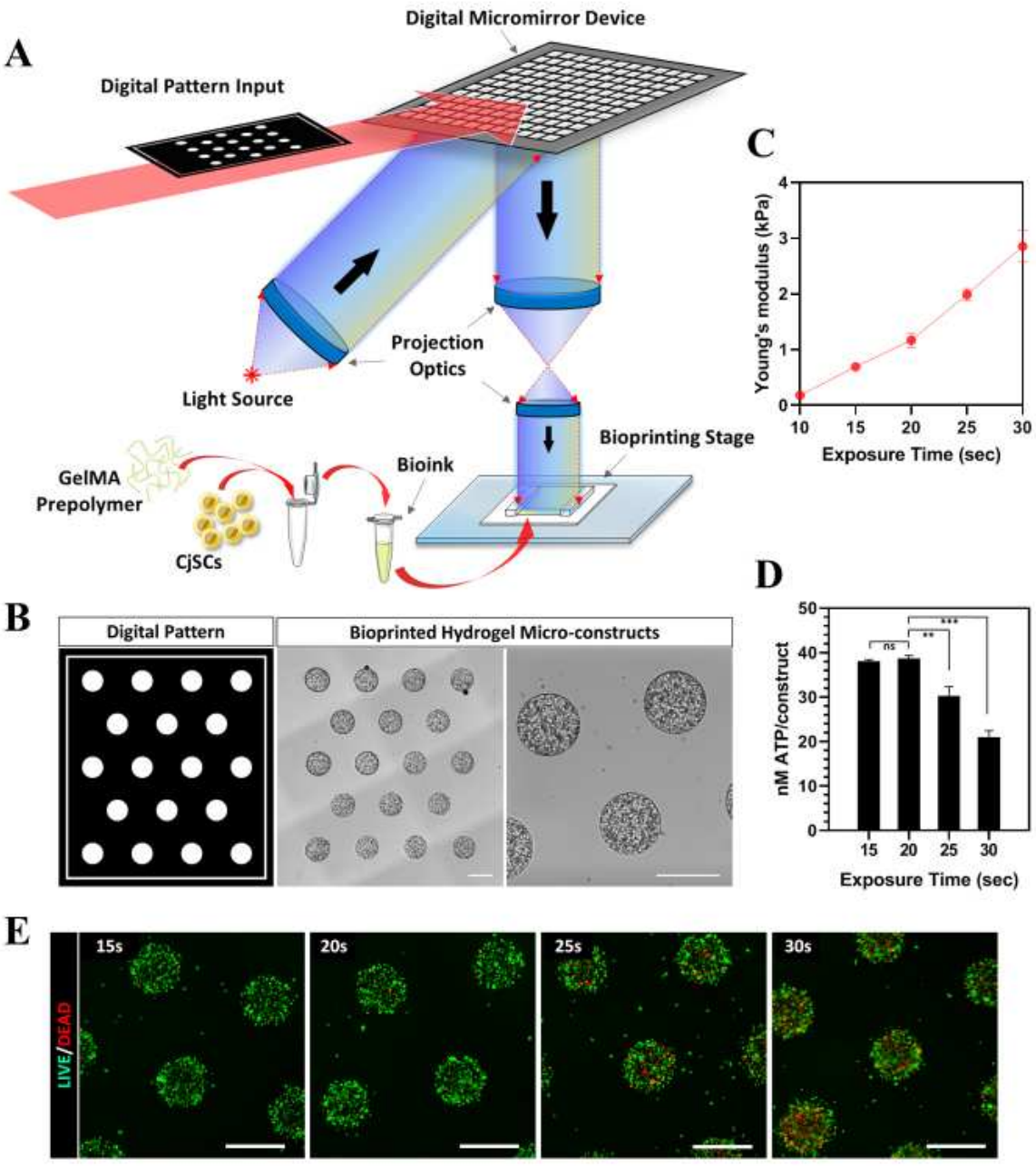

Figure 3.2. Bioprinting of CjSC-loaded Hydrogel Micro-constructs with Tunable Mechanical Properties. (A) Schematic of the DLP-based rapid bioprinting process to fabricate hydrogel micro-constructs loaded with CjSCs. (B) Designed digital patterns and the representative corresponding hydrogel micro-constructs encapsulating 107 cells/ml of CjSCs. Scale bars: 500 μm. (C) Plot of compressive modulus of the hydrogel micro-constructs versus light exposure time (mean ± SD, n = 3). (D) Plot of metabolic activity (ATP content/construct) of the bioprinted constructs versus light exposure time (mean ± SD, n = 6, **: $P < 0.01$, ***: $P < 0.001$.). The metabolic activity was measured using CellTiter-Glo® 3D cell viability assay. (E) Representative images of Live/DeadTM staining of the CjSC-loaded hydrogel micro-constructs fabricated under different exposure times. Scale bars: 100 μm.

3.3.2 DLP-based rapid bioprinting of hydrogel micro-constructs support the viability of encapsulated CjSCs

Upon establishing stable *in vitro* expansion conditions, we next developed an injectable cell delivery system for CjSCs as a strategy towards a potential clinically translatable stem cell therapy. It is critical to ensure that both the biochemical and biophysical properties are optimized to ensure appropriate viability and functionality of CjSCs. Among the different biofabrication techniques available, DLP-based bioprinting systems enable rapid and scalable fabrication of cellularized hydrogel micro-constructs with precise geometrical control [48,51,52,54,55]. Our DLP-based bioprinter utilizes a DMD chip that converts user-defined digital designs into optical patterns to rapidly photopolymerize hydrogel constructs encapsulating cells into well-defined microscale patterns (Fig. 3.2A). More importantly, the ability to spatiotemporally regulate light exposure enables direct control over crosslinking density and thus the tunability of hydrogel mechanical properties [51,64]. In particular, GelMA has been widely used in biomedical applications including 3D encapsulation of various types of stem cells [70]. Therefore, we chose GelMA to fabricate hydrogel micro-constructs encapsulating CjSCs as a delivery vehicle. The GelMA pre-polymer solution was mixed with the CjSCs solution to form the bioink for DLP-based bioprinting (Fig. 3.2A). Through parallel projection printing, a total of 18 GelMA-based microscale cylinders (500 μm in diameter; 500 μm in height) encapsulating CjSCs at the density of 107 cells/ml were fabricated in a single print within 30 seconds (Fig. 3.2B). To optimize the stem cell niche, we tuned the exposure time to adjust the mechanical properties of the hydrogel scaffolds and monitored the change of the encapsulated CjSCs (Supplementary S3.2A). Mechanical testing results showed a positive linear relationship between the Young's modulus of

the hydrogel micro-constructs and the light exposure time for photo-crosslinking, where increasing exposure time correlated to an increase in hydrogel stiffness ranging from 0.2-3 kPa over a 10 to 30 seconds exposure time range (Fig. 3.2C). In addition, CellTiter-Glo® 3D cell viability assay was performed to measure the cellular metabolic activity of hydrogel micro-constructs (Fig. 3.2D). After 24 hours in culture, the amount of ATP generated per construct significantly decreased in the groups with 25 seconds exposure (i.e. 30.32 ± 2.04 nM/construct) and with 30 seconds exposure (i.e. 21.04 ± 1.43 nM/construct) compared to the group with 20 seconds exposure (i.e. 38.71 ± 0.64 nM/construct). Consistently, Live/DeadTM staining showed an increased number of dead cells in the groups with higher exposure time of 25 seconds and 30 seconds (Fig.3. 2E). To confirm the preservation of stem cell phenotype upon varied exposure times, the bioprinted CjSCs were evaluated by real time qPCR for the mRNA expression of the stemness marker P63 (Supplementary S2B). Consistently, the P63 mRNA expression was significantly down-regulated in groups with over 20 seconds exposure. Based on these findings, all subsequent bioprinting experiments encapsulating CjSCs were fabricated at 20 seconds exposure. Furthermore, we have tested the biodegradability of our hydrogel materials under this printing setting and confirmed the hydrogel constructs to be biodegradable (Supplementary S3.2C, D).

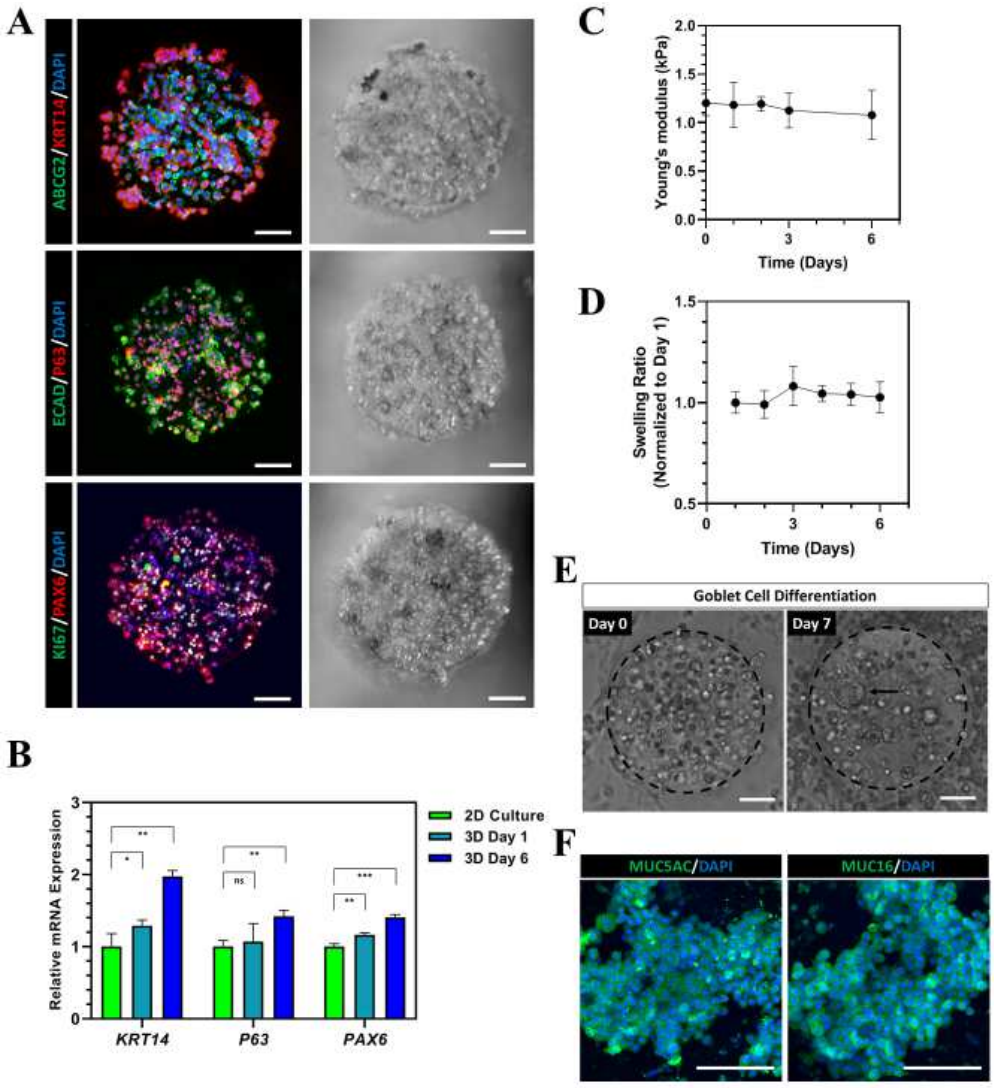

Figure 3.3. Bioprinted Hydrogel Micro-constructs Support 3D Culture of Functional CjSCs. (A) Representative fluorescence and corresponding bright field images of immunofluorescence staining on bioprinted CjSC-loaded hydrogel micro-constructs after 2 days in culture with CjSCM showing positive expression for ABCG2/KRT14, E-Cad/P63, KI67/PAX6. Scale bars: 100 μm. (B) Real time qPCR showing mRNA expression of stem cell markers (i.e. KRT14, P63) and lineage marker (PAX6) in the encapsulated CjSCs in 3D culture (3D Day 1, 3D Day 6), and CjSCs in 2D culture with CjSCM (2D Culture) for 6 days. The relative mRNA expression was normalized by the mRNA expression of 2D Culture (mean ± SD, n = 3, ns: non-significant, *: $P < 0.05$, **: $P < 0.01$, ***: $P < 0.001$.). (C) Plot of compressive modulus of the 3D hydrogel micro-constructs versus time in culture (mean ± SD, n = 3). (D) Plot of equilibrium swelling ratio of the acellular 3D hydrogel micro-constructs versus time in culture (mean ± SD, n = 3). (E) Representative bright field images of 3D hydrogel micro-constructs at day 0 and day 7 of conjunctival goblet cell differentiation. The arrow highlights the cell aggregate in the construct during differentiation. Scale bars: 100 μm. (F) Immunofluorescence staining of representative hydrogel micro-constructs after 7 days of conjunctival goblet cell differentiation showing positive expression of MUC5AC and MUC16. Scale bars: 100 μm.

3.3.3 Bioprinted hydrogel micro-constructs support encapsulated CjSC phenotype and differentiation potential

Next, we examined whether the bioprinted hydrogel micro-constructs can support stem cell phenotype and differentiation potential of encapsulated CjSCs within a 3D microenvironment. Immunofluorescence staining showed positive expression of the stem cell markers (i.e. ABCG2, KRT14, P63) as well as the lineage markers (i.e. E-Cad, PAX6) after 3 days in culture, which is consistent with the expected expression profile of CjSCs in 2D culture (Fig. 3.3A). Real time qPCR showed a significant up-regulation of P63, KRT14 and PAX6 in the hydrogel micro-constructs after 6 days in culture relative to hydrogel micro-constructs after one day in culture and the 2D culture group cultured with CjSCM for 6 days. All qPCR data were normalized to the 2D culture group (Fig. 3.3B). These results indicate that the 3D microenvironment significantly enhanced the stem cell phenotype of the encapsulated CjSCs. Building on this observation, we also examined the mechanical stability of the hydrogel micro-constructs over time. Mechanical testing data showed that the compressive modulus of the hydrogel micro-constructs did not significantly change over time and remained stable under physiological conditions (Fig. 3.3C). Moreover, the equilibrium swelling ratio measurements of acellular hydrogel micro-constructs found no significant changes after 6 days in 1X PBS at 37°C (Fig. 3.3D). Next, we assessed the functionality of the encapsulated CjSCs in the hydrogel micro-constructs by inducing goblet cell differentiation. After 7 days of differentiation, characteristic large cell aggregates were observed in hydrogel micro-constructs (Fig. 3.3E). Moreover, immunofluorescence staining confirmed the expression of MUC5AC and MUC16 in the hydrogel micro-constructs and demonstrated that the differentiation potential of the encapsulated CjSCs was preserved (Fig. 3.3F).

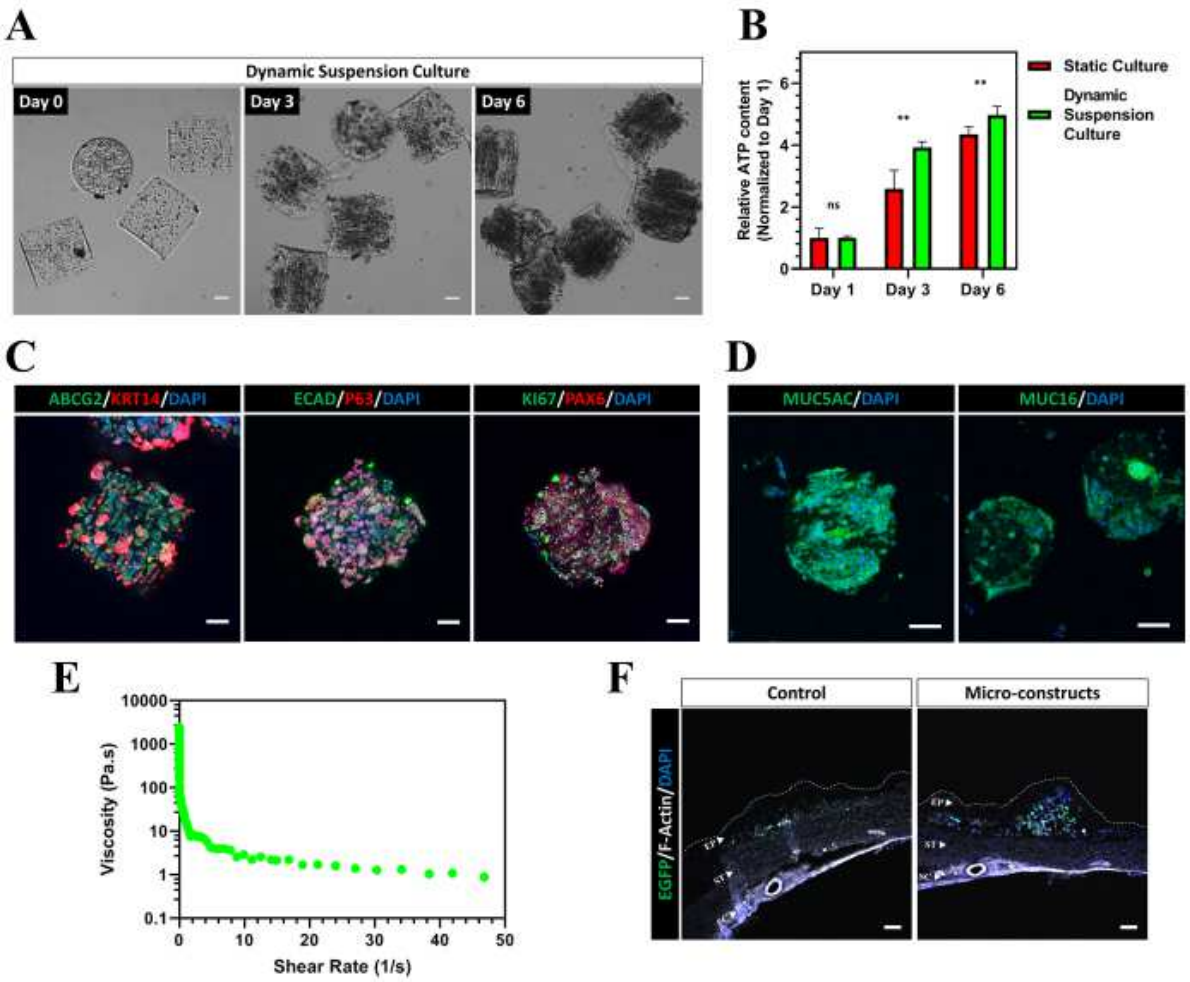

Figure 3.4. Dynamic Suspension Culture and Subconjunctival Injectable Delivery of CjSC-loaded Hydrogel Micro-constructs. (A) CjSC-loaded hydrogel micro-constructs in dynamic suspension culture for 6 days. Scale bars: 100 μm. (B) Plot of relative ATP content of the hydrogel micro-constructs in dynamic suspension culture or in static culture over time (mean ± SD, n = 6, **: $P < 0.01$.). The ATP content was measured via CellTiter-Glo® 3D cell viability assay and the relative ATP content was calculated by normalizing the data at each time point with the corresponding data at day 1. (C) Immunofluorescence staining of representative hydrogel micro-constructs samples after 6 days under dynamic suspension culture with ABCG2/KRT14, E-Cad/P63, KI67/PAX6. Scale bars: 100 μm. (D) Immunofluorescence staining showing positive expression of MUC5AC and MUC16 for representative hydrogel micro-constructs cultured dynamically in suspension after 7 days of conjunctival goblet cell differentiation. Scale bars: 100 μm. (E) Continuous flow rheometry test for the hydrogel composition of the micro-constructs demonstrating shear thinning with increased shear rate (mean, n = 3). (F) Confocal images of the cryosectioned ocular surface containing the conjunctiva and sclera after subconjunctival injection of hydrogel micro-constructs or cell-only control. Sections were stained with anti-EGFP antibody and phalloidin (anti F-Actin) to visualize the histological structures. The EGFP positive signals correspond to the transplanted CjSCs. The white dotted line outlines the boundaries of the conjunctival epithelium. EP: conjunctival epithelium; ST: conjunctival stroma; SC: sclera. Scale bars: 100 μm.

3.3.4 Dynamic suspension culture of bioprinted hydrogel micro-constructs maintains encapsulated CjSCs phenotype, proliferation, and differentiation capacity

To be clinically translatable, the production of cell-based constructs transplants needs to be scalable to meet the high cell demands within the clinic and provide a cost-effective strategy for large scale in vitro culture. Suspension culture has been largely employed in the form of bioreactors including fed-batch and perfusion setups to efficiently culture cells at a large scale [71]. As a result, we subjected our CjSC-loaded hydrogel micro-constructs to dynamic suspension culture and evaluated their efficacy as a potential clinically translatable stem cell expansion system. Samples were cultured in a 6-well plate under constant agitation at 95 rpm and a significant increase in cell density was observed over time as visualized in Fig. 4A. More importantly, CellTiter-Glo® 3D cell viability assay demonstrated that dynamic suspension culture significantly enhanced cell viability compared to hydrogel micro-constructs cultured under static conditions at both day 3 and day 6 (Fig. 3.4B). These results also demonstrated that dynamic suspension culture enabled high cell density culture of CjSCs while maintaining the cell viability (Supplementary S3.3A). Immunofluorescence staining showed positive expression of the markers ABCG2, KRT14, P63, E-Cad and PAX6 in the hydrogel micro-constructs after 6 days in dynamic suspension culture, which indicated the retention of CjSCs properties in this culture system (Fig. 3.4C). Goblet cell differentiation was also performed to evaluate the functionality of the CjSCs after dynamic suspension culture. After 7 days of differentiation under dynamic suspension conditions, immunofluorescence staining confirmed positive expression of MUC5AC and MUC16 in the hydrogel micro-constructs (Fig. 3.4D).

3.3.5 Subconjunctival cell delivery of bioprinted CjSC-loaded hydrogel micro-constructs

Subconjunctival injection is a commonly used and minimally invasive approach for drug delivery to the ocular surface. Taking advantage of the ability to fabricate micron scale constructs via bioprinting, hydrogel micro-constructs containing CjSCs were produced as cylinders measuring in 100 μm diameter and 100 μm in height based on the inner diameter of a 30-gauge needle (i.e., 0.159 mm). We performed rheometry to assess if the bioprinted hydrogels experience shear thinning, which is a necessary property to retain the hydrogel construct's fidelity after subjecting it to syringe injection (Fig.3. 4E, Supplementary S3.3B, C). As the shear rate increases, the viscosity drastically decreases, indicating the hydrogel is shear thinning. To test the injectability directly, hydrogel micro-constructs were repeatedly aspirated and ejected with a 30-gauge syringe needle for 3 times. The geometrical integrity of the hydrogel micro-constructs was unchanged after the repeated aspiration and ejection, indicating the physical robustness of the hydrogel micro-constructs (Supplementary S3.3D). The samples were then cultured under dynamic suspension as previously described and Live/DeadTM staining at end point (i.e., day 7) showed high viability of the encapsulated CjSCs, which were comparable to the untreated controls (Supplementary S3.3E). We further tested the subconjunctival injection of the hydrogel micro-constructs on rabbit eyeballs. For ease of visualization, we used lentiviral vectors to label CjSCs with enhanced GFP (EGFP). Hydrogel micro-constructs cultured for 5 days in CjSCM were delivered by subconjunctival injection into the bulbar conjunctival epithelium while single cell suspensions at 106 cells/ml in 100 μl DPBS were also injected as controls. The injections were performed symmetrically on the four points (Supplementary S3.3C, red arrows) of the rabbit ocular surface with 30-gauge needles using a stereomicroscope. After injection, the rabbit eyeballs were incubated with DF12 supplemented with EGF for 24 hours with constant agitation at 95 rpm.

Tissue samples were then analyzed via immunofluorescence staining which confirmed a dense localization of the hydrogel micro-constructs containing EGFP positive CjSCs within the subconjunctival region compared to sparse fluorescence signals in the controls (Fig. 3.4F). Collectively, these results supported that the bioprinted hydrogel micro-constructs can be used to deliver CjSCs into the subconjunctival regions via injection and help immobilize them to the targeted area.

3.4 Discussion

Over the past few decades, regenerative medicine and stem cell therapies for ocular surface diseases have become a popular field with the growing demand for clinically translatable regenerative approaches [1,19,21]. However, CjSCs, one of the major stem cells on the ocular surface, have not yet been efficiently expanded *in vitro* [22,24,26]. Moreover, the lack of knowledge of the CjSC niche has made the development of 3D matrices supporting CjSCs growth a challenge [20,72]. Approaches involving minimally invasive ocular surface cell transplantation are critical to the successful application of CjSCs as a cell-based therapy [45]. Here, we present a clinically translatable approach using rapid bioprinting to fabricate hydrogel micro-constructs encapsulating CjSCs for subconjunctival injectable delivery on an ocular surface. We first established an efficient feeder-free in vitro culture system for CjSCs expansion using a culture medium containing a small molecule cocktail (i.e. A83-01 + DMH1 + Y27632). Then, we used DLP-based rapid bioprinting technology to fabricate injectable conjunctival GelMA hydrogel micro-constructs for the subconjunctival delivery of CjSCs. By varying the light exposure time and thus the stiffness of the resulting hydrogel using our bioprinting system, we generated hydrogel micro-constructs that supported the viability and stem cell behavior of the encapsulated CjSCs.

The hydrogel micro-constructs also enabled dynamic suspension culture of CjSCs for scalable and efficient expansion. In addition, ex vivo studies highlighted the ability of our CjSC-loaded hydrogel micro-constructs for successful subconjunctival delivery using clinically-relevant 30-gauge syringe needles and immobilization into the subconjunctival target site.

CjSCs have been popular in the last decade as they can potentially be applied in stem cell therapy to treat multiple ocular surface diseases [24,26]. However, an efficient *in vitro* expansion method for CjSCs derived from the primary conjunctival epithelium with high purity has not yet been reported [22,37]. To expand the CjSCs, we tested a small molecule cocktail that inhibited dual SMAD signaling and ROCK signaling. dSMADi and ROCKi, as well as their synergistic combination, have been reported to support sustained culture of basal stem cells in many other epithelia such as the airway, intestine and skin [28,29]. During primary culture, the formulation with A83-01, DMH1, Y27632 extensively promoted the growth of CjSCs in comparison with the epithelial basal medium. As such, we integrated these small molecules into the epithelial stem cell growth medium and developed the novel culture medium, CjSCM, tailored to support CjSCs proliferation. In this work, we successfully cultured highly homogenous CjSCs in vitro that can be expanded for more than 60 cell doublings while retaining the stem cell properties and the differentiation capacity into conjunctival goblet cells. These findings highlighted a significant step in establishing stable CjSCs in vitro expansion towards the understanding of CjSC-based developmental biology study and the development of novel therapies to treat ocular surface diseases.

Recent studies have revealed that the mechanical properties of extracellular matrix play a key role in cell fate determinant for resident stem cells [19,35,36]. However, despite efforts in locating the stem cell population within the conjunctiva, the mechanical properties of CjSC niche

remain largely unknown [22]. Therefore, a biofabrication system with control of biophysical property is needed to recapitulate the CjSC niche. DLP-based rapid bioprinting enables well-controlled tuning of the mechanical properties of the printed structures by simply changing the light exposure time for photo-crosslinking [51,52,54,64]. Due to the tunability of our bioprinting process to control the mechanical properties, we tested a range of hydrogel micro-constructs fabricated using different light exposure times to determine the optimal printing conditions. Our findings revealed that hydrogel micro-constructs fabricated with a 20 second light exposure resulted in the highest viability and retention of stem cell phenotype in CjSCs. Notably, our bioprinting system enables the fabrication of 18 cellularized hydrogel micro-constructs simultaneously with customizable geometries in less than a minute. This throughput can be further improved by adjusting the optical system in the bioprinter. Such a high throughput is required for scalable manufacturing applications. Interestingly, the measured modulus of our optimized hydrogel micro-constructs is different from the reported bulk modulus of conjunctival epithelium [73,74]. This result indicates the heterogeneity in mechanical properties of conjunctival epithelial microenvironments and that a relatively soft niche may be favored by resident CjSCs.

Various types of substrates, including 2D substrates such as AM and engineered gelatin membrane as well as 3D matrixes composed of compressed collagen and synthetic polymers have been reported to support ex vivo or in vitro culture of conjunctival epithelial cells [3,16,27,39,75]. However, the expansion of CjSCs has not been well addressed. Maintenance of these stem cell properties in CjSCs is critically important towards the development of effective therapies. In our study, the hydrogel micro-constructs were able to support the culture of encapsulated CjSCs while maintaining expression of the stem cell identity markers as confirmed by both immunofluorescences staining and real time qPCR. Furthermore, we found a significant up-

regulation in transcriptional expression of the stem cell markers (i.e. KRT14, P63) and lineage marker (i.e. PAX6) in the hydrogel micro-constructs after 6 days of static culture, suggesting that the hydrogel micro-constructs favorably recapitulated the biomechanical and biochemical matrix properties of native niche for CjSCs to maintain their stem cell phenotype. The hydrogel micro-constructs were also physically stable after prolonged incubation under physiological conditions as no notable changes in the modulus or the equilibrium swelling ratio were detected after 6 days. Furthermore, successful goblet cell differentiation in the hydrogel micro-constructs under static conditions showed preserved functionality of the encapsulated CjSCs. Overall, these results agreed well with the previous findings on the supportive role of bioprinted hydrogel micro-constructs in stem cell culture [51,52,54]. Integrated with bioprinting technology, this platform would broaden the utility of CjSCs for cell-based therapies and in vitro disease modeling [76].

Scalable manufacturing is a necessary step towards the development of a clinically translatable product and suspension culture has been favorable for the enhanced uptake of nutrients, reduced cost, and increased scalability [19,71]. Dynamic suspension culture with hydrogel has been found to facilitate stem cell expansion [77–79]. To explore the potential application of our bioprinted hydrogel micro-constructs as a clinically relevant cell-based delivery system we performed dynamic suspension culture. The encapsulated stem cells proliferated rapidly under dynamic suspension culture compared with static culture conditions, as the suspension group was 1.5-fold more viable than the static control after 3 days of dynamic suspension culture. This was coupled with significantly higher metabolic activities in the dynamic suspension culture samples compared to the static culture controls. These results indicated that dynamic suspension culture promoted the proliferation and viability of encapsulated CjSCs. In addition, encapsulated CjSCs reserved the stem cell identity and were able to be differentiated towards conjunctival goblet cells

post dynamic suspension culture. In summary, dynamic suspension culture promoted viability, proliferation, and retained the stem cell properties and the differentiation potential of CjSC-loaded hydrogel micro-constructs and demonstrated their potential for scalable culturing applications.

Patients with severe ocular surface disorders are commonly treated with surgical transplantation of allografts, such as AM [13–17], which involves suture-based surgical transplantation and requires time consuming postsurgical recovery [41]. To address these challenges, we fabricated injectable CjSC-loaded hydrogel micro-constructs applicable for clinical subconjunctival cell delivery. We confirmed with rheometry that the bulk 5% GelMA hydrogel is shear thinning and therefore is a good candidate for an injectable hydrogel application to ensure minimally invasive delivery is maintained and to eliminate potential leakage after injection. We chose to use a 30-gauge syringe needle that is commonly employed in clinical practice for subconjunctival injection. The shear thinning hydrogel also protected the encapsulated cells from shear forces during injection while delivering cells at high densities into the targeted region. To test the injectability of our hydrogel micro-constructs, we prepared hydrogel micro-constructs measuring 100 μm diameter and 100 μm in height, which were designed to fit inside a 30-gauge syringe needle that has an inner diameter of 0.159 mm for injectable delivery. Our findings demonstrated that our bioprinted hydrogel micro-constructs were able to preserve the viability of encapsulated CjSCs after multiple injections through the 30-gauge syringe needle. Furthermore, the rheological properties of hydrogel as well as the tensile nature of the conjunctival epithelium both support the immobilization of hydrogel micro-constructs [73,80,81]. Subconjunctival injection of the hydrogel micro-constructs was able to deliver a relatively large number of cells (approximately 30,000 cells per construct) into the subconjunctival region of rabbit eyeballs with a single injection and facilitated the retention of the transplanted cells within the target region. This

work has laid the foundation for future in vivo tests in animal models of ocular surface diseases such as Stevens-Johnson syndrome that would further support clinical applications.

3.5 Conclusion

DLP-based rapid bioprinting was applied to fabricate injectable hydrogel micro-constructs loaded with CjSCs for ocular stem cell transplantation. By incorporating a small molecule cocktail in the culture medium, we were able to produce homogenous CjSCs with high replicative potential and differentiation capacity. The tunability for mechanical properties, granted by our bioprinting system, enabled the rapid fabrication of hydrogel micro-constructs that promoted the viability and stem cell properties of encapsulated CjSCs. The hydrogel micro-constructs could also be applied to dynamic suspension culture of CjSCs for potential large-scale production in clinical applications. Furthermore, our hydrogel micro-constructs were readily injected through a 30-gauge syringe needle without compromising cell viability or physical deformation and were suitable for subconjunctival delivery as well as immobilization to the target subconjunctival region as demonstrated in an ex vivo rabbit eyeball model.

The efficient CjSCs feeder-free in vitro expansion approach developed in this study can be translated to different cell therapy applications and provide insight on the stem cell population within the conjunctiva. Our injectable hydrogel micro-constructs can also be extended to incorporate patient-derived cells for autograft or iPSC-derived cells and donor cells for allograft to treat patients requiring ocular surface regeneration. Besides, this study has illustrated the application of bioprinting on CjSCs and provided insight on the mechanical properties that supported the CjSCs encapsulation, which can be translated to future studies with clinically relevant materials and overcome the regulatory limits of GelMA. In addition, our minimally

invasive CjSCs delivery approach can serve as a potential strategy for the treatment of ocular diseases such as the ocular cicatricial pemphigoid, Stevens-Johnson syndrome, and toxic epidermal necrolysis. Implications from the successful expansion of CjSCs are beneficial for the further studies focused on the understanding of eye development and pathogenesis of many ocular surface diseases. The versatility of our hydrogel micro-constructs platform also allows the flexibility to incorporate multiple cell types and/or bioactive constituents for injectable delivery for next generation cell-based therapies such as the injectable delivery of stem cell-derived cytokines or exosomes to enhance the efficacy of clinical treatments.

Acknowledgements

Chapter 3, in full, is a reprint of the published article, "Rapid Bioprinting of Conjunctival Stem Cell Micro-constructs for Subconjunctival Ocular Injection", Z. Zhong, X. Deng, P. Wang, C. Yu, W. Kiratitanaporn, X. Wu, J. Schimelman, M. Tang, A. Balayan, E. Yao, J. Tian, L. Chen, K. Zhang, S.C. Chen, *Biomaterials*, 2020. The dissertation author was the primary investigator and author of this paper. This work was supported in part by grants from the National Institutes of Health (R21 EY031122, R01 EB02185) and National Science Foundation (1937653). This material is based upon work supported by the National Science Foundation Graduate Research Fellowship Program under Grant No. DGE-1650112.

Supplementary Information

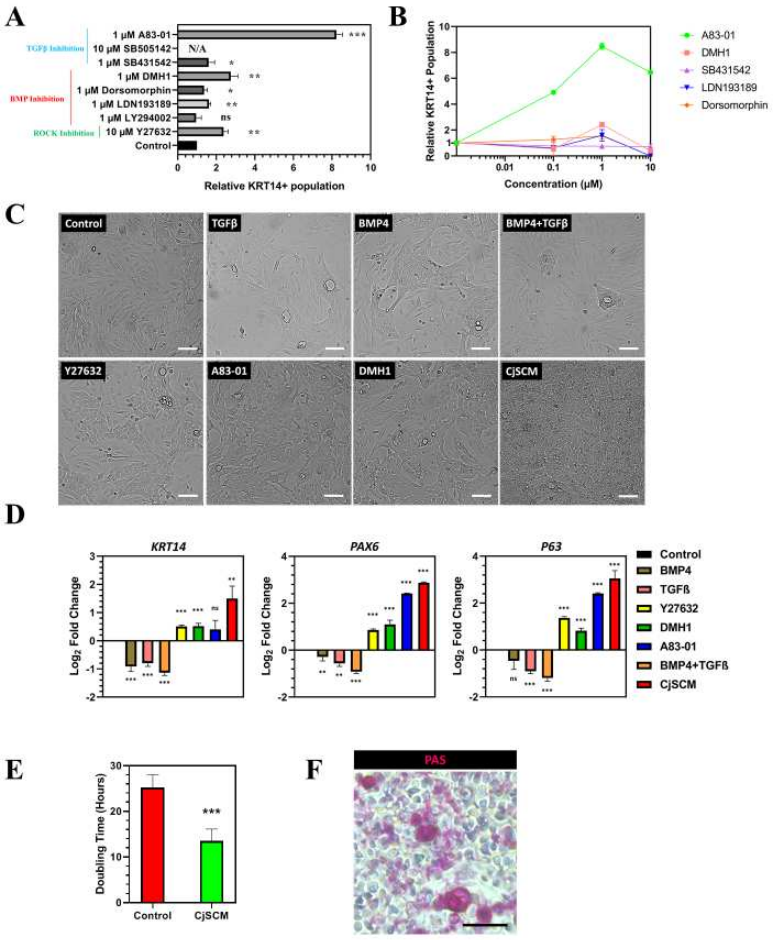

Supplementary Figure S3.1. Component test. (A) Flow cytometry analysis of primary conjunctival epithelial cells cultured in various conditions for 5 days (mean ± SD, n = 3, ns: non-significant; *: $P < 0.05$; **: $P < 0.01$; ***: $P < 0.001$). The cells were stained with anti-KRT14 antibody. The KRT14 positive population was considered as the stem cell population. The number of KRT14 positive cells was normalized by the number of positive cells in the control. Different components used in the test were grouped by their targeting signaling pathways (i.e. TGFβ, BMP, ROCK). (B) Flow cytometry analysis of KRT14 positive population in primary conjunctival epithelial cells cultured in media with different concentrations of the components (mean ± SD). (C) Cell morphologies of primary conjunctival epithelial cells cultured in various conditions (i.e. 100 ng/ml TGFβ, 100 ng/ml BMP4, 100 ng/ml TGFβ + 100 ng/ml BMP4, 1 μM A83-01, 1 μM DMH, 10 μM Y27632) for 4 days. Scale bars: 100 μm. (D) Real time qPCR showing the relative mRNA expression of stem cell markers (i.e. KRT14, P63) and lineage marker (i.e. PAX6) in primary conjunctival epithelial cells under various culture conditions for 4 days (mean ± SD, n = 3, ns: non-significant; **: $P < 0.01$; ***: $P < 0.001$). (E) Average cell doubling time of conjunctival epithelial cells in culture with control medium and CjSCM from P0 to P10 (mean ± SD, n = 3; ***: $P < 0.001$). (F) Periodic acid–Schiff (PAS) staining of the differentiated cells. Purple staining indicates presence of mucin. Scale bars: 100 μm.

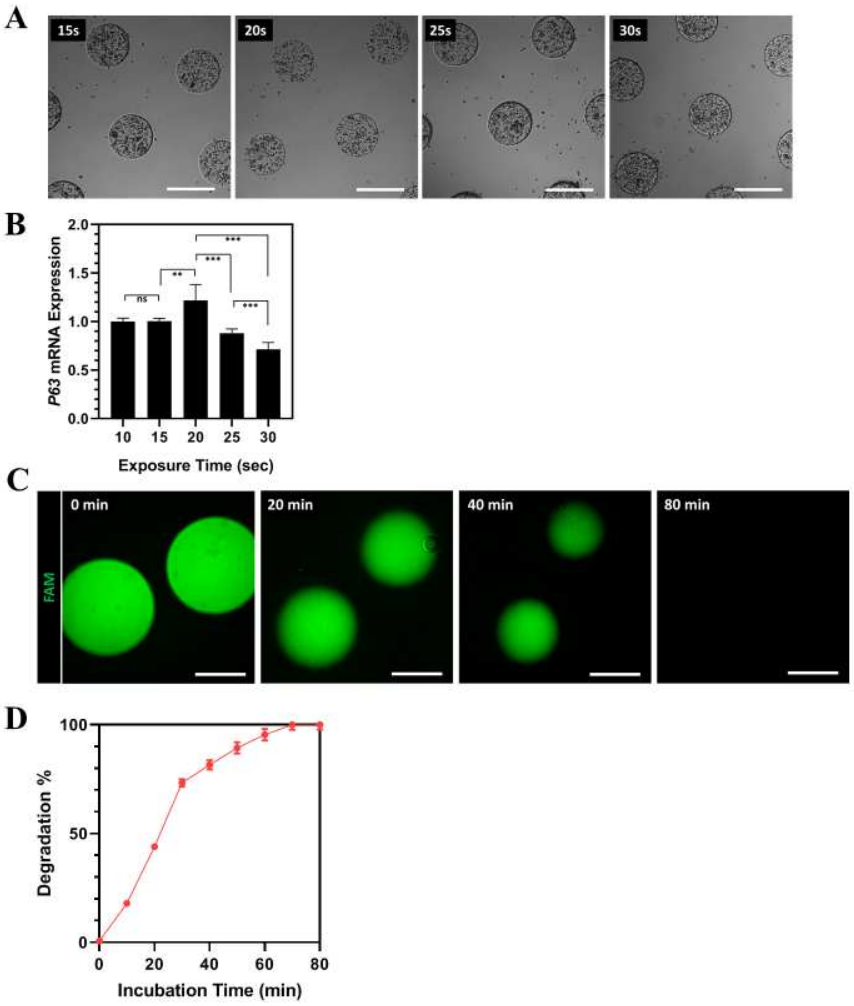

Supplementary Figure S3.2. 3D viability and biodegradability. (A) Representative images of CjSC-loaded hydrogel micro-constructs (107 cells/ml) fabricated with different exposure times. Scale bars: 500 µm. (B) Real time qPCR of the stemness marker P63 on CjSC-loaded hydrogel micro-constructs printed under different exposure times. The mRNA expression of P63 was normalized with the group with 10s exposure (mean ± SD, n = 3, ns: non-significant; **: $P < 0.01$; ***: $P < 0.001$). (C) Representative fluorescent images of fluorescein (FAM)-loaded acellular hydrogel constructs incubated with 10 µg/ml collagenase solution for different period of time. Scale bars: 1 mm. (D) Plot of degradation of the FAM-loaded acellular hydrogel constructs versus time (mean ± SD, n = 6).

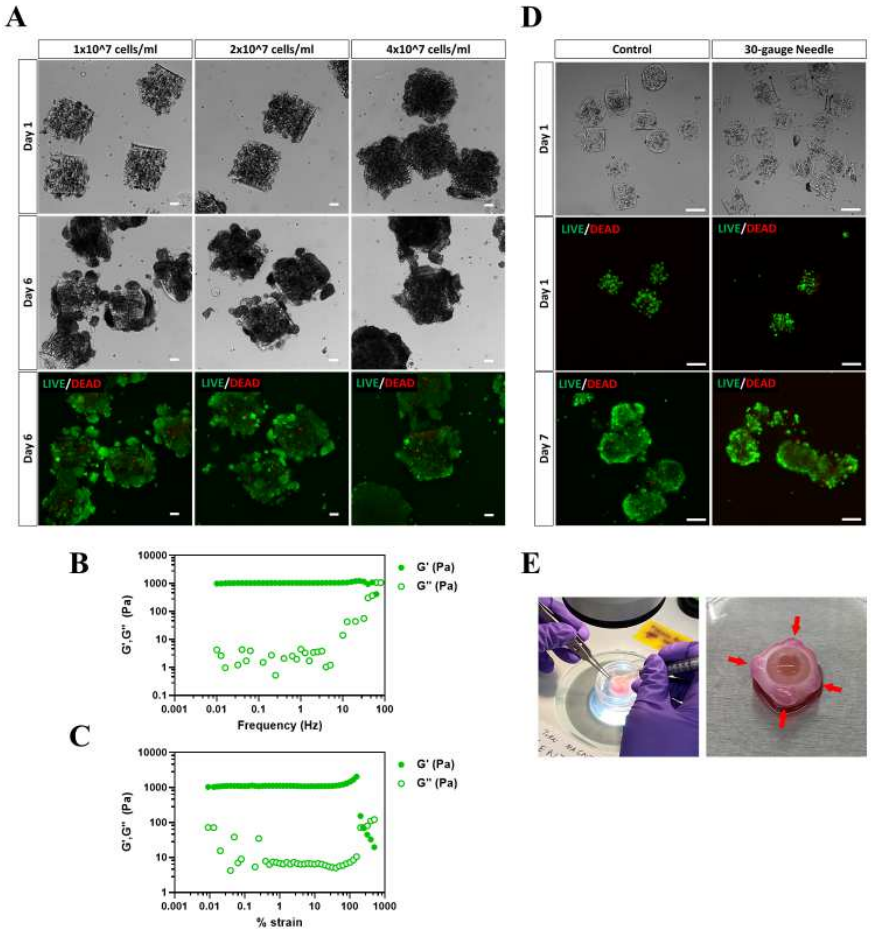

Supplementary Figure S3.3. Dynamic suspension culture and injectable delivery of CjSCs. (A) Representative images of hydrogel micro-constructs encapsulated with different concentrations of CjSCs in dynamic suspension culture. At day 6 of culture, the hydrogel micro-constructs were subjected to Live/Dead^{TM} staining to evaluate the viability. Scale bars: 100 µm. (B) Rheometry frequency sweep and (C) stain sweep for the hydrogel composition of the micro-constructs demonstrating a predominate and consistent elastic response (G', storage modulus) as compared to the viscous response (G", loss modulus) across both sweeps (mean, n = 3). (D) CjSC-loaded hydrogel micro-constructs (5×106 cells/ml) after repeated aspiration and ejection through a 30-gauge syringe while non-treated samples served as the control. All the CjSC-loaded hydrogel micro-constructs were kept in dynamic suspension culture post repeated ejection and aspiration tests. Live/DeadTM staining was performed on the repeatedly injected and non-treated samples at day 1 and day 7 of culture. Scale bars: 100 µm. (E) Subconjunctival delivery of the injectable transplants encapsulating CjSCs where the red arrows highlight the injected sites.

Supplementary Table 3.1. Antibody List

Antibody	Catalog	Vendor	Dilution
Anti-mouse IgG (H+L), F(ab')2 Fragment (Alexa Fluor® 488 Conjugate) #4408	4408S	Cell Signaling Technologies	1:500
Anti-rabbit IgG (H+L), F(ab')2 Fragment (Alexa Fluor® 555 Conjugate) #4413	4413S	Cell Signaling Technologies	1:500
Anti-rabbit IgG (H+L), F(ab')2 Fragment (Alexa Fluor® 488 Conjugate) #4412	4412S	Cell Signaling Technologies	1:500
Anti-mouse IgG (H+L), F(ab')2 Fragment (Alexa Fluor® 647 Conjugate) #4410	4410S	Cell Signaling Technologies	1:500
E-Cadherin (4A2) Mouse mAb	14472S	Cell Signaling Technologies	1:100
Keratin 14 Polyclonal Antibody, Purified	905301	BioLegend	1:100
Purified anti-Pax-6 Antibody	901301	BioLegend	1:200
Purified Mouse Anti-Ki-67	550609	BD Pharmagin	1:100
MUC5AC Monoclonal Antibody (45M1)	12178	Invitrogen	1:100
Anti p63 antibody[N2C1]	GTX102425	GeneTex	1:200
Anti-BCRP/ABCG2 antibody[BXP-21] (ab3380)	AB3380	Abcam	1:100
Anti-MUC16 antibody[X75]	ab1107	Abcam	1:100
DAPI (4',6-Diamidino-2-Phenylindole, Dihydrochloride)	D1306	ThermoFisher Scientific	1:500
Flash Phalloidin™ Red 594	424203	BioLegend	1:100

Supplementary Table 3.2. Primers for Real Time qPCR.

Gene		5' → 3'
Pax6	Forward	GTATTCTTGCTTCAGGTAGAT
	Reverse	GAGGCTCAAATGCGACTTCAGCT
Krt14	Forward	CCCAGTTCTCCTCGGGCTCT
	Reverse	GTGGGAGGACACCACCTTGC
p63	Forward	GAACGGCTCCTCGTCCACCA
	Reverse	GACGGCGAGAGGGCATCGAA
Gapdh	Forward	TGGTGAAGGTCGGAGTGAAC
	Reverse	ATGTAGTGGAGGTCAATGAATGG

Reference

[1] P. Nguyen, S. Khashabi, S. C, Ocular Surface Reconstitution, in: Prog. Mol. Environ. Bioeng. - From Anal. Model. to Technol. Appl., 2011. https://doi.org/10.5772/22879.

[2] I.K. Gipson, Goblet cells of the conjunctiva: A review of recent findings, Prog. Retin. Eye

Res. (2016). https://doi.org/10.1016/j.preteyeres.2016.04.005.

[3] S. Barabino, M. Rolando, G. Bentivoglio, C. Mingari, S. Zanardi, R. Bellomo, G. Calabria, Role of amniotic membrane transplantation for conjunctival reconstruction in ocular-cicatricial pemphigoid, Ophthalmology. (2003). https://doi.org/10.1016/S0161-6420(02)01892-4.

[4] D.G. Gregory, The ophthalmologic management of acute Stevens-Johnson syndrome, Ocul. Surf. (2008). https://doi.org/10.1016/S1542-0124(12)70273-2.

[5] M. Li, M. Zhu, Y. Yu, L. Gong, N. Zhao, M.J. Robitaille, Comparison of conjunctival autograft transplantation and amniotic membrane transplantation for pterygium: A meta-analysis, Graefe's Arch. Clin. Exp. Ophthalmol. (2012). https://doi.org/10.1007/s00417-011-1820-8.

[6] D. Meller, R.T.F. Pires, R.J.S. Mack, F. Figueiredo, A. Heiligenhaus, W.C. Park, P. Prabhasawat, T. John, S.D. McLeod, K.P. Steuhl, S.C.G. Tseng, Amniotic membrane transplantation for acute chemical or thermal burns, Ophthalmology. (2000). https://doi.org/10.1016/S0161-6420(00)00024-5.

[7] H. Hashemi, M. Khabazkhoob, A. Yekta, E. Jafarzadehpour, H. Ostadimoghaddam, H. Kangari, The prevalence and determinants of pterygium in rural areas, J. Curr. Ophthalmol. (2017). https://doi.org/10.1016/j.joco.2016.09.002.

[8] B. Rzany, M. Mockenhaupt, S. Baur, W. Schröder, U. Stocker, J. Mueller, N. Holländer, R. Bruppacher, E. Schöpf, Epidemiology of erythema exsudativum multiforme majus, Stevens-Johnson syndrome, and toxic epidermal necrolysis in Germany (1990-1992): Structure and results of a population-based registry, J. Clin. Epidemiol. (1996). https://doi.org/10.1016/0895-4356(96)00035-2.

[9] P. Bernard, L. Vaillant, B. Labeille, C. Bedane, B. Arbeille, J.P. Denoeux, G. Lorette, J.M. Bonnetblanc, C. Prost, Incidence and Distribution of Subepidermal Autoimmune Bullous Skin Diseases in Three French Regions, Arch. Dermatol. (1995). https://doi.org/10.1001/archderm.1995.01690130056010.

[10] A.J. Lee, J. Lee, S.M. Saw, G. Gazzard, D. Koh, D. Widjaja, D.T.H. Tan, Prevalence and risk factors associated with dry eye symptoms: A population based study in Indonesia, Br. J. Ophthalmol. (2002). https://doi.org/10.1136/bjo.86.12.1347.

[11] M.T. Rodríguez-Ares, Prevalence of pinguecula and pterygium in a general population in Spain, Eye. (2011). https://doi.org/10.1038/eye.2010.204.

[12] S. Barabino, Y. Chen, S. Chauhan, R. Dana, Ocular surface immunity: Homeostatic mechanisms and their disruption in dry eye disease, Prog. Retin. Eye Res. (2012). https://doi.org/10.1016/j.preteyeres.2012.02.003.

[13] E. Clearfield, V. Muthappan, X. Wang, I.C. Kuo, Conjunctival autograft for pterygium, Cochrane Database Syst. Rev. (2016). https://doi.org/10.1002/14651858.CD011349.pub2.

[14] P. V. Morgan, J.D. Suh, C.J. Hwang, Nasal floor mucosa: New donor site for mucous membrane grafts, Ophthal. Plast. Reconstr. Surg. (2016). https://doi.org/10.1097/IOP.0000000000000451.

[15] J. Liu, H. Sheha, Y. Fu, L. Liang, S.C.G. Tseng, Update on amniotic membrane transplantation, Expert Rev. Ophthalmol. (2010). https://doi.org/10.1586/eop.10.63.

[16] S. Dehghani, M. Rasoulianboroujeni, H. Ghasemi, S.H. Keshel, Z. Nozarian, M.N. Hashemian, M. Zarei-Ghanavati, G. Latifi, R. Ghaffari, Z. Cui, H. Ye, L. Tayebi, 3D-Printed membrane as an alternative to amniotic membrane for ocular surface/conjunctival defect reconstruction: An in vitro & in vivo study, Biomaterials. (2018). https://doi.org/10.1016/j.biomaterials.2018.05.013.

[17] Q. Pan, A. Angelina, M. Marrone, W.J. Stark, E.K. Akpek, Autologous serum eye drops for dry eye, Cochrane Database Syst. Rev. (2017). https://doi.org/10.1002/14651858.CD009327.pub3.

[18] S.C.G. Tseng, H. He, S. Zhang, S.Y. Chen, Niche Regulation of Limbal Epithelial Stem Cells: Relationship between Inflammation and Regeneration, Ocul. Surf. (2016). https://doi.org/10.1016/j.jtos.2015.12.002.

[19] H. Xia, X. Li, W. Gao, X. Fu, R.H. Fang, L. Zhang, K. Zhang, Tissue repair and regeneration with endogenous stem cells, Nat. Rev. Mater. 3 (2018) 174–193. https://doi.org/10.1038/s41578-018-0027-6.

[20] T. Nakamura, T. Inatomi, C. Sotozono, N. Koizumi, S. Kinoshita, Ocular surface reconstruction using stem cell and tissue engineering, Prog. Retin. Eye Res. (2016). https://doi.org/10.1016/j.preteyeres.2015.07.003.

[21] R. Williams, R. Lace, S. Kennedy, K. Doherty, H. Levis, Biomaterials for Regenerative Medicine Approaches for the Anterior Segment of the Eye, Adv. Healthc. Mater. 7 (2018). https://doi.org/10.1002/adhm.201701328.

[22] R.M.K. Stewart, C.M. Sheridan, P.S. Hiscott, G. Czanner, S.B. Kaye, Human Conjunctival Stem Cells are Predominantly Located in the Medial Canthal and Inferior Forniceal Areas, Invest. Ophthalmol. Vis. Sci. 56 (2015) 2021–2030. https://doi.org/10.1167/iovs.14-16266.

[23] J.H. Stern, Y. Tian, J. Funderburgh, G. Pellegrini, K. Zhang, J.L. Goldberg, R.R. Ali, M. Young, Y. Xie, S. Temple, Regenerating Eye Tissues to Preserve and Restore Vision, Cell Stem Cell. (2018). https://doi.org/10.1016/j.stem.2018.05.013.

[24] T. Ramos, D. Scott, S. Ahmad, An Update on Ocular Surface Epithelial Stem Cells: Cornea and Conjunctiva, Stem Cells Int. (2015). https://doi.org/10.1155/2015/601731.

[25] H. Ouyang, Y. Xue, Y. Lin, X. Zhang, L. Xi, S. Patel, H. Cai, J. Luo, M. Zhang, M. Zhang, Y. Yang, G. Li, H. Li, W. Jiang, E. Yeh, J. Lin, M. Pei, J. Zhu, G. Cao, L. Zhang, B. Yu, S. Chen, X.D. Fu, Y. Liu, K. Zhang, WNT7A and PAX6 define corneal epithelium homeostasis and pathogenesis, Nature. (2014). https://doi.org/10.1038/nature13465.

[26] F. Majo, A. Rochat, M. Nicolas, G.A. Jaoudé, Y. Barrandon, Oligopotent stem cells are distributed throughout the mammalian ocular surface, Nature. (2008). https://doi.org/10.1038/nature07406.

[27] M. Bertolin, C. Breda, S. Ferrari, S.I. Van Acker, N. Zakaria, E. Di Iorio, A. Migliorati, D. Ponzin, B. Ferrari, Z. Lužnik, V. Barbaro, Optimized protocol for regeneration of the conjunctival epithelium using the cell suspension technique, Cornea. (2019). https://doi.org/10.1097/ICO.0000000000001670.

[28] H. Mou, V. Vinarsky, P.R. Tata, K. Brazauskas, S.H. Choi, A.K. Crooke, B. Zhang, G.M. Solomon, B. Turner, H. Bihler, J. Harrington, A. Lapey, C. Channick, C. Keyes, A. Freund, S. Artandi, M. Mense, S. Rowe, J.F. Engelhardt, Y.C. Hsu, J. Rajagopal, Dual SMAD Signaling Inhibition Enables Long-Term Expansion of Diverse Epithelial Basal Cells, Cell Stem Cell. (2016). https://doi.org/10.1016/j.stem.2016.05.012.

[29] C. Zhang, H.J. Lee, A. Shrivastava, R. Wang, T.J. McQuiston, S.S. Challberg, B.A. Pollok, T. Wang, Long-Term In Vitro Expansion of Epithelial Stem Cells Enabled by Pharmacological Inhibition of PAK1-ROCK-Myosin II and TGF-β Signaling, Cell Rep. 25 (2018) 598-610.e5. https://doi.org/10.1016/j.celrep.2018.09.072.

[30] K. Kobielak, N. Stokes, J. De La Cruz, L. Polak, E. Fuchs, Loss of a quiescent niche but not follicle stem cells in the absence of bone morphogenetic protein signaling, Proc. Natl. Acad. Sci. U. S. A. (2007). https://doi.org/10.1073/pnas.0703004104.

[31] N. Oshimori, E. Fuchs, Paracrine TGF-β signaling counterbalances BMP-mediated repression in hair follicle stem cell activation, Cell Stem Cell. (2012). https://doi.org/10.1016/j.stem.2011.11.005.

[32] X.C. He, J. Zhang, W.G. Tong, O. Tawfik, J. Ross, D.H. Scoville, Q. Tian, X. Zeng, X. He, L.M. Wiedemann, Y. Mishina, L. Li, BMP signaling inhibits intestinal stem cell self-renewal through suppression of Wnt-β-catenin signaling, Nat. Genet. (2004). https://doi.org/10.1038/ng1430.

[33] P.R. Tata, H. Mou, A. Pardo-Saganta, R. Zhao, M. Prabhu, B.M. Law, V. Vinarsky, J.L. Cho, S. Breton, A. Sahay, B.D. Medoff, J. Rajagopal, Dedifferentiation of committed epithelial cells into stem cells in vivo, Nature. (2013). https://doi.org/10.1038/nature12777.

[34] M. Amano, M. Nakayama, K. Kaibuchi, Rho-kinase/ROCK: A key regulator of the cytoskeleton and cell polarity, Cytoskeleton. (2010). https://doi.org/10.1002/cm.20472.

[35] S.W. Lane, D.A. Williams, F.M. Watt, Modulating the stem cell niche for tissue regeneration, Nat. Biotechnol. (2014). https://doi.org/10.1038/nbt.2978.

[36] K.H. Vining, D.J. Mooney, Mechanical forces direct stem cell behaviour in development and regeneration, Nat. Rev. Mol. Cell Biol. (2017). https://doi.org/10.1038/nrm.2017.108.

[37] D. Meller, V. Dabul, S.C.G. Tseng, Expansion of conjunctival epithelial progenitor cells on amniotic membrane, Exp. Eye Res. (2002). https://doi.org/10.1006/exer.2001.1163.

[38] J.R.S. Ricardo, P.C. Cristovam, P.A.N. Filho, C.C. Farias, A.L. De Araujo, R.R. Loureiro, J.L. Covre, J.N. De Barros, T.P. Barreiro, M.S. Dos Santos, J.A.P. Gomes, Transplantation of conjunctival epithelial cells cultivated ex vivo in patients with total limbal stem cell deficiency, Cornea. (2013). https://doi.org/10.1097/ICO.0b013e31825034be.

[39] C.C. Drechsler, A. Kunze, A. Kureshi, G. Grobe, S. Reichl, G. Geerling, J.T. Daniels, S. Schrader, Development of a conjunctival tissue substitute on the basis of plastic compressed collagen, J. Tissue Eng. Regen. Med. 11 (2017) 896–904. https://doi.org/10.1002/term.1991.

[40] A.Y. Cheung, E. Sarnicola, M. Eslani, K.H. Kurji, B.M. Genereux, A. Govil, E.J. Holland, Infectious keratitis after ocular surface stem cell transplantation, Cornea. (2018). https://doi.org/10.1097/ICO.0000000000001690.

[41] A. Riemens, L.C.J. Te Boome, V. Kalinina Ayuso, J.J.W. Kuiper, S.M. Imhof, H.M. Lokhorst, R. Aniki, Impact of ocular graft-versus-host disease on visual quality of life in patients after allogeneic stem cell transplantation: Questionnaire study, Acta Ophthalmol. (2014). https://doi.org/10.1111/aos.12047.

[42] N. Nassiri, M. Eslani, N. Panahi, S. Mehravaran, A. Ziaei, A.R. Djalilian, Ocular graft versus host disease following allogeneic stem cell transplantation: A review of current knowledge and recommendations, J. Ophthalmic Vis. Res. (2013). https://doi.org/10.1038/s41409-018-0090-z.

[43] U. Agraval, P. Rundle, I.G. Rennie, S. Salvi, Fresh frozen amniotic membrane for conjunctival reconstruction after excision of neoplastic and presumed neoplastic conjunctival lesions, Eye. (2017). https://doi.org/10.1038/eye.2016.322.

[44] N.N. Ashraf, M.I. Adhi, Outcome of application of amniotic membrane graft in ocular surface disorders, J. Pak. Med. Assoc. (2017).

[45] Z. Zhang, Injectable biomaterials for stem cell delivery and tissue regeneration, Expert Opin. Biol. Ther. 17 (2017) 49–62. https://doi.org/10.1080/14712598.2017.1256389.

[46] L. Koivusalo, J. Karvinen, E. Sorsa, I. Jönkkäri, J. Väliaho, P. Kallio, T. Ilmarinen, S. Miettinen, H. Skottman, M. Kellomäki, Hydrazone crosslinked hyaluronan-based hydrogels for therapeutic delivery of adipose stem cells to treat corneal defects, Mater. Sci. Eng. C. (2018). https://doi.org/10.1016/j.msec.2017.12.013.

[47] Y. Ke, Y. Wu, X. Cui, X. Liu, M. Yu, C. Yang, X. Li, Polysaccharide hydrogel combined with mesenchymal stem cells promotes the healing of corneal alkali burn in rats, PLoS One. (2015). https://doi.org/10.1371/journal.pone.0119725.

[48] X. Qu, W. Zhu, S. Huang, Y.S. Li, S. Chien, K. Zhang, S. Chen, Relative impact of uniaxial alignment vs. form-induced stress on differentiation of human adipose derived stem cells, Biomaterials. (2013). https://doi.org/10.1016/j.biomaterials.2013.09.009.

[49] P. Soman, J.W. Lee, A. Phadke, S. Varghese, S. Chen, Spatial tuning of negative and positive Poisson's ratio in a multi-layer scaffold, Acta Biomater. (2012). https://doi.org/10.1016/j.actbio.2012.03.035.

[50] K.C. Hribar, Y.S. Choi, M. Ondeck, A.J. Engler, S. Chen, Digital plasmonic patterning for localized tuning of hydrogel stiffness, Adv. Funct. Mater. (2014). https://doi.org/10.1002/adfm.201400274.

[51] C. Yu, X. Ma, W. Zhu, P. Wang, K.L. Miller, J. Stupin, A. Koroleva-Maharajh, A. Hairabedian, S. Chen, Scanningless and continuous 3D bioprinting of human tissues with decellularized extracellular matrix, Biomaterials. 194 (2019) 1–13. https://doi.org/10.1016/j.biomaterials.2018.12.009.

[52] X. Ma, X. Qu, W. Zhu, Y.S. Li, S. Yuan, H. Zhang, J. Liu, P. Wang, C.S.E. Lai, F. Zanella, G.S. Feng, F. Sheikh, S. Chien, S. Chen, Deterministically patterned biomimetic human iPSC-derived hepatic model via rapid 3D bioprinting, Proc. Natl. Acad. Sci. U. S. A. (2016). https://doi.org/10.1073/pnas.1524510113.

[53] P. Soman, B.T.D. Tobe, J.W. Lee, A.M. Winquist, I. Singec, K.S. Vecchio, E.Y. Snyder, S. Chen, Three-dimensional scaffolding to investigate neuronal derivatives of human embryonic stem cells, Biomed. Microdevices. (2012). https://doi.org/10.1007/s10544-012-9662-7.

[54] C. Yu, W. Zhu, B. Sun, D. Mei, M. Gou, S. Chen, Modulating physical, chemical, and biological properties in 3D printing for tissue engineering applications, Appl. Phys. Rev. 5 (2018). https://doi.org/10.1063/1.5050245.

[55] K.C. Hribar, D. Finlay, X. Ma, X. Qu, M.G. Ondeck, P.H. Chung, F. Zanella, A.J. Engler, F. Sheikh, K. Vuori, S.C. Chen, Nonlinear 3D projection printing of concave hydrogel microstructures for long-term multicellular spheroid and embryoid body culture, Lab Chip. (2015). https://doi.org/10.1039/c5lc00159e.

[56] S. Raghava, M. Hammond, U.B. Kompella, Periocular routes for retinal drug delivery, Expert Opin. Drug Deliv. (2004). https://doi.org/10.1517/17425247.1.1.99.

[57] J.A. Nowak, E. Fuchs, Isolation and culture of epithelial stem cells, Methods Mol. Biol. (2009). https://doi.org/10.1007/978-1-59745-060-7_14.

[58] H.A. McCauley, G. Guasch, Three cheers for the goblet cell: Maintaining homeostasis in mucosal epithelia, Trends Mol. Med. (2015). https://doi.org/10.1016/j.molmed.2015.06.003.

[59] J.T. Henriksson, T.G. Coursey, D.B. Corry, C.S. De Paiva, S.C. Pflugfelder, IL-13 stimulates proliferation and expression of mucin and immunomodulatory genes in cultured conjunctival goblet cells, Investig. Ophthalmol. Vis. Sci. (2015). https://doi.org/10.1167/iovs.14-15496.

[60] H.A. McCauley, C.Y. Liu, A.C. Attia, K.A. Wikenheiser-Brokamp, Y. Zhang, J.A. Whitsett, G. Guasch, TGFβ signaling inhibits goblet cell differentiation via SPDEF in conjunctival epithelium, Dev. (2014). https://doi.org/10.1242/dev.117804.

[61] M. Tang, Q. Xie, R.C. Gimple, Z. Zhong, T. Tam, J. Tian, R.L. Kidwell, Q. Wu, B.C. Prager, Z. Qiu, A. Yu, Z. Zhu, P. Mesci, H. Jing, J. Schimelman, P. Wang, D. Lee, M.H. Lorenzini, D. Dixit, L. Zhao, S. Bhargava, T.E. Miller, X. Wan, J. Tang, B. Sun, B.F. Cravatt, A.R. Muotri, S. Chen, J.N. Rich, Three-dimensional bioprinted glioblastoma microenvironments model cellular dependencies and immune interactions, Cell Res. (2020). https://doi.org/10.1038/s41422-020-0338-1.

[62] H. Shirahama, B.H. Lee, L.P. Tan, N.J. Cho, Precise tuning of facile one-pot gelatin methacryloyl (GelMA) synthesis, Sci. Rep. (2016). https://doi.org/10.1038/srep31036.

[63] P. Wang, X. Li, W. Zhu, Z. Zhong, A. Moran, W. Wang, K. Zhang, S. Chen, 3D bioprinting of hydrogels for retina cell culturing, Bioprinting. (2018). https://doi.org/10.1016/j.bprint.2018.e00029.

[64] X. Ma, C. Yu, P. Wang, W. Xu, X. Wan, C.S.E. Lai, J. Liu, A. Koroleva-Maharajh, S. Chen, Rapid 3D bioprinting of decellularized extracellular matrix with regionally varied mechanical properties and biomimetic microarchitecture, Biomaterials. (2018). https://doi.org/10.1016/j.biomaterials.2018.09.026.

[65] M.H. Chen, L.L. Wang, J.J. Chung, Y.H. Kim, P. Atluri, J.A. Burdick, Methods to Assess Shear-Thinning Hydrogels for Application As Injectable Biomaterials, ACS Biomater. Sci. Eng. (2017). https://doi.org/10.1021/acsbiomaterials.7b00734.

[66] H. Alam, L. Sehgal, S.T. Kundu, S.N. Dalal, M.M. Vaidya, Novel function of keratins 5 and 14 in proliferation and differentiation of stratified epithelial cells, Mol. Biol. Cell. (2011). https://doi.org/10.1091/mbc.E10-08-0703.

[67] S. Merjava, A. Neuwirth, M. Tanzerova, K. Jirsova, The spectrum of cytokeratins expressed in the adult human cornea, limbus and perilimbal conjunctiva, Histol. Histopathol. (2011). https://doi.org/10.14670/HH-26.323.

[68] G. Pellegrini, E. Dellambra, O. Golisano, E. Martinelli, I. Fantozzi, S. Bondanza, D. Ponzin, F. McKeon, M. De Luca, p63 identifies keratinocyte stem cells, Proc. Natl. Acad. Sci. U. S.

A. (2001). https://doi.org/10.1073/pnas.061032098.

[69] I.K. Gipson, S. Spurr-Michaud, A. Tisdale, Human conjunctival goblet cells express the membrane associated mucin MUC16: Localization to mucin granules, Exp. Eye Res. (2016). https://doi.org/10.1016/j.exer.2015.12.009.

[70] S. Xiao, T. Zhao, J. Wang, C. Wang, J. Du, L. Ying, J. Lin, C. Zhang, W. Hu, L. Wang, K. Xu, Gelatin Methacrylate (GelMA)-Based Hydrogels for Cell Transplantation: an Effective Strategy for Tissue Engineering, Stem Cell Rev. Reports. 15 (2019) 664–679. https://doi.org/10.1007/s12015-019-09893-4.

[71] S. Eaker, E. Abraham, J. Allickson, T.A. Brieva, D. Baksh, T.R.J. Heathman, B. Mistry, N. Zhang, Bioreactors for cell therapies: Current status and future advances, Cytotherapy. (2017). https://doi.org/10.1016/j.jcyt.2016.09.011.

[72] S. Schrader, M. Notara, M. Beaconsfield, S.J. Tuft, J.T. Daniels, G. Geerling, Tissue engineering for conjunctival reconstruction: Established methods and future outlooks, Curr. Eye Res. (2009). https://doi.org/10.3109/02713680903198045.

[73] S. Kasbekar, S.B. Kaye, R.L. Williams, R.M.K. Stewart, S. Leow-Dyke, P. Rooney, Development of decellularized conjunctiva as a substrate for the ex vivo expansion of conjunctival epithelium, J. Tissue Eng. Regen. Med. 12 (2018) e973–e982. https://doi.org/10.1002/term.2419.

[74] R.M. Gouveia, G. Lepert, S. Gupta, R.R. Mohan, C. Paterson, C.J. Connon, Assessment of corneal substrate biomechanics and its effect on epithelial stem cell maintenance and differentiation, Nat. Commun. (2019). https://doi.org/10.1038/s41467-019-09331-6.

[75] M. He, T. Storr-Paulsen, A.L. Wang, C.E. Ghezzi, S. Wang, M. Fullana, D. Karamichos, T.P. Utheim, R. Islam, M. Griffith, M.M. Islam, R.R. Hodges, G.E. Wnek, D.L. Kaplan, D.A. Dartt, Artificial polymeric scaffolds as extracellular matrix substitutes for autologous conjunctival goblet cell expansion, Investig. Ophthalmol. Vis. Sci. (2016). https://doi.org/10.1167/iovs.16-20081.

[76] X. Ma, J. Liu, W. Zhu, M. Tang, N. Lawrence, C. Yu, M. Gou, S. Chen, 3D bioprinting of functional tissue models for personalized drug screening and in vitro disease modeling, Adv. Drug Deliv. Rev. (2018). https://doi.org/10.1016/j.addr.2018.06.011.

[77] C. Luan, P. Liu, R. Chen, B. Chen, Hydrogel based 3D carriers in the application of stem cell therapy by direct injection, Nanotechnol. Rev. (2017). https://doi.org/10.1515/ntrev-2017-0115.

[78] B. Jiang, L. Yan, J.G. Shamul, M. Hakun, X. He, Stem Cell Therapy of Myocardial Infarction: A Promising Opportunity in Bioengineering, Adv. Ther. (2020). https://doi.org/10.1002/adtp.201900182.

[79] Y. Lei, D. V. Schaffer, A fully defined and scalable 3D culture system for human pluripotent stem cell expansion and differentiation, Proc. Natl. Acad. Sci. U. S. A. (2013). https://doi.org/10.1073/pnas.1309408110.

[80] K.J. Roberts, A.M. Kershner, P.A. Beachy, The Stromal Niche for Epithelial Stem Cells: A Template for Regeneration and a Brake on Malignancy, Cancer Cell. (2017). https://doi.org/10.1016/j.ccell.2017.08.007.

[81] C.H. Lee, S.G. Joe, S.J. Yang, Subconjunctival Injection of Viscoelastic Material for Leaking Sclerotomy in Transconjunctival Sutureless Vitrectomy, J. Ophthalmol. (2016). https://doi.org/10.1155/2016/9659675.

Chapter 4 Rapid 3D Bioprinting of Multicellular Model Recapitulating Pterygium Microenvironment

Abstract

Pterygium is an ocular surface disorder with high prevalence that can lead to vision impairment. As a pathological outgrowth of conjunctiva, pterygium involves neovascularization and chronic inflammation, but its pathogenesis remains largely unknown. Over the last decade, various types of disease models have been built to study pterygium. Here, we developed a 3D multicellular in vitro pterygium model using the digital light processing (DLP)-based 3D bioprinting of human conjunctival stem cells (hCjSCs). A novel feeder-free culture system was adopted and efficiently expanded the primary hCjSCs with homogeneity, stemness and differentiation potency. The DLP-based 3D bioprinting was able to fabricate hydrogel scaffolds that support the viability and biological integrity of the encapsulated hCjSCs. The bioprinted 3D pterygium model was fabricated with hCjSCs, immune cells and vascular cells to recapitulate the disease microenvironment. Transcriptomic analysis using RNA sequencing (RNA-seq) identified a distinct profile correlated to inflammation response, angiogenesis, and epithelial mesenchymal transition in the bioprinted 3D pterygium model. In addition, the pterygium signatures and disease relevance of the bioprinted model was validated with the public RNA-seq data of patient-derived pterygium tissues. By integrating the stem cell technology and 3D bioprinting, this is the first reported 3D in vitro disease model for pterygium that can be utilized by future studies towards the investigation of pterygium disease mechanisms and the drug screening.

4.1 Introduction

As an essential part of the ocular surface, the conjunctiva is a mucosal stratified epithelial membrane that covers the major surface of sclera and lines the eyelid and functions in lubrication, mechanical support, and immune responses [1,2]. The conjunctival epithelium contains goblet cells producing mucins that comprise the tear film, which is a dynamic fluidic layer critical for the homeostasis of the ocular surface [3,4]. The damage and inflammation of conjunctiva caused by disease or injury could lead to a variety of symptoms, including dry eye and vision impairment [5,6]. Despite of the high prevalence, the pathogenetic mechanism for many of the conjunctival diseases are unclean [5,6]. Pterygium is a pathological overgrowth of vascularized conjunctiva that could invade the cornea across the limbus and compromise the vision [7,8]. With minor pharmaceutical treatments reported, patients with severe pterygium often require surgical interventions to restore basic visual functions, but the prevention of post-surgical recurrence can be challenging [9–11]. Although chronic inflammation and angiogenesis in pterygium have been well characterized, comprehensive understanding in the pathological development and the molecular background of pterygium remain debatable [8,12–16]. One of the major challenges is the development disease models. Existing pterygium disease models were 2D cultured human patient-derived pterygium epithelial cells that failed to recapitulate the multicellular microenvironment or animal models developed using the subconjunctival injection of human animal cells that could be limited by the reproducibility and heterogeneity [17–20].

In the past decade, with the development of stem cell technologies, disease modeling based on the tissue engineering of human stem cell have been widely explored to develop clinical-relevant patient-specific models to replace the small-animal models for personalized medicine [21,22]. 3D bioprinting is a rising technology for the fabrication of functional 3D tissue structures

with tailored biological and mechanical properties [23,24]. Among different 3D bioprinting techniques, direct light processing (DLP)-based 3D bioprinting stands out for the rapid fabrication, superior microscale and nanoscale resolution, and the high post-fabrication cell integrity [23,25]. The DLP-based bioprinting have been utilized to fabricate synthetic tissues for the disease modeling of multiple organs and tissues, including heart, liver, brain, alveoli, spinal cord and bone [26–31]. Conjunctival stem cells (CjSCs) are the bipotent endogenous stem cells that can give rise to both the conjunctival goblet cells and the conjunctival keratinocytes, and thereby hold tremendous potential in modeling the conjunctival microenvironment [4,32–34]. However, the lack of knowledge in the habited microenvironment and the in vitro expansion method have limited the applications of CjSCs in tissue engineering [35–39]. We have previously reported the DLP-based 3D bioprinting of microscale hydrogel constructs encapsulating rabbit CjSCs with the stem cell properties and differentiation potency preserved [40]. But the bioprinting of human CjSCs (hCjSCs) and the disease modeling using CjSCs were not yet studied.

In this study, we explored the DLP-based 3D bioprinting of primary hCjSCs and developed a bioprinted multicellular pterygium model. We first harvested the hCjSCs from donor tissues and expanded them with a feeder-free in vitro culture system. Using a custom DLP-based 3D bioprinter, we printed hydrogel scaffolds that were able to support the viability, stemness, and differentiation potency of the encapsulated hCjSCs. Next, we performed a multicellular bioprinting that combined hCjSCs along with immune cells and vasculature to develop the bioprinted 3D pterygium model. The bioprinted pterygium model was then subjected to global transcriptomic analysis to in-depth characterized the disease phenotypes. Furthermore, we validated our bioprinted model with published dataset of patient derived pterygium tissues. To the best of our knowledge, this is the first report of a 3D in vitro disease model mimicking the multicellular microenvironment of

pterygium. The DLP-based 3D bioprinting of hCjSCs developed here can be translatable for the use in personalized medicine. The cellular interactions and signaling pathways revealed from the multicellular bioprinted model are also implicative to understand the pathogenesis of pterygium.

4.2 Materials and Methods

Primary cell isolation, cell culture and cell doubling quantification

Fresh corneoscleral tissues were provided by One Legacy or Saving Sight eye banks with the consent for research use. The human corneoscleral tissue handling protocol has been evaluated and exempted by the University of California, Los Angeles (UCLA) Institutional Review Boards (IRB#12-000363). The experiments were designed and performed adhered to the tenets of the Declaration of Helsinki and the overall procedure was consent by the University of California San Diego Institutional Biosafety Committee. Primary human conjunctival epithelial cells were isolated from the bulbar conjunctiva on the scleral surface that was 2-4mm away to the limbus. Dissected tissues were subjected to mincing and a 30–60-minute digestion with 0.5% type IV collagenase (Sigma Aldrich) at 37℃ under agitation. Following the collagen digestion, the cells were further digested with 0.25% trypsin-EDTA (ThermoFisher Scientific).

The isolated CjSCs were cultured on the collagen I (ThermoFisher Scientific) surface as previously described [40]. The epithelial cell culture medium was made with Dulbecco's Modified Eagle Medium (DMEM) /F-12 (3:1) supplemented with 10% (v/v) fetal bovine serum (FBS, ThermoFisher Scientific), 1% (v/v) penicillin–streptomycin (ThermoFisher Scientific), 1% (v/v) insulin-transferrin-selenium (ThermoFisher Scientific), 400 ng/ml hydrocortisone (Sigma Aldrich), 0.1 nM cholera toxin (Sigma Aldrich), 10 ng/ml recombinant human epidermal growth factor (EGF, R&D System), and 2 nM reverse T3 (Sigma Aldrich). The conjunctival stem cell culture medium

(CjSCM) was made by adding 10 μM ROCK inhibitor Y27632 (Tocris Bioscience), 1 μM A83-01 (STEMCELL Technologies) and 1 μM DMH1 (STEMCELL Technologies) and used for the CjSC culture. The conjunctival goblet cell differentiation was performed using Keratinocyte SFM (ThermoFisher Scientific) supplemented with bovine pituitary extract (BPE), 10 ng/ml recombinant KGF (Biolegend), 10 ng/ml recombinant EGF (Biolegend), 1% (v/v) P-S, 10 ng/ml recombinant BMP4 (R&D System), and 100 ng/ml IL13 (Biolegend) [39–41]. M2 macrophages were acquired by differentiating THP-1 monocytes. THP-1 cells were maintained with RPMI1640 medium (ThermoFisher Scientific) with 10% (v/v) FBS, and the M2 differentiation was done by incubating the THP-1 cells in 200 ng/ml tetradecanoyl phorbol acetate (PMA, Sigma Aldrich) for 48 hours, following by incubation in complete RPMI 1640 medium for 24 hours, and then in 20 ng/ml interleukin 4 (IL4, Biolegend) and 20 ng/ml interleukin 13 (IL13, Biolegend) for another 48 hours. Human umbilical vein endothelial cells (HUVECs) are cultured with Endothelial Cell Growth Medium-2 (EGMTM-2, Lonza). C3H/10T1/2 mouse embryonic fibroblast (10T1/2s) was cultured with DMEM with 10% (v/v) FBS. For the cell culture of the 3D bioprinted pterygium model and the corresponding 2D control, complete EGMTM-2 was mixed 1:1 with the epithelial cell culture medium and supplemented with 10 μM Y27632.

For the quantification of cell doubling, pre-cultured cells isolated from primary conjunctival epithelium were seeded on collagen I coated 6-well plate (Corning) with 10,000 cells per well. The epithelial cell culture medium was used as the control medium, and the cells were then cultured with either CjSCM or control medium. The cells were passaged when the confluence reached 90% and the cell numbers were measured manually every time with a hemocytometer (Fisher Scientific). The same number of cells (10,000 cells) were seeded on the next round and repeated the process. The cell doubling time (DT) was calculated as: $DT = \Delta T \cdot ln\ 2\ /ln\ (Q2/Q1)$.

ΔT: culture time. Q1, Q2: the number of cells at the beginning and at the end.

Material synthesis

The materials for bioprinting, gelatin methacryloyl (GelMA) and hyaluronic acid glycidyl methacrylate (HAGM), were prepared as previously described [40,42–44]. For the synthesis of GelMA, type A porcine skin gelatin (Sigma Aldrich) was dissolved in a 0.25 M carbonate-bicarbonate (3:7) solution (pH 9) to make a 10% (w/v) solution. Then, methacrylic anhydride (Sigma Aldrich) was added dropwise, following by 1-hour reaction at 50℃ with constant stirring. The products were dialyzed using 13.5 kDa dialysis membranes (Repligen), lyophilized, and stored at -80℃. The synthesized GelMA has an approximate degree of methacrylation of 95% [43]. For HAGM, 1% (w/v) hyaluronic acid solution was made by dissolving sodium hyaluronate (Lifecore Biomedical) in water: acetone (1:1) solution with continuous stirring in dark at room temperature and incubated overnight. Next, triethylamine (Sigma Aldrich) was slowly added in the reaction and mixed thoroughly, then glycidyl methacrylate (GM, Sigma Aldrich) was also added dropwise, and reacted overnight at room temperature with Argon seal and constant stirring, followed by acetone precipitation. The products were collected with vacuum filtration, dissolved again with DI water, dialyzed, lyophilized and stored at -80℃. The resultant HAGM has an approximate degree of methacrylation of 35% [42].

The photoinitiator lithium phenyl-2,4,6-trimethylbenzoylphosphinate (LAP) was synthesized following previous publication [40,42]. Briefly, dimethyl phenylphosphonite (Sigma Aldrich) was added dropwise to an equimolar amount of 2,4,6-trimethylbenzoyl chloride (Acros Organics), and reacted for 18 hours at room temperature with constant stirring. Then, a solution of

lithium bromide (Sigma Aldrich) in 2-butanone (Sigma Aldrich) was added into the reaction, and incubated overnight at room temperature, following by filter-washing with 2-butanone. The resultant solidified LAP was made into powder and stored in the dark at 4 ℃.

DLP-based 3D bioprinting

A customized DLP-based 3D bioprinting system was built with projection optics suppled with a 365 nm light source (Hamamatsu), a motion controller (Newport) and a digital micromirror device (DMD, Texas Instruments). The digital patterns were generated with MATLAB and inputted to the DMD chip through a custom-built coordination software. The thickness of the printed structures was controlled by the motion controller covered with polydimethylsiloxane (PDMS). The bioprinted hydrogel structures were printed on methacrylated coverslips upon light exposure, then rinsed with warm DPBS before subjected to culture in 5% CO2 at 37℃.

The pre-polymer solution for the printing was made by dissolving GelMA, HAGM and LAP with DPBS (ThermoFisher Scientific) and filtered with 0.22 μm syringe filter (Millipore Sigma). 5% or 8% (w/v) GelMA with 0.25% (w/v) LAP, and 2.5% (w/v) GelMA with 1% (w/v) HAGM and 0.25% (w/v) LAP were made accordingly. The 5% (w/v) GelMA was used as the soft condition for hCjSC bioprinting while the 8% (w/v) GelMA was used as the stiff condition. 2.5% (w/v) GelMA with 1% (w/v) HAGM was used for the bioprinting of HUVECs and 10T1/2s. Before the printing, the cells were digested, filtered with 70 μm cell strainers (Corning), quantified for the cell concentration, and pelleted with desired quantity. For the hCjSC bioprinting, the bioink contained 2×107 cells/mL of hCjSCs. For the multilayered printing of 3D pterygium model, the stem cell layer contained 2×107 cells/mL of hCjSCs plus 1×107 cells/mL of macrophages while

the vascular layer contained 2×107 cells/mL of HUVECs and 4×105 cells/mL of 10T1/2s (50:1).

Mechanical characterization

The compressive Young's modulus was measured using Microsquisher (CellScale) following manufacturer's instructions. GelMA cylinders with 500 μm-diameter and 500 μmin-thickness were printed and incubated overnight in DPBS at 37℃. Briefly, two cycles of predetermined compression were done to remove the hysteresis of the samples. Then, the samples were compressed by 10% strain with a rate of 2 μm/s while the force and displacement were recorded. The data was then processed with a custom-made MATLAB script.

Immunoassays and flow cytometry

For the immunofluorescence staining of 2D cultured cells, cells grown on Millicell EZ slides (Millipore Sigma) were washed twice with DPBS and fixed with 4% (w/v) paraformaldehyde (PFA, FUJIFILM Wako). The fixed samples were permeabilized and blocked with 5% bovine serum albumin (BSA, Sigma Aldrich) with 0.3% triton X-100 (Sigma Aldrich) and 0.1% TWEEN® 20 (Sigma Aldrich) for 1 hour at room temperature. For the staining of mucin, samples were permeabilized with 0.2% triton X-100 in DPBS for 10 minutes, following by 1-hour blocking with 5% BSA. Then, the samples were incubated with primary antibody solution overnight. The secondary antibody with different conjugated fluorophores (Alexa Fluor®, Cell Signaling Technology) were diluted with 5% BSA and incubated with the samples for 1 hour at room temperature. The antibody information was enclosed at Supplementary Table X. The samples were stained with 4',6-Diamidino-2-Phenylindole (DAPI, ThermoFisher Scientific) for the nuclear

illustration and mounted with Fluoromount-G™ Mounting Medium (ThermoFisher Scientific). For the staining of the bioprinted samples, samples were fixed and stained following the same procedures, expect the last step of mounting.

For flow cytometry, encapsulated cells were released from the bioprinted scaffolds by enzymatical digestion with collagenase IV. The released cells were further digested with 0.25% trypsin-EDTA and filtered with a 70 μm cell strainer to obtain single cell suspension. The samples were then subjected to direct staining or fixed with Cytofix™ Fixation Buffer (BD). For the immunostaining, fixed cells were permeabilized with 0.2% triton X-100 in Cell Staining Buffer (Biolegend) for 2 minutes, and then incubated for 20 minutes with the diluted primary antibody, and secondary antibody, respectively. The cells were washed with Cell Staining Buffer between each step. BD Accuri™ C6 flow cytometer was used in the experiment and the resultant data was processed using FlowJo.

Viability Tests

The viability of the encapsulated cells was evaluated using flow cytometry with propidium iodide (PI, Biolegend) staining and the LIVE/DEAD® viability/cytotoxicity kit (ThermoFisher Scientific). For the PI staining, samples were incubated with diluted PI solution (10 μl per million cells in 0.5 ml/test) for 15 minutes at 4 °C before analysis. For the LIVE/DEAD® staining, samples were incubated with 2 μM calcein acetoxymethyl ester and 4 μM ethidium homodimer diluted in DPBS, for 30 min at 37℃, following by imaging.

RNA extraction, RNA sequencing and transcriptomic analysis

For the RNA sequencing (RNA-seq), hCjSCs were labeled with GFP with lentiviral vectors before subjected to bioprinting and culture. The GFP-labeled hCjSCs were isolated from the bioprinted scaffolds by enzymatic digestion and fluorescence-activated cell sorting (FACS). RNA was isolated with a method based on TRIzol® reagent (Ambion Thermo Fisher) with Direct-zol™ RNA Purification kit (Zymo Research) following manufacturer's protocol. The RNA products were quantified using NanoDrop™ 2000 (Thermo Fisher Scientific). The library preparation and RNA-seq were performed on Illumina platform by Novogene (Sacramento, CA).

For the transcriptomic data analysis, reads were filtered and trimmed with Trim Galore (version 0.4.1) followed by mapping to the human genome (GRCh38.12) using Hisat2. Differential expression analysis was performed using DESeq (Adjusted P-value<0.01). For the differently expressed genes, protein to protein interaction enrichment analysis were constructed through Cytoscape. GO Enrichment Analysis were carried out through Geneontology. PCA was calculated by using all the genes. Gene set enrichment analysis was performed using the online GSEA webportal (http://software.broadinstitute.org/gsea/msigdb/annotate.jsp) and the GSEA desktop application (http://software.broadinstitute.org/gsea/downloads.jsp).

Imaging and Statistics

Imaging in this study was conducted using Leica SP8 confocal microscope and Leica DMI 6000-B fluorescence microscope. Images were processed with LAS X and ImageJ.

Statistical analysis was performed using Microsoft Excel and GraphPad Prism. The data was presented as mean ± standard deviations with two-tailed Student's t-test or one way ANOVA used to determine the significance. P-value was presented in the figures with asterisks (*: $P < 0.05$; **: $P < 0.01$; ***: $P < 0.001$.).

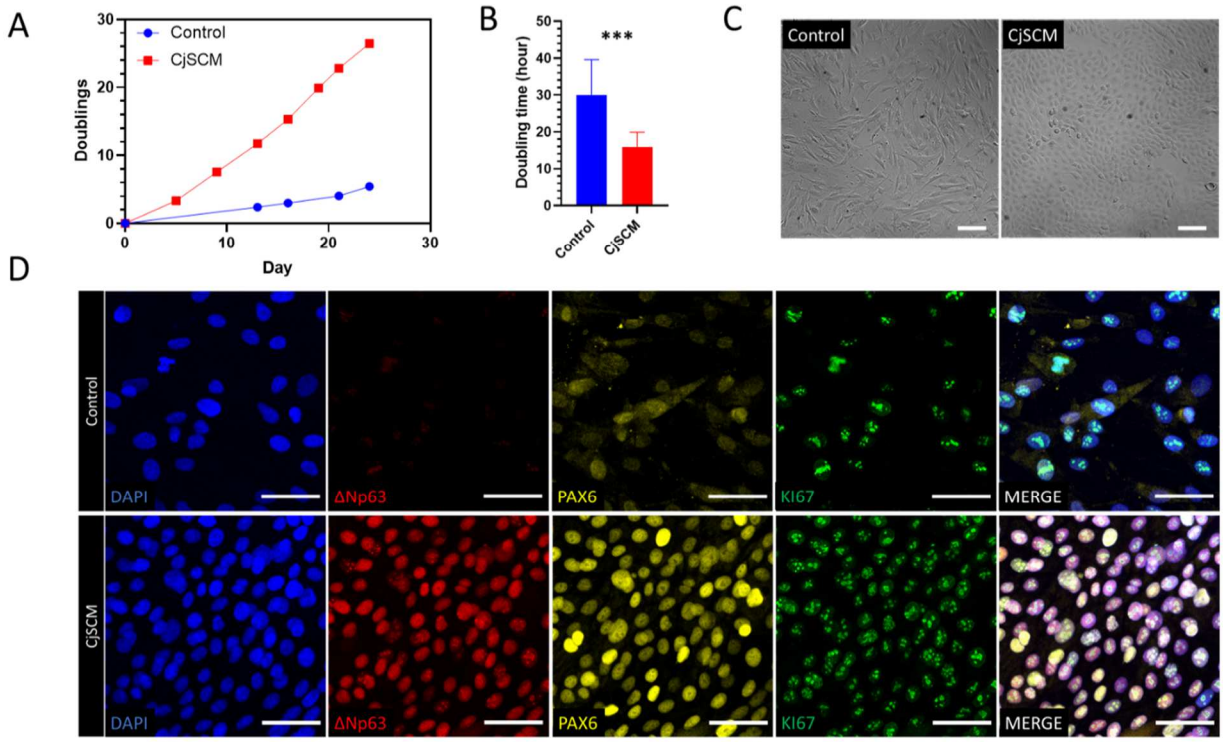

Figure. 4.1. *In vitro* expansion of primary hCjSCs using CjSCM. (A) Representative cumulative quantification plot showed the cell doublings versus the culture time of human primary conjunctival epithelial cells in culture with CjSCM or control medium that without small molecule inhibitors. (B) Average cell doubling time of human conjunctival epithelial cells in culture with control medium and CjSCM from passage 1 to 8 (mean ± SD, n = 3; ***: $P < 0.001$). (C) Cell morphologies of primary human conjunctival epithelial cells cultured with CjSCM or control medium at passage 3. Scale bars: 100 μm. (D) Immunofluorescence staining of P63, PAX6 and KI67 on hCjSCs expanded in CjSCM or control medium at passage 3. Scale bars: 50 μm.

4.3 Results

4.3.1 *In vitro* expansion of primary hCjSCs

The hCjSCs are one of the predominant stem cells on the ocular surface with high value in clinical applications, but the in vitro expansion of hCjSCs has been a challenge [35,36,39]. We have previously reported the feeder-free culture of primary rabbit CjSCs using the CjSCM containing a cocktail of small molecules inhibiting transforming growth factor-beta (TGF-β) signaling, bone morphogenetic proteins (BMP) signaling, and Rho-associated protein kinase

(ROCK) signaling [40]. Given the promise of the results on rabbit cells, we validate the expansion efficacy of CjSCM on primary hCjSCs isolated from donor tissue. As shown with the accumulative quantification of cell doublings, compared to the cells cultured with control medium that contained no inhibitor cocktail, the cells cultured with CjSCM showed faster proliferation and higher replicative potency (Figure 4.1A, Supplementary Figure S4.1A). They also had significantly shorter cell doubling time, as the control cells had an averaged doubling time of 30.01±9.58 hours while the CjSCM group had an averaged doubling time of 15.95±3.93 hours (Figure 4.1B). As for the cell morphology, the cells expanded with CjSCM exhibited more compacted, cuboidal, and uniform morphology whereas the control cells were elongated, spindle-shaped, and variable-sized (Figure 4.1C). In addition, the transcriptional difference in cells was measured with real time qPCR. As a result, the mRNA expression of epithelial stem cell markers, P63 and keratin 14 (KRT14), as well as the ocular lineage marker, PAX6, and proliferation marker, KI67, was significantly upregulated in the CjSCM group, while the expression of mesenchymal markers, vitronectin (VIM) and collagen IA (COL1A), was significantly upregulated in the control cells (Figure 4.1D). The immunofluorescence staining of stem cell markers (ΔNP63, P63, ABCG2, KRT14), lineage markers (PAX6, E-cadherin (ECAD)), and proliferation marker KI67 indicated the predominant presence of hCjSCs in the CjSCM group (Figure 4.1E, Supplementary Figure S4.1B). To validate the potency, we have induced the goblet cell differentiation on the expanded hCjSCs. After 7 days of differentiation, the generation of conjunctival goblet cells was confirmed by the protein expression of mucin 1 (MUC1), mucin 5AC (MUC5AC), and mucin 16 (MUC16), as shown by immunofluorescence staining (Supplementary Figure S4.1C). These results collectively demonstrated that the primary hCjSCs were efficiently expanded in vitro using CjSCM with high homogeneity and the stem cell phenotypes and potency preserved.

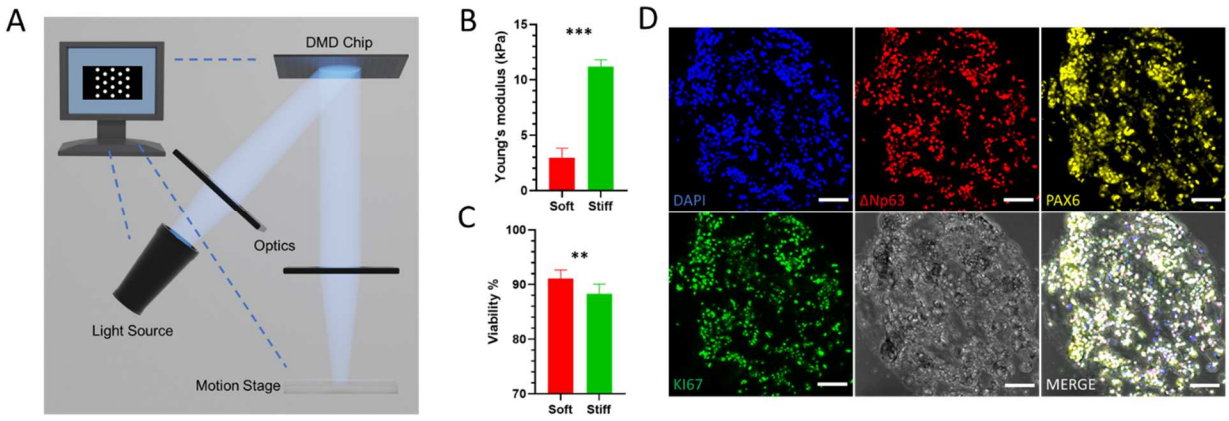

Figure. 4.2. DLP-based 3D bioprinting of hydrogel scaffolds supporting the stemness and functionality of the encapsulated hCjSCs. (A) Schematic of the DLP 3D bioprinter setup. (B) Compressive modulus of the hCjSCs encapsulated in soft and stiff bioprinted scaffolds (mean ± SD, n = 3). (C) The ration of PI-negative population measured with flow cytometry representing the percentage of viable cells in soft and stiff bioprinted scaffolds cultured for 5 days (mean ± SD, n = 3). (D) Representative immunofluorescence staining and corresponding bright field images of on bioprinted hydrogel scaffolds encapsulating hCjSCs after 2 days in culture showing the positive expression for P63, PAX6 and KI67. Scale bars: 100 μm.

4.3.2 DLP-based 3D Bioprinting of hCjSCs

To support the use of hCjSCs in disease modeling, we next explored the 3D bioprinting of hCjSCs. With the rapid, scalable process, high fabrication resolution and versatile material choice, DLP-based 3D bioprinting has been used in fabricating hydrogel scaffolds encapsulating various types of human stem cells for disease modeling and therapeutic purposes [25,29,42,43]. The DLP 3D bioprinter we used in this study was assembled with a motion control stage, a DMD chip that can translate digital inputs to light patterns, a 365 nm laser source and projection optics (Figure 4.2A). GelMA was adopted as bioink material because it has excellent cell binding capacity and has been used for encapsulating multiple cell types, including rabbit CjSCs [25,40,45]. Mechanical properties of the extracellular matrix (ECM), such as stiffness, have been proved to manipulate essential functions and cell behaviors of stem cells [46,47]. To test the biomechanical condition for hCjSCs, GelMA cylinders (diameter: 500 μm; thickness: 500 μm) were printed in different

stiffness to encapsulate the hCjSCs, as the soft condition being around 3 kPa while the stiff condition is around 11 kPa (Figure 4.2B). After incubating for 5 days, the viability of encapsulated hCjSCs was evaluated with PI staining and flow cytometry. As a result, both the soft and stiff condition showed over 85% cell viability, but the soft condition had significant higher viability (Figure 4.2C). The results were also confirmed by LIVE/DEAD® staining (Supplementary Figure S4.2A). In addition, as examined using real time qPCR, the transcriptional expression of P63, KRT14, PAX6, and KI67 was significantly higher in the soft condition, compared with 2D control and stiff condition (Figure 4.2D). Thus, we adopted the soft printing condition for the following experiments. With immunofluorescence staining, the stem cell identity of the encapsulated hCjSCs was confirmed (Figure 4.2E, Supplementary Figure 4.2B). To test the functionality of the encapsulated hCjSCs, we conducted the 3D differentiation on the bioprinted scaffolds encapsulating hCjSCs and found the expression of characteristic mucins after 7 days (Supplementary Figure 4.2C). Together, we achieved the DLP-based 3D bioprinting of hCjSCs with GelMA while preserving the cell viability, stemness and functionality.

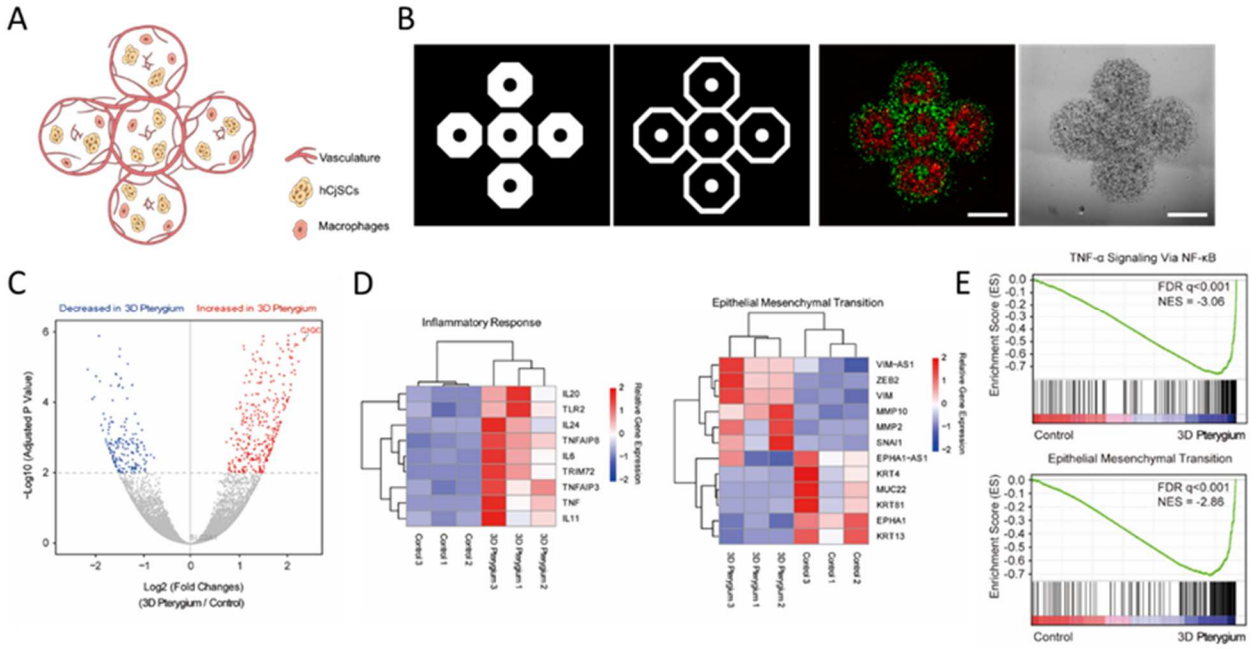

Figure. 4.3. DLP-based 3D bioprinting of multicellular pterygium model with distinct transcriptomic profiles. (A) Illustration of the bioprinted multicellular model. (B) Representative images of the 3D pterygium model. Red: hCjSCs and macrophages; green: HUVECs and fibroblasts. Scale bars: 1mm. (C) Volcano plot of global transcriptomic landscape comparing the bioprinted 3D pterygium model and the 2D control. The *x*-axis represents log2 transformed fold changes, and the *y*-axis shows the log 10 transformed *p*-value adjusted for multiple test correction (n =3 per condition). (D) Heatmap of representative DEGs correlated to inflammatory response and epithelial mesenchymal transition in the 3D pterygium model versus the 2D control. Scale bars represent relative gene expression (log2). (E) Representative GSEA showing the enrichment of TNF-α/NF-κB signaling and EMT comparing the 3D pterygium model with the control. FDR: false discovery rate, NES: normalized enrichment score.

4.3.3 3D Bioprinted Multicellular Pterygium Model

With the background of extensive chronic inflammation in pterygium, the angiogenesis and the infiltration of immune cells dominate the cellular interactions in the pterygium microenvironment [14,17,44,48,49]. In existing pterygium models, patient-derived pterygium epithelial cells or mouse embryonic fibroblasts were injected to the subconjunctival regions of the animal eye to induce immune response and neovascularization [17,18,20]. Other study had also implicated the stem cell origination and the presence of stem cell population inside pterygium [14,50]. Taking the advantage of the 3D bioprinting of hCjSCs, we developed a 3D bioprinted

pterygium model combining hCjSCs, macrophages, vascular endothelial cells, and fibroblasts to recapitulate the multicellular microenvironment of pterygium (Figure 3A). Different population of cells were patterned following our printing masks (Figure 3B). The bioprinted models were then subjected to culture and characterization.

4.3.4 3D Pterygium Model Displayed Distinct Transcriptomic Profiles Compared to 2D Culture

To comprehensively characterize the bioprinted 3D pterygium model, we bioprinted the models with hCjSCs from 3 healthy donors and performed global transcriptomic profiling with RNA-seq on the bioprinted hCjSCs in the 3D pterygium model as the hCjSCs cultured in 2D condition were used as control. Principal component analysis (PCA) showed a drastic transcriptomic difference between the hCjSCs in the 3D pterygium model and the control (Supplementary Figure S3A). Differentially expressed gene (DEG) analysis identified markers with significant transcriptional expression difference between the cells in 3D pterygium model and the control, as the volcano plot shows that 420 genes were significantly upregulated, whereas 170 genes were downregulated ($p < 0.05$, $|\text{fold change}| > 2$) (Figure 3C) Unsupervised hierarchical clustering with the top markers distinguished between the 3D pterygium and the control (Supplementary Figure S3B). Based on the DEG analysis comparing with the 2D control, the 3D pterygium models showed significantly upregulated expression of genes correlated to interleukin cascade, tumor necrosis factor (TNF) signaling, and other inflammatory response (Figure 3D). We have also noticed the upregulation of mesenchymal markers and markers of epithelial mesenchymal transition (EMT), along with the downregulation of conjunctival epithelial markers (Figure 3D). In addition, genes involved in TGF-β/BMP signaling were upregulated in the 3D pterygium model (Supplementary Figure S3C). Markers of other principle signaling pathways in

the epithelial stem cell were also investigated (Supplementary Figure S3C). These results have underlined that the encapsulated hCjSCs in the bioprinted 3D pterygium model were assaulted by inflammatory stimulus from the synthetic microenvironment and undergoing EMT that was potentially mediated by TGF-β/BMP signaling [51–53].

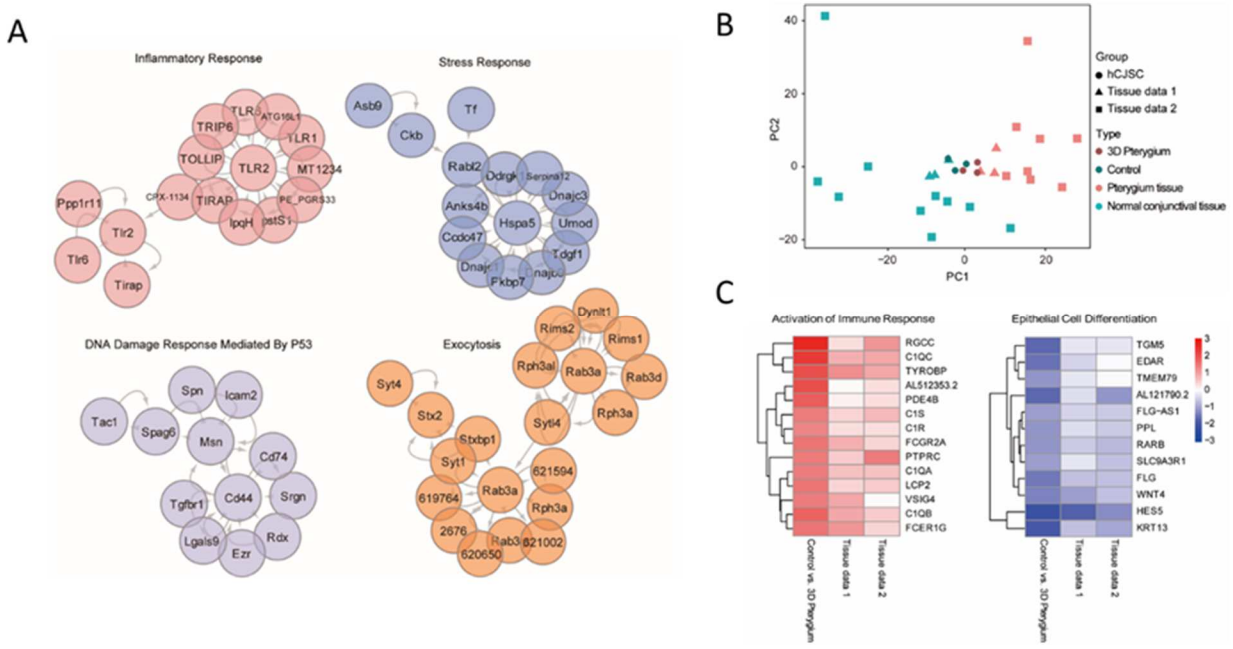

Figure. 4.4. Transcriptome profiles of 3D pterygium model resemble patient-derived pterygium tissue. (A) PPI enrichment analysis based on the DEGs between the 3D pterygium model and the control. (B) PCA of the global transcriptomic profiles of the hCjSCs from the bioprinted model (3D pterygium) and 2D culture (Control), and human tissues from healthy individuals (normal conjunctival tissue) and pterygium patients (Pterygium tissue). (C) Heatmap of consistent DEGs correlated to activation of immune response and epithelial cell differentiation. Tissue data 1 (X. Liu, et al.) and tissue data 2 (Y. Chen, et al.) represent human tissue data from two independent studies. Scale bar represents normalized fold change.

4.3.5 3D Pterygium Model Exhibited Transcriptomic Signatures of Pterygium

We performed further analysis to interrogate if our model exhibited molecular features relevant to pterygium. Gene set enrichment analysis (GSEA) revealed that the 3D pterygium model expressed enriched gene hallmarks of EMT, TNF-α/NF-κB signaling, EGF signaling and

Neuregulin-1 (NRG1) signaling while the control showed enrichment involved in epithelial differentiation and keratinization (Figure 3E, Supplementary Figure S4A). Gene ontology (GO) enrichment analysis showed the overrepresented GO terms correlated to the organization of cell-cell and cell-substrate junction, EMT, Notch signaling, DNA damage response, endoplasmic reticulum (ER) unfolded protein response (UPR), interleukin production, and angiogenesis regulation in the 3D pterygium model while GO terms correlated to epithelial cell differentiation, keratinization, canonical Wnt signaling were down-regulated (Supplementary Figure S4B). Protein-protein interaction (PPI) enrichment analysis highlighted the protein networks correlated to inflammatory response, stress response, DNA damage response mediated by P53, and exocytosis in the 3D pterygium model (Figure 4A). Furthermore, to determine the correlation between our 3D pterygium model with actual pterygium tissues, we combined the RNA-seq data of normal human conjunctiva and patient-derived pterygium sample from published databases for comparative analysis [54,55]. Based on the matrix analysis with PCA, the 3D pterygium model exhibited a closer transcriptome state to patient-derived pterygium tissues while the transcriptomic profiles of hCjSCs cultured in 2D condition was close to the normal conjunctival tissue data (Figure 4B). GO enrichment analysis on consistent DEGs comparing different datasets revealed that the 3D pterygium model had up-regulation GO terms consistent with the pterygium tissues correlated to activation of immune response, the regulation of cell-cell junctions and cell-substrate junctions, EMT, vascular endothelial growth factor (VEGF) production, integrin-mediated signaling pathways, non-canonical Wnt signaling (planar cell polarity), TGF-β/SMAD signaling (Figure 4C, Supplementary Figure S4C). These results indicated that the bioprinted 3D pterygium model was able to model the disease microenvironment of pterygium and tune the hCjSCs from healthy donors into pterygium-relevant pathological state.

4.4 Conclusion

Pterygium is a pathological conjunctival overgrowth with chronic inflammation and angiogenesis that could jeopardize the vision [7,8,16]. Effective and reproducible disease models are needed to decipher the pathogenesis and explore new therapeutic approach of pterygium [18,19]. Here, based on the in vitro expansion and DLP-based 3D bioprinting of hCjSCs, we developed a 3D bioprinted multicellular pterygium in vitro disease model. We first used a novel feeder-free culture method to efficiently expand the primary hCjSCs. Then, we validated the DLP-based 3D bioprinting of hCjSCs with GelMA bioink while preserving the viability, stemness and functionality. With the DLP 3D bioprinter, we fabricated a 3D pterygium model with hCjSCs from healthy donors, macrophages, HUVECs and fibroblasts mimicking the multicellular pterygium microenvironment. By performing global transcriptomic analysis with RNA-seq, we found that the hCjSCs in the bioprinted 3D model exhibited pathological features highlighting inflammatory response and EMT. Further comparative analysis with published data of patient-derived pterygium tissues confirmed the presence of pterygium signatures in our bioprinted 3D pterygium model.

Despite of the foreseeable clinically translatable value of hCjSCs, the efficient generation and the effective tissue engineering approach for hCjSCs were under investigation [33,35,38]. Consistent with other reported culture of human epithelial stem cells and our previous report on rabbit CjSCs, CjSCM with the inhibition on TGF-β signaling and BMP signaling, as well as the ROCK signaling, was able to support the efficient in vitro expansion of hCjSCs while maintained the stemness and differentiation potency [40,56,57]. As we generated large number of cells from a small number of starting materials for the experiment, our culture method could combine with impression cytology for the future clinical study [58]. In addition, with the DLP-based 3D bioprinting, we fabricated hydrogel scaffolds with GelMA supporting the viability and stem cell

properties of the encapsulated hCjSCs. The rapid, scalable, reproducible fabrication with DLP-based 3D bioprinting made this model highly valuable and clinically translatable for personalized medicine [59]. The flexible pattern design also enabled convenient modification on the models to adapt different biomedical applications in the future.

To recapitulate the pterygium microenvironment, we integrated hCjSCs with immune cells and vascular cells, in the bioprinting to develop a 3D pterygium model and performed RNA-seq to evaluate the model [12,49]. Vast difference in gene expression was found in DEG analysis comparing the hCjSCs from the 3D pterygium model and the 2D control, indicating the bioprinted synthetic multicellular 3D microenvironment significantly alternated the state of encapsulated cells. The GSEA and GO enrichment analysis have indicated the hCjSCs in the 3D pterygium model were under ER stress and DNA damage induced by the inflammatory stimulus through TNF-α/NF-κB signaling and interleukin cascade and undergoing EMT that was potentially mediated by integrin signaling, TGF-β/SMAD signaling, and Notch signaling [51,60–66]. In addition, GSEA has identified the activation of EGF signaling and NRG signaling in the 3D pterygium model, underlining the crosstalk between epithelial cells and macrophages [67,68]. Notably, by comparing our data with the transcriptomic signatures identified in the patient-derived tissues, the bioprinted 3D pterygium model was grouped into the pterygium tissues while the 2D control classified into normal conjunctival tissues, which further confirmed the pathological changes of healthy hCjSCs in the bioprinted model [54,55]. Moreover, the key events and signaling pathways that were highlighted by the transcriptomic analysis are potential targets for developing pharmaceutical treatment of pterygium.

In conclusion, based on the DLP-based 3D bioprinting of hCjSCs, we have developed a bioprinted 3D pterygium model presenting the multicellular microenvironment and transcriptomic

signatures of pterygium. This is the first reported 3D in vitro disease model for pterygium recapitulating pathological features consistent with patient-derived pterygium tissues. Supported by the DLP-based 3D bioprinting technology, this model is valuable for different applications for the future study.

Acknowledgements

Chapter 4, in full, a reprint of the unpublished manuscript in review, “Rapid 3D Bioprinting of Multicellular Model Recapitulating Pterygium Microenvironment”, Z. Zhong, J. Wang, J. Tian, X. Deng, A. Balayan, Y. Sun, C. Ma, J. Schimelman, M. Tang, X. Shi, E. Yao, S. Deng, S.C. Chen. The dissertation author was the primary investigator and author of this paper. This work was supported in part by grants from the NIH to S.C. (R21EY031122, R01EB02185) and S.D. (R01EY021797), National Science Foundation (NSF) to S.C. (1937653), and California Institute for Regenerative Medicine to S.D. (CLIN1-08686 and CLIN2-11650).

Supplementary Information

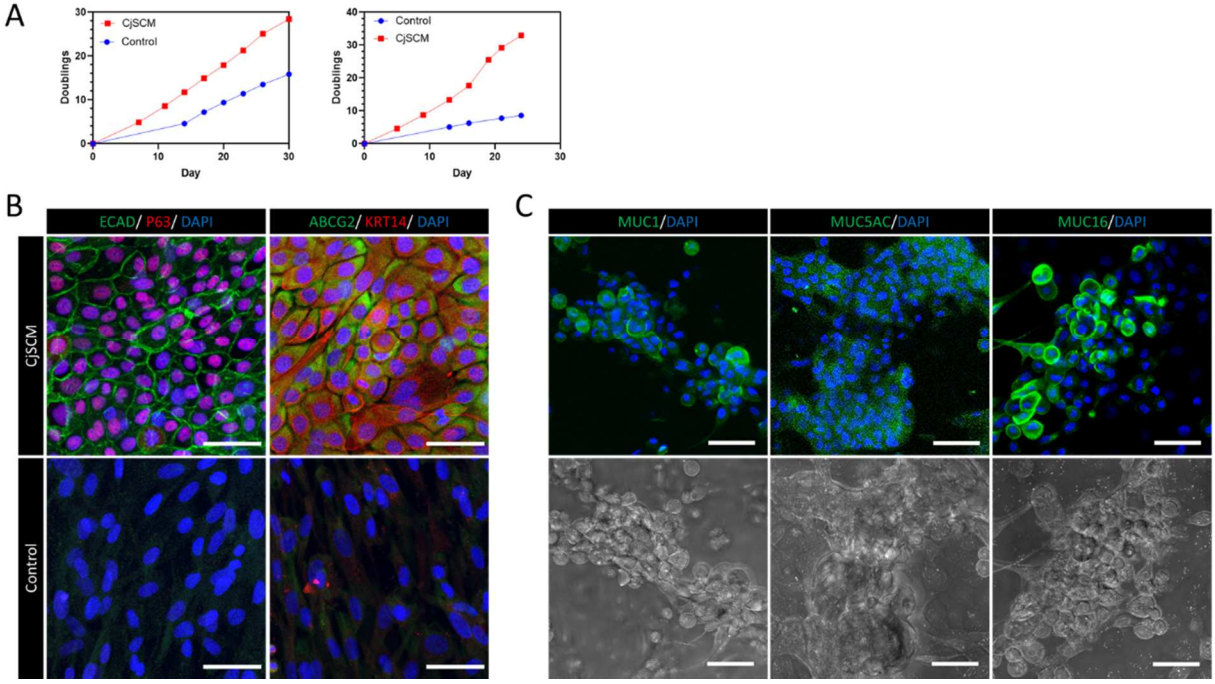

Supplementary Figure S4.1. Characterization of 2D hCjSCs. (A) Cumulative quantification plots of the cell doublings versus the culture time of primary conjunctival epithelial cells from different donors in culture with CjSCM or control medium. (B) Immunofluorescence staining of ECAD/P63 and ABCG2/KRT14 on hCjSCs expanded in CjSCM or control medium at passage 3. Scale bars: 50 μm. (C) Immunofluorescence staining of MUC1, MUC5AC and MUC16, and the corresponding bright field images on the conjunctival goblet cells differentiated from hCjSCs. Scale bars: 50 μm.

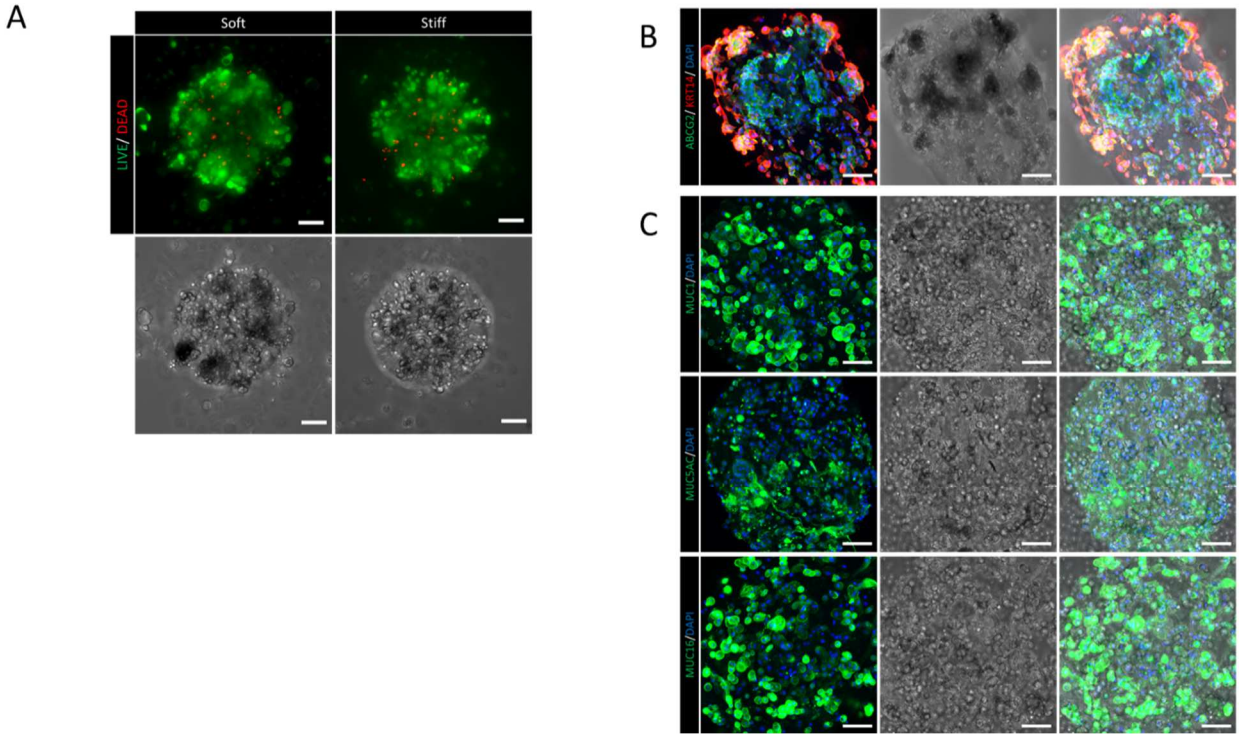

Supplementary Figure S4.2. Characterization of 3D hCjSCs. (A) Live/Dead™ staining was performed on the hydrogel scaffolds encapsulated with hCjSCs to compare cell viability in soft and stiff bioprinted scaffolds. Scale bars: 100 μm. (B) Immunofluorescence staining of ABCG2 and KRT14 on bioprinted hydrogel scaffolds encapsulating hCjSCs after 2 days in culture. Scale bars: 100 μm. (C) Immunofluorescence staining of MUC1, MUC5AC and MUC16 on hydrogel scaffolds encapsulating hCjSCs after 7 days of conjunctival goblet cell differentiation. Scale bars: 100 μm.

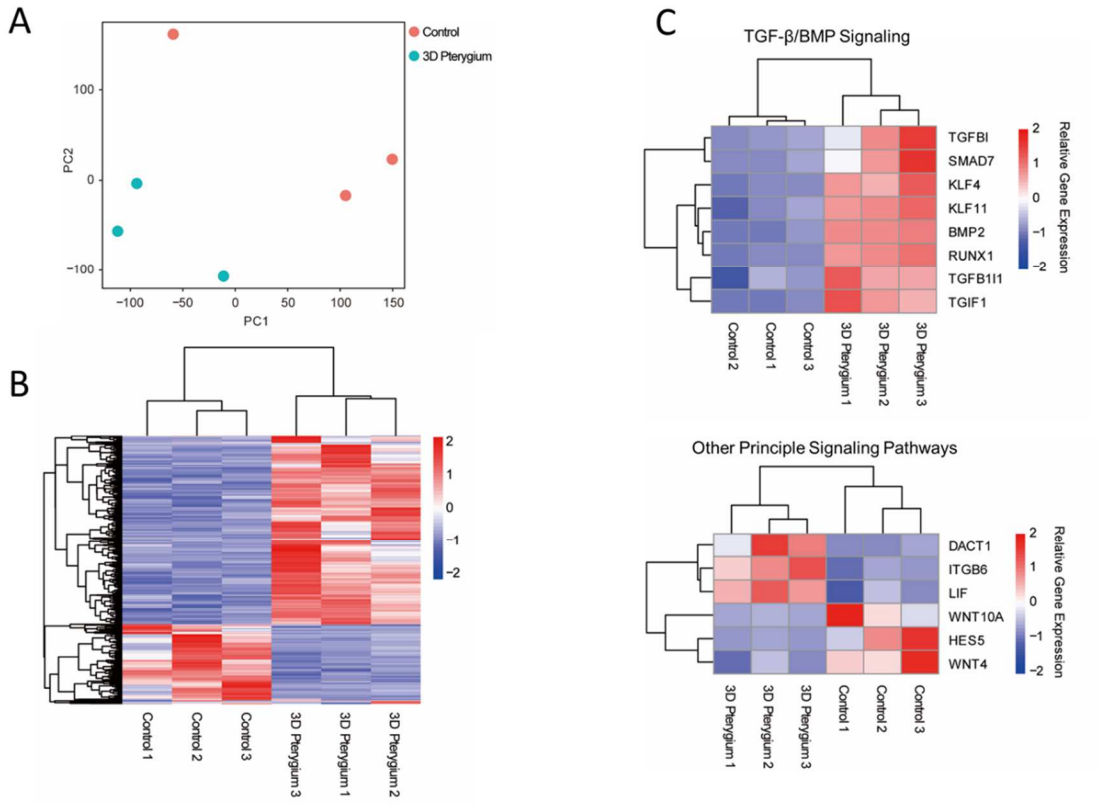

Supplementary Figure S4.3. Transcriptomic analysis. (A) PCA result of the global transcriptomic profiles of the 3D pterygium model and the control. (B) Heatmap showing total DEGs culture control and (C) the representative DEGs correlated to TGF-β/BMP signaling and other principal signaling pathways in the 3D pterygium model compared to the 2D culture control. Scale bars represent log2 transformed fold changes

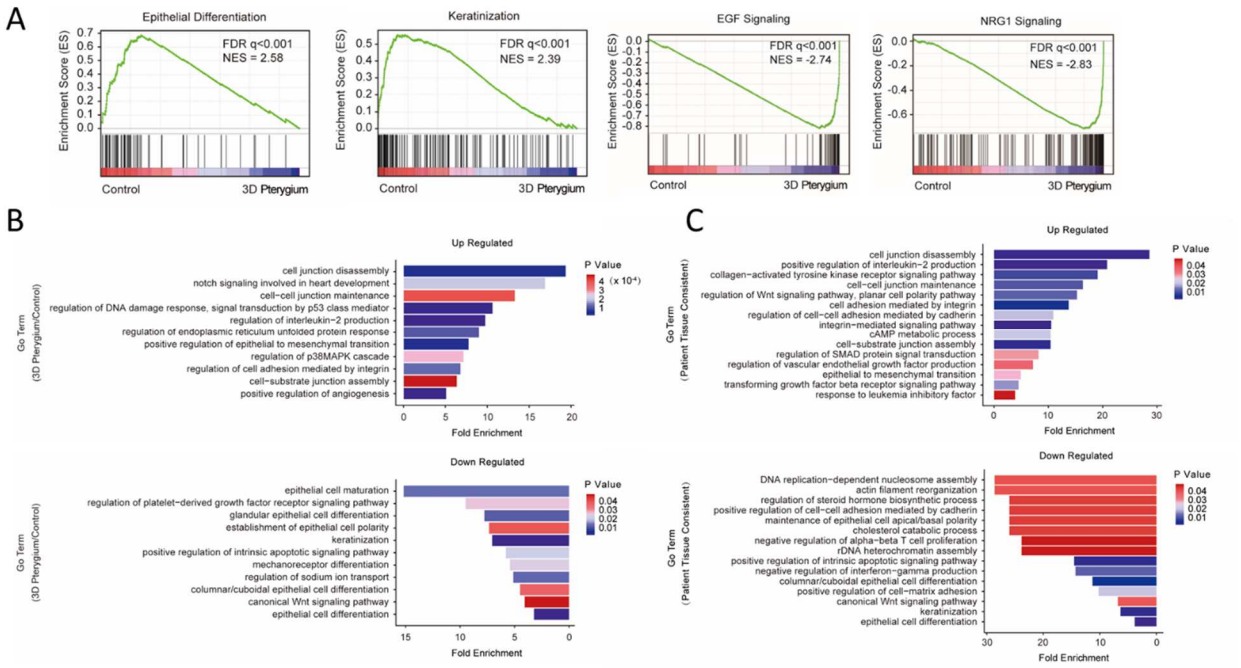

Supplementary Figure S4.4. Gene enrichment analysis. (A) Representative GSEA showing the enrichment of epithelial differentiation and keratinization in the control compared to the 3D pterygium. (B) GO terms enriched in hCjSCs cultured in the 3D pterygium model versus 2D control. (C) GO enrichment analysis on the consistent DEGs in 3D pterygium model and human patient samples.

Reference

[1] T.M. Harvey, A.G.A. Fernandez, R. Patel, D. Goldman, J. Ciralsky, Conjunctival Anatomy and Physiology, in: Ocul. Surf. Dis. Cornea, Conjunctiva Tear Film, Elsevier Inc., 2013: pp. 23–27. https://doi.org/10.1016/B978-1-4557-2876-3.00004-3.

[2] E.K. Akpek, J.D. Gottsch, Immune of defense at the ocular surface, Eye. 17 (2003) 949–956. https://doi.org/10.1038/sj.eye.6700617.

[3] J.B. Foster, W.B. Lee, The Tear Film: Anatomy, Structure and Function, in: Ocul. Surf. Dis. Cornea, Conjunctiva Tear Film, Elsevier Inc., 2013: pp. 17–21. https://doi.org/10.1016/B978-1-4557-2876-3.00003-1.

[4] I.K. Gipson, Goblet cells of the conjunctiva: A review of recent findings, Prog. Retin. Eye Res. 54 (2016) 49–63. https://doi.org/10.1016/j.preteyeres.2016.04.005.

[5] D. Thorel, S. Ingen-Housz-Oro, G. Royer, A. Delcampe, N. Bellon, C. Bodemer, A. Welfringer-Morin, D. Bremond-Gignac, M.P. Robert, M. Tauber, F. Malecaze, O. Dereure, V. Daien, A. Colin, C. Bernier, C. Couret, B. Vabres, F. Tetart, B. Milpied, T. Cornut, B. Ben Said, C. Burillon, N. Cordel, L. Beral, N. De Prost, P. Wolkenstein, M. Muraine, J. Gueudry,

Management of ocular involvement in the acute phase of Stevens-Johnson syndrome and toxic epidermal necrolysis: French national audit of practices, literature review, and consensus agreement, Orphanet J. Rare Dis. 15 (2020) 259. https://doi.org/10.1186/s13023-020-01538-x.

[6] T. Yamaguchi, Inflammatory response in dry eye, Investig. Ophthalmol. Vis. Sci. 59 (2018) DES192–DES199. https://doi.org/10.1167/iovs.17-23651.

[7] E. Clearfield, V. Muthappan, X. Wang, I.C. Kuo, Conjunctival autograft for pterygium, Cochrane Database Syst. Rev. 2016 (2016) CD011349. https://doi.org/10.1002/14651858.CD011349.pub2.

[8] J. Chui, N. di Girolamo, D. Wakefield, M.T. Coroneo, The pathogenesis of pterygium: Current concepts and their therapeutic implications, Ocul. Surf. 6 (2008) 24–43. https://doi.org/10.1016/S1542-0124(12)70103-9.

[9] D.G. Said, L.A. Faraj, M.S. Elalfy, A. Yeung, A. Miri, U. Fares, A.M. Otri, I. Rahman, S. Maharajan, H.S. Dua, Intra-lesional 5 fluorouracil for the management of recurrent pterygium, Eye. 27 (2013) 1123–1129. https://doi.org/10.1038/eye.2013.135.

[10] Y. Monden, F. Hotokezaka, R. Yamakawa, Recurrent pterygium treatment using mitomycin C, double amniotic membrane transplantation, and a large conjunctival flap, Int. Med. Case Rep. J. 11 (2018) 47–52. https://doi.org/10.2147/IMCRJ.S150969.

[11] W.K. Chu, H.L. Choi, A.K. Bhat, V. Jhanji, Pterygium: new insights, Eye. 34 (2020) 1047–1050. https://doi.org/10.1038/s41433-020-0786-3.

[12] F. Zhao, S. Cai, Z. Huang, P. Ding, C. Du, Optical Coherence Tomography Angiography in Pinguecula and Pterygium, Cornea. 39 (2020) 99–103. https://doi.org/10.1097/ICO.0000000000002114.

[13] S. Ling, L. Liang, H. Lin, W. Li, J. Xu, Increasing lymphatic microvessel density in primary pterygia, Arch. Ophthalmol. 130 (2012) 735–742. https://doi.org/10.1001/archophthalmol.2012.293.

[14] J. Chui, M.T. Coroneo, L.T. Tat, R. Crouch, D. Wakefield, N. Di Girolamo, Ophthalmic pterygium: A stem cell disorder with premalignant features, Am. J. Pathol. 178 (2011) 817–827. https://doi.org/10.1016/j.ajpath.2010.10.037.

[15] E. Cárdenas-Cantú, J. Zavala, J. Valenzuela, J.E. Valdez-García, Molecular Basis of Pterygium Development, Semin. Ophthalmol. 31 (2014) 1–17. https://doi.org/10.3109/08820538.2014.971822.

[16] C. Liu, Y. Song, X. Wang, Z. Lai, C. Li, P. Wan, N. Xu, D. Huang, Y. Liu, Z. Wang, The key role of vegf in the cross talk between pterygium and dry eye and its clinical significance, Ophthalmic Res. 63 (2020) 320–331. https://doi.org/10.1159/000503636.

[17] Minsup Lee; Seohyeon Yun; So Yeon Choi; JaeWook Yang, Corneal neovascularization and inflammation in pterygium mouse model induced by subconjunctival injection of human pterygium epithelial cells, Invest. Ophthalmol. Vis. Sci. 58 (2017). https://iovs.arvojournals.org/article.aspx?articleid=2642050 (accessed May 27, 2021).

[18] J. Zavala, J.C. Hernandez-Camarena, B. Salvador-Gálvez, J.E. Pérez-Saucedo, A. Vela-Martinez, J.E. Valdez-García, Extracellular matrix and fibroblast injection produces pterygium-like lesion in rabbits, Biol. Res. 51 (2018) 15. https://doi.org/10.1186/s40659-018-0165-8.

[19] N. Di Girolamo, N. Tedla, R.K. Kumar, P. McCluskey, A. Lloyd, M.T. Coroneo, D. Wakefield, Culture and characterisation of epithelial cells from human pterygia, Br. J. Ophthalmol. 83 (1999) 1077–1082. https://doi.org/10.1136/bjo.83.9.1077.

[20] H.S. Lee, J.H. Lee, J.W. Yang, Effect of porcine chondrocyte-derived extracellular matrix on the pterygium in mouse model, Graefe's Arch. Clin. Exp. Ophthalmol. 252 (2014) 609–618. https://doi.org/10.1007/s00417-014-2592-8.

[21] K.H. Benam, S. Dauth, B. Hassell, A. Herland, A. Jain, K.J. Jang, K. Karalis, H.J. Kim, L. MacQueen, R. Mahmoodian, S. Musah, Y.S. Torisawa, A.D. Van Der Meer, R. Villenave, M. Yadid, K.K. Parker, D.E. Ingber, Engineered in vitro disease models, Annu. Rev. Pathol. Mech. Dis. 10 (2015) 195–262. https://doi.org/10.1146/annurev-pathol-012414-040418.

[22] C. Argentati, I. Tortorella, M. Bazzucchi, F. Morena, S. Martino, Harnessing the potential of stem cells for disease modeling: Progress and promises, J. Pers. Med. 10 (2020). https://doi.org/10.3390/jpm10010008.

[23] X. Ma, J. Liu, W. Zhu, M. Tang, N. Lawrence, C. Yu, M. Gou, S. Chen, 3D bioprinting of functional tissue models for personalized drug screening and in vitro disease modeling, Adv. Drug Deliv. Rev. 132 (2018) 235–251. https://doi.org/10.1016/j.addr.2018.06.011.

[24] K. Walus, S. Beyer, S.M. Willerth, Three-dimensional bioprinting healthy and diseased models of the brain tissue using stem cells, Curr. Opin. Biomed. Eng. 14 (2020) 25–33. https://doi.org/10.1016/j.cobme.2020.03.002.

[25] C. Yu, J. Schimelman, P. Wang, K.L. Miller, X. Ma, S. You, J. Guan, B. Sun, W. Zhu, S. Chen, Photopolymerizable Biomaterials and Light-Based 3D Printing Strategies for Biomedical Applications, Chem. Rev. 120 (2020) 10695–10743. https://doi.org/10.1021/acs.chemrev.9b00810.

[26] X. Ma, X. Qu, W. Zhu, Y.S. Li, S. Yuan, H. Zhang, J. Liu, P. Wang, C.S.E. Lai, F. Zanella, G.S. Feng, F. Sheikh, S. Chien, S. Chen, Deterministically patterned biomimetic human iPSC-derived hepatic model via rapid 3D bioprinting, Proc. Natl. Acad. Sci. U. S. A. 113 (2016) 2206–2211. https://doi.org/10.1073/pnas.1524510113.

[27] J. Zhang, Q. Hu, S. Wang, J. Tao, M. Gou, Digital light processing based three-dimensional printing for medical applications, Int. J. Bioprinting. 6 (2020) 12–27. https://doi.org/10.18063/ijb.v6i1.242.

[28] B. Grigoryan, S.J. Paulsen, D.C. Corbett, D.W. Sazer, C.L. Fortin, A.J. Zaita, P.T. Greenfield, N.J. Calafat, J.P. Gounley, A.H. Ta, F. Johansson, A. Randles, J.E. Rosenkrantz, J.D. Louis-Rosenberg, P.A. Galie, K.R. Stevens, J.S. Miller, Multivascular networks and functional intravascular topologies within biocompatible hydrogels, Science (80-.). 364 (2019) 458–464. https://doi.org/10.1126/science.aav9750.

[29] J. Koffler, W. Zhu, X. Qu, O. Platoshyn, J.N. Dulin, J. Brock, L. Graham, P. Lu, J. Sakamoto, M. Marsala, S. Chen, M.H. Tuszynski, Biomimetic 3D-printed scaffolds for spinal cord injury repair, Nat. Med. 25 (2019) 263–269. https://doi.org/10.1038/s41591-018-0296-z.

[30] D. Dean, J. Wallace, A. Siblani, M.O. Wang, K. Kim, A.G. Mikos, J.P. Fisher, Continuous digital light processing (cDLP): Highly accurate additive manufacturing of tissue engineered bone scaffolds: This paper highlights the main issues regarding the application of Continuous Digital Light Processing (cDLP) for the production of highly accurate PPF scaffolds with layers as thin as 60 μm for bone tissue engineering, Virtual Phys. Prototyp. 7 (2012) 13–24. https://doi.org/10.1080/17452759.2012.673152.

[31] J. Liu, K. Miller, X. Ma, S. Dewan, N. Lawrence, G. Whang, P. Chung, A.D. Mcculloch, S. Chen, Direct 3D bioprinting of cardiac micro-tissues mimicking native myocardium, (2020). https://doi.org/10.1016/j.biomaterials.2020.120204.

[32] R.M.K. Stewart, C.M. Sheridan, P.S. Hiscott, G. Czanner, S.B. Kaye, Human Conjunctival Stem Cells are Predominantly Located in the Medial Canthal and Inferior Forniceal Areas, Invest. Ophthalmol. Vis. Sci. 56 (2015) 2021–2030. https://doi.org/10.1167/iovs.14-16266.

[33] S. Schrader, M. Notara, M. Beaconsfield, S.J. Tuft, J.T. Daniels, G. Geerling, Tissue engineering for conjunctival reconstruction: Established methods and future outlooks, Curr. Eye Res. 34 (2009) 913–924. https://doi.org/10.3109/02713680903198045.

[34] T. Ramos, D. Scott, S. Ahmad, An Update on Ocular Surface Epithelial Stem Cells: Cornea and Conjunctiva, Stem Cells Int. 2015 (2015). https://doi.org/10.1155/2015/601731.

[35] M. Bertolin, C. Breda, S. Ferrari, S.I. Van Acker, N. Zakaria, E. Di Iorio, A. Migliorati, D. Ponzin, B. Ferrari, Z. Lužnik, V. Barbaro, Optimized protocol for regeneration of the conjunctival epithelium using the cell suspension technique, Cornea. 38 (2019) 469–479. https://doi.org/10.1097/ICO.0000000000001670.

[36] N. Wu, C. Yan, J. Chen, Q. Yao, Y. Lu, F. Yu, H. Sun, Y. Fu, Conjunctival reconstruction via enrichment of human conjunctival epithelial stem cells by p75 through the NGF-p75-SALL2 signaling axis, Stem Cells Transl. Med. 9 (2020) 1448–1461. https://doi.org/10.1002/sctm.19-0449.

[37] D. Meller, V. Dabul, S.C.G. Tseng, Expansion of conjunctival epithelial progenitor cells on amniotic membrane, Exp. Eye Res. 74 (2002) 537–545. https://doi.org/10.1006/exer.2001.1163.

[38] S.J. Spurr-Michaud, I.K. Gipson, Methods for culture of human corneal and conjunctival epithelia, Methods Mol. Biol. 945 (2013) 31–43. https://doi.org/10.1007/978-1-62703-125-7_3.

[39] K. Nomi, R. Hayashi, Y. Ishikawa, Y. Kobayashi, T. Katayama, A.J. Quantock, K. Nishida, Generation of functional conjunctival epithelium, including goblet cells, from human iPSCs, Cell Rep. 34 (2021) 108715. https://doi.org/10.1016/j.celrep.2021.108715.

[40] Z. Zhong, X. Deng, P. Wang, C. Yu, W. Kiratitanaporn, X. Wu, J. Schimelman, M. Tang, A. Balayan, E. Yao, J. Tian, L. Chen, K. Zhang, S. Chen, Rapid bioprinting of conjunctival stem cell micro-constructs for subconjunctival ocular injection, Biomaterials. 267 (2021) 120462. https://doi.org/10.1016/j.biomaterials.2020.120462.

[41] H.A. McCauley, G. Guasch, Three cheers for the goblet cell: Maintaining homeostasis in mucosal epithelia, Trends Mol. Med. 21 (2015) 492–503. https://doi.org/10.1016/j.molmed.2015.06.003.

[42] P. Wang, X. Li, W. Zhu, Z. Zhong, A. Moran, W. Wang, K. Zhang, S. Chen, 3D bioprinting of hydrogels for retina cell culturing, Bioprinting. 12 (2018). https://doi.org/10.1016/j.bprint.2018.e00029.

[43] M. Tang, Q. Xie, R.C. Gimple, Z. Zhong, T. Tam, J. Tian, R.L. Kidwell, Q. Wu, B.C. Prager, Z. Qiu, A. Yu, Z. Zhu, P. Mesci, H. Jing, J. Schimelman, P. Wang, D. Lee, M.H. Lorenzini, D. Dixit, L. Zhao, S. Bhargava, T.E. Miller, X. Wan, J. Tang, B. Sun, B.F. Cravatt, A.R. Muotri, S. Chen, J.N. Rich, Three-dimensional bioprinted glioblastoma microenvironments model cellular dependencies and immune interactions, Cell Res. 30 (2020) 833–853. https://doi.org/10.1038/s41422-020-0338-1.

[44] H. Shirahama, B.H. Lee, L.P. Tan, N.J. Cho, Precise tuning of facile one-pot gelatin methacryloyl (GelMA) synthesis, Sci. Rep. (2016). https://doi.org/10.1038/srep31036.

[45] M. Zhu, Y. Wang, G. Ferracci, J. Zheng, N.J. Cho, B.H. Lee, Gelatin methacryloyl and its hydrogels with an exceptional degree of controllability and batch-to-batch consistency, Sci. Rep. 9 (2019) 1–13. https://doi.org/10.1038/s41598-019-42186-x.

[46] K.H. Vining, D.J. Mooney, Mechanical forces direct stem cell behaviour in development and regeneration, Nat. Rev. Mol. Cell Biol. 18 (2017) 728–742. https://doi.org/10.1038/nrm.2017.108.

[47] J.H. Wen, L.G. Vincent, A. Fuhrmann, Y.S. Choi, K.C. Hribar, H. Taylor-Weiner, S. Chen, A.J. Engler, Interplay of matrix stiffness and protein tethering in stem cell differentiation, Nat. Mater. 13 (2014) 979–987. https://doi.org/10.1038/nmat4051.

[48] Ü. Beden, M. Irkeç, D. Orhan, M. Orhan, The roles of T-lymphocyte subpopulations (CD4 and CD8), intercellular adhesion molecule-1 (ICAM-1), HLA-DR receptor, and mast cells in etiopathogenesis of pterygium, Ocul. Immunol. Inflamm. 11 (2003) 115–122. https://doi.org/10.1076/ocii.11.2.115.15913.

[49] S. Tsironi, E. Ioachim, M. Machera, M. Aspiotis, N. Agnanti, K. Psilas, Presence and possible significance of immunohistochemically demonstrable metallothionein expression in pterygium versus pinguecula and normal conjunctiva, Eye. 15 (2001) 89–96. https://doi.org/10.1038/eye.2001.20.

[50] N. Dushku, T.W. Reid, Immunohistochemical evidence that human pterygia originate from an invasion of vimentin-expressing altered limbal epithelial basal cells, Curr. Eye Res. 13 (1994) 473–481. https://doi.org/10.3109/02713689408999878.

[51] J. Xu, S. Lamouille, R. Derynck, TGF-B-induced epithelial to mesenchymal transition, Cell Res. 19 (2009) 156–172. https://doi.org/10.1038/cr.2009.5.

[52] M. Holtmann, M. Neurath, Differential TNF-Signaling in Chronic Inflammatory Disorders, Curr. Mol. Med. 4 (2005) 439–444. https://doi.org/10.2174/1566524043360636.

[53] S. Lamouille, J. Xu, R. Derynck, Molecular mechanisms of epithelial-mesenchymal transition, Nat. Rev. Mol. Cell Biol. 15 (2014) 178–196. https://doi.org/10.1038/nrm3758.

[54] Y. Chen, H. Wang, Y. Jiang, X. Zhang, Q. Wang, Transcriptional profiling to identify the key genes and pathways of pterygium, PeerJ. 2020 (2020). https://doi.org/10.7717/peerj.9056.

[55] X. Liu, J. Zhang, D. Nie, K. Zeng, H. Hu, J. Tie, L. Sun, L. Peng, X. Liu, J. Wang, Comparative Transcriptomic Analysis to Identify the Important Coding and Non-coding RNAs Involved in the Pathogenesis of Pterygium, Front. Genet. 12 (2021) 646550. https://doi.org/10.3389/fgene.2021.646550.

[56] C. Zhang, H.J. Lee, A. Shrivastava, R. Wang, T.J. McQuiston, S.S. Challberg, B.A. Pollok, T. Wang, Long-Term In Vitro Expansion of Epithelial Stem Cells Enabled by Pharmacological Inhibition of PAK1-ROCK-Myosin II and TGF-β Signaling, Cell Rep. 25 (2018) 598-610.e5. https://doi.org/10.1016/j.celrep.2018.09.072.

[57] H. Mou, V. Vinarsky, P.R. Tata, K. Brazauskas, S.H. Choi, A.K. Crooke, B. Zhang, G.M. Solomon, B. Turner, H. Bihler, J. Harrington, A. Lapey, C. Channick, C. Keyes, A. Freund, S. Artandi, M. Mense, S. Rowe, J.F. Engelhardt, Y.C. Hsu, J. Rajagopal, Dual SMAD Signaling Inhibition Enables Long-Term Expansion of Diverse Epithelial Basal Cells, Cell Stem Cell. 19 (2016) 217–231. https://doi.org/10.1016/j.stem.2016.05.012.

[58] R. Singh, A. Joseph, T. Umapathy, N.L. Tint, H.S. Dua, Impression cytology of the ocular surface, Br. J. Ophthalmol. 89 (2005) 1655–1659. https://doi.org/10.1136/bjo.2005.073916.

[59] X. Ma, J. Liu, W. Zhu, M. Tang, N. Lawrence, C. Yu, M. Gou, S. Chen, 3D bioprinting of functional tissue models for personalized drug screening and in vitro disease modeling, Adv. Drug Deliv. Rev. (2018). https://doi.org/10.1016/j.addr.2018.06.011.

[60] M.S. Hayden, S. Ghosh, Regulation of NF-κB by TNF family cytokines, Semin. Immunol. 26 (2014) 253–266. https://doi.org/10.1016/j.smim.2014.05.004.

[61] C. Soria-Valles, A. López-Soto, F.G. Osorio, C. López-Otín, Immune and inflammatory responses to DNA damage in cancer and aging, Mech. Ageing Dev. 165 (2017) 10–16. https://doi.org/10.1016/j.mad.2016.10.004.

[62] G. Sökeland, U. Schumacher, The functional role of integrins during intra- and extravasation within the metastatic cascade, Mol. Cancer. 18 (2019) 1–19. https://doi.org/10.1186/s12943-018-0937-3.

[63] K. Zhang, R.J. Kaufman, From endoplasmic-reticulum stress to the inflammatory response, Nature. 454 (2008) 455–462. https://doi.org/10.1038/nature07203.

[64] B. Feldkoren, R. Hutchinson, Y. Rapaport, A. Mahajan, V. Margulis, Integrin signaling potentiates transforming growth factor-beta 1 (TGF-β1) dependent down-regulation of E-Cadherin expression – Important implications for epithelial to mesenchymal transition (EMT) in renal cell carcinoma, Exp. Cell Res. 355 (2017) 57–66. https://doi.org/10.1016/j.yexcr.2017.03.051.

[65] D.M. Gonzalez, D. Medici, Signaling mechanisms of the epithelial-mesenchymal transition, Sci. Signal. 7 (2014) re8. https://doi.org/10.1126/scisignal.2005189.

[66] Z. Wang, Y. Li, D. Kong, F. H. Sarkar, The Role of Notch Signaling Pathway in Epithelial-Mesenchymal Transition (EMT) During Development and Tumor Aggressiveness, Curr. Drug Targets. 11 (2010) 745–751. https://doi.org/10.2174/138945010791170860.

[67] T. Jardé, W.H. Chan, F.J. Rossello, T. Kaur Kahlon, M. Theocharous, T. Kurian Arackal, T. Flores, M. Giraud, E. Richards, E. Chan, G. Kerr, R.M. Engel, M. Prasko, J.F. Donoghue, S. ichi Abe, T.J. Phesse, C.M. Nefzger, P.J. McMurrick, D.R. Powell, R.J. Daly, J.M. Polo, H.E. Abud, Mesenchymal Niche-Derived Neuregulin-1 Drives Intestinal Stem Cell Proliferation and Regeneration of Damaged Epithelium, Cell Stem Cell. 27 (2020) 646-662.e7. https://doi.org/10.1016/j.stem.2020.06.021.

[68] J.H. Ko, H.J. Kim, H.J. Jeong, H.J. Lee, J.Y. Oh, Mesenchymal Stem and Stromal Cells Harness Macrophage-Derived Amphiregulin to Maintain Tissue Homeostasis, Cell Rep. 30 (2020) 3806-3820.e6. https://doi.org/10.1016/j.celrep.2020.02.062.

Chapter 5 Conclusions and Future Perspectives

1.1 Conclusions

In this dissertation, the 3D bioprinting of different types of ocular stem cells and the therapeutic and disease modeling applications were explored.

In Chapter 2, the dual-ECM bioprinting of primary LSCs is reported. This method applied DLP-based 3D bioprinting to fabricate engineered microscale hydrogel scaffolds based on GelMA and HAGM. The scaffolds both supported the viability of encapsulated primary LSCs but exhibited differential regulation. LSCs were found to actively proliferated in the GelMA-based scaffolds and took on quiescent characteristics in the HAGM-based scaffolds. Based on this, a bioprinted dual-ECM 'Yin-Yang' model encapsulating both active and quiescent LSCs was fabricated. These results illustrated an innovative engineering approach for disease modeling, drug screening and the development of an LSC-based regenerative therapy for the treatment of related ocular diseases.

In Chapter 3, the bioprinting of injectable hydrogel construct encapsulating rabbit CjSCs is reported. DLP-based 3D bioprinting was applied to fabricate hydrogel microscale constructs encapsulating CjSCs. By incorporating a small molecule cocktail in the culture medium, homogenous CjSCs with high replicative potential and potency were produced. The tunability for mechanical properties enabled the rapid fabrication of hydrogel constructs that promoted the viability and stem cell properties of encapsulated CjSCs and could be applied to dynamic suspension culture of CjSCs. The hydrogel constructs encapsulating CjSCs were injectable without compromising cell viability or physical deformation, and were suitable for subconjunctival as demonstrated in an *ex vivo* rabbit eyeball model

In Chapter 4, the bioprinting of human CjSCs and the development to bioprinted pterygium model are reported. Primary hCjSCs were efficiently expand using a novel feeder-free culture

method. DLP-based 3D bioprinting of hCjSCs with GelMA bioink preserved hCjSCs' viability, stemness and functionality. Based on this, a 3D bioprinted pterygium model containing hCjSCs from healthy donors, macrophages, and vascular cells was fabricated to recapitulate the multicellular pterygium microenvironment. With RNA-seq, we found that the hCjSCs in the bioprinted 3D model exhibited pathological features of pterygium and the comparative analysis with published data of patient-derived pterygium tissues produced consistent results.

1.2 Perspectives

3D bioprinting recapitulating ocular surface microenvironment

As we have explored the bioprinting of two epithelial stem cells on the ocular surface, LSCs and CjSCs, the epithelial cells, stromal cells, and immune cells orchestrate the ocular surface homeostasis [1–3]. In Chapter 4, we have discussed the integration of hCjSCs with macrophages and vascular cells to recapitulate the disease microenvironment of pterygium, which is under chronic inflammation. Using similar strategy, we can further explore the intercellular crosstalk between the epithelial stem cells and the mesenchymal cells in the stroma, which was mediated by the macrophages and contributed to the tissue regeneration. Moreover, as we have discussed in Chapter 2, the integration of different materials can variate the cell phenotypes in the scaffolds. Other than that, stiffness of the scaffold can also regulate the encapsulated cells and our DLP bioprinter can fabricated scaffolds with variable stiffness [4]. Thereby, the bioprinting of scaffolds mimicking the heterogeneity in ECM and mechanical properties of ocular surface can be further explored. The design can also be changed to adapt bioreactor or microfluidic device to produce powerful engineered tools for high-throughput drug screening.

3D bioprinted injectable hydrogel constructs for combinational therapy

We have explored the injectable hydrogel constructs in Chapter 3 and the idea can be applied to develop many therapeutic products. The design of the bioprinted constructs can be further optimized for fluidic dynamic and the shape can be modified for the immobilization in different tissues [5]. Replacing the endogenous stem cells with iPSC-derived cells or progenitor cells can overcome the difficulty of isolation and expansion as well as the age, source, conditions of the donor [6,7]. With the help of gene editing, the disease-related genetic alternation, inherit mutation, and immunogenicity can be corrected or alleviated after the reprograming [8,9]. In addition, as stem cell therapy combining stem cell transplantation and gene therapy, or the administration of drugs or bioactive molecules, including cytokines and exosome [10–12]. This approach can be integrated in the bioprinted constructs design as we can have a core-shell structure to simultaneously deliver different cargos. Furthermore, programmable degradation of the hydrogel can be applied in the bioprinted injectable constructs to better control the delivery [13].

Reference

[1] A. Naji, B. Favier, F. Deschaseaux, N. Rouas-Freiss, M. Eitoku, N. Suganuma, Mesenchymal stem/stromal cell function in modulating cell death, Stem Cell Res. Ther. 2019 101. 10 (2019) 1–12. https://doi.org/10.1186/S13287-019-1158-4.

[2] J.H. Ko, H.J. Kim, H.J. Jeong, H.J. Lee, J.Y. Oh, Mesenchymal Stem and Stromal Cells Harness Macrophage-Derived Amphiregulin to Maintain Tissue Homeostasis, Cell Rep. 30 (2020) 3806-3820.e6. https://doi.org/10.1016/j.celrep.2020.02.062.

[3] D.J. Prockop, J. Youn Oh, Mesenchymal stem/stromal cells (MSCs): Role as guardians of inflammation, Mol. Ther. 20 (2012) 14–20. https://doi.org/10.1038/mt.2011.211.

[4] M. Tang, S.K. Tiwari, K. Agrawal, M. Tan, J. Dang, T. Tam, J. Tian, X. Wan, J. Schimelman, S. You, Q. Xia, T.M. Rana, S. Chen, Rapid 3D Bioprinting of Glioblastoma Model Mimicking Native Biophysical Heterogeneity, Small. 17 (2021) 2006050. https://doi.org/10.1002/smll.202006050.

[5] K. Liang, K.H. Bae, M. Kurisawa, Recent advances in the design of injectable hydrogels for stem cell-based therapy, J. Mater. Chem. B. 7 (2019) 3775–3791. https://doi.org/10.1039/C9TB00485H.

[6] S. Yamanaka, Pluripotent Stem Cell-Based Cell Therapy—Promise and Challenges, Cell Stem Cell. 27 (2020) 523–531. https://doi.org/10.1016/j.stem.2020.09.014.

[7] M. Madrid, C. Sumen, S. Aivio, N. Saklayen, Autologous Induced Pluripotent Stem Cell–Based Cell Therapies: Promise, Progress, and Challenges, Curr. Protoc. 1 (2021) e88. https://doi.org/10.1002/cpz1.88.

[8] J. Jacków, Z. Guo, C. Hansen, H.E. Abaci, Y.S. Doucet, J.U. Shin, R. Hayashi, D. DeLorenzo, Y. Kabata, S. Shinkuma, J.C. Salas-Alanis, A.M. Christiano, CRISPR/Cas9-based targeted genome editing for correction of recessive dystrophic epidermolysis bullosa using iPS cells, Proc. Natl. Acad. Sci. U. S. A. 116 (2019) 26846–26852. https://doi.org/10.1073/pnas.1907081116.

[9] R. Araki, M. Uda, Y. Hoki, M. Sunayama, M. Nakamura, S. Ando, M. Sugiura, H. Ideno, A. Shimada, A. Nifuji, M. Abe, Negligible immunogenicity of terminally differentiated cells derived from induced pluripotent or embryonic stem cells, Nature. 494 (2013) 100–104.

[10] I.K. Cho, C.E. Hunter, S. Ye, A.L. Pongos, A.W.S. Chan, Combination of stem cell and gene therapy ameliorates symptoms in Huntington's disease mice, Npj Regen. Med. 4 (2019) 1–9. https://doi.org/10.1038/s41536-019-0066-7.

[11] S.J. Park, R.Y. Kim, B.W. Park, S. Lee, S.W. Choi, J.H. Park, J.J. Choi, S.W. Kim, J. Jang, D.W. Cho, H.M. Chung, S.H. Moon, K. Ban, H.J. Park, Dual stem cell therapy synergistically improves cardiac function and vascular regeneration following myocardial infarction, Nat. Commun. 10 (2019) 1–12. https://doi.org/10.1038/s41467-019-11091-2.

[12] A.K. Riau, H.S. Ong, G.H.F. Yam, J.S. Mehta, Sustained delivery system for stem cell-derived exosomes, Front. Pharmacol. 10 (2019) 1368. https://doi.org/10.3389/fphar.2019.01368.

[13] Y. Wang, Programmable hydrogels, Biomaterials. 178 (2018) 663–680. https://doi.org/10.1016/j.biomaterials.2018.03.008.